APPLICATION OF GEOPHYSICAL METHODS TO DELINEATE KAOLIN DEPOSITS AND SURVEY FOR GROUND WATER POTENTIALITIES AT MINJIBIR, KANO STATE.

.

by

Neelum Aggarwai

A thesis submitted to the Postgraduate School, Ahmadu Bello University, in partial fulfillment of the requirements for the degree of Masters of Science in Applied Geophysics.

Department of Physics,
Faculty of Science,
Ahmadu Bello University, Zaria,

November, 1983.

DECLARATION

I hereby declare that, this thesis is an original work carried out by the author under the supervision of Professor D.E. Ajakaiye, Head of Department of Physics and Dr. M.B. Awad, the Geophysics Course Co-ordinator.

To the best of my knowledge no part thereof has been submitted elsewhere for the award of a degree or diploma. The work of others is duly acknowledged and referenced.

Author.

Supervisor.

A.B.U., Zaria.

November, 1983.

ACKNOWLEDGEMENT

I would like to express my sincere thanks to Professor D.E. Ajakaiye, Head of Physics Department, Ahmadu Bello University, Zaria for inspiration and very useful suggestions during this work. I am deeply indebted to my supervisor, Dr. M.B. Awad for his invaluable guidance, keen interest and the advice which he readily gave at all times during my project work and the writing of this report.

My special thanks goes to Ministry of Rural and Community Development, Kano, (Rural Water Supply) for allowing me to use their Terrameter SAS 300 for the field work and to the staff of Ministry of Works and Transport, Soil and Materials Laboratory, Kano, for their assistance in helping me to test the soil and rock samples. I am also grateful to Geological Survey Department at Kano for the information on the possible location of Kaolin in Minjibir District and Federal Ministry of Water Resources, Kano for the log of borehole at Wasai, and Ministry of Land and Survey, Kano for the survey maps for Minjibir District.

Finally, I wish to express my sincere gratitude to my Father, Mr. H.R. Aggarwal, for the encouragement and support he has given to me throughout the project.

ABSTRACT

Three different geophysical methods namely resistivity, self-potential (S.P.) and very low frequency (V.L.F.) have been employed to delineate the extent of kaolin deposits and explore possible places for groundwater aquifers in the vicinity of Minjibir, Kano State. A reconnaissance survey was carried out along three long profiles, while detail work was done on a 200x400 m grid located in the vicinity of an existing kaolin pit.

The detail resistivity survey results indicate a three layer sub—strata with resistivities of 600 to 1,175 ohm meter for the first layer, 100 to 235 ohm m for the middle layer and 2,400 XL-m and above for the third layer. It shows a thickness varying from 1.1 to 1.7 m for the top layer and 11.4 + 2.4 m to 21.7 $\pm$ 1.3 m for the second layer. These results are in agreement with those deduced from the V.L.F. detail survey and the available borehole data of the survey area.

Using resistivity profiling and S.P. methods, the extent of the kaolin deposit was delineated and its total mass was estimated to be around 1.7 $\pm$ 0.2 million tons. Two prospective places to drill boreholes for water supply have been suggested based on the results of

the V.L.F., S.P., and resistivity surveys. The results of mechanical analysis of the top soils have been correlated with the heights of the sampling points. Silt and coarse sand provides the highest multiple correlation factor, approximately 0.6 with height, which indicates that the upper most layers are composed of coarse sand covered by silt.

TABLE OF CONTENTS

	Page
ACKNOWLEDGEMENT	iii
ABSTRACT	iv
TABLE OF CONTENTS	vi
LIST OF TABLES	ix
LIST OF FIGURES	x
ABBREVIATIONS, GLOSSARIES AND SYMBOLS	xiv
Chapter 1 - INTRODUCTION	1
1.1 General	1
1.2 Composition, properties and uses of kaolin	2
1.3 Area of survey	5
1.4 Choice of methods	7
Chapter 2 - GEOLOGY	11
2.1 General geology	11
2.2 Local geology	13
2.3 Soil formations in Nigeria	19
2.4 Laterite deposits	20
2.5 Geology of kaolin	21
Chapter 3 - METHODS OF SURVEY	23
3.1 Resistivity	23
3.2 Self-potential (S.P.)	35
3.3 Very low frequency (V.L.F.)	38
Chapter 4 - SOILS AND THEIR MECHANICAL ANALYSIS ..	45
4.1 Definition	45

Page

4.2 Soil classification 45

4.3 Soil sampling procedure 46

4.4 Laboratory tests 48

4.5 Interpretation 51

4.5.1 Minjibir-Wasai section.. 51

4.5.2 Dry stream bed section.. 58

4.5.3 Minjibir-Bagurawa section 60

4.6 Comparative study between topography and its mechanical analysis 60

4.6.1 Correlation coefficients between two different sets of data 60

4.6.2 Results of correlation.. 68

Chapter 5 - REGIONAL SURVEY 72

5.1 Resistivity survey 72

5.1.1 Interpretation of resistivity profiling 73

5.2 Self-potential survey 78

5.2.1 Interpretation of regional self-potential survey 78

5.3 Very low frequency survey 82

5.3.1 Interpretation of regional V.L.F. survey 84

Chapter 6 - DETAILED INVESTIGATION OF THE AREA AROUND THE KAOLIN PIT AND ITS INTERPRETATION 88

6.1 Field configuration 88

6.2 Resistivity survey 88

Page

6.3 Vertical electrical soundings 88

6.3.1 Interpretation of the vertical electrical soundings conducted around the kaolin pit 90

6.3.2 Coefficient of correlation and equivalence 98

6.3.3 Geological deductions for area surrounding the kaolin pit from iso-resistivity contours 103

6.3.4 Deduction of sub-surface structure of the area surrounding the kaolin pit from anomalous body characteristics 117

6.4 Resistivity profiling 124

6.4.1 Interpretation of resistivity profiling 126

6.5 Interpretation of self-potential survey 131

6.6 Interpretation of V.L.F. survey 135

hapter 7 - CONCLUSIONS 140

7.1 Summary 140

7.2 Suggestions 143

EFERENCES 144

LIST OF TABLES

		Page
1.1	Physical parameters of some rock materials ..	10
3.1	Different transmitting stations	44
4.1	Unified soil classification system..	47
4.2	Range of particle size of the various soil constituents	50
4.3	Correlation of porosity with soil constituents along the three profiles	59
4.4	Lithological description of soils along Minjibir to Wasai profile	61
4.5	Lithological description of soils along dry river bed profile	64
4.6	Lithological description of soils along Minjibir to Bagurawa profile	66
4.7	Multiple correlation coefficient of actual data points	70
6.1	Resistivity values and thickness of the layers at the sounding points..	92
6.2	Correlation coefficient of actual and observed VES points..	102
6.3	Calculated values of relief, maximum gradient, mean radius and area of anomalous body with respect to various depths	118
6.4	Calculated volume of anomalous body with respect to depths	118

LIST OF FIGURES

		Page
1.1	Schematic structure of kaolinite	3
1.2	Map of the surveyed area	6
1.3	Approximate ranges for the electric resistivity of rocks and soils	9
2.1	The geological formations in Nigeria	12
2.2	Geological map of northern Nigeria	14
2.3	Geological map of Kano State..	16
2.4	Geological map of Kano State at a depth of 50 m...	17
2.5	Lithology of borehole at Wasai	18
3.1	Scheme of simple field apparatus for resistivity measurements	26
3.2	Schlumberger arrangement for vertical sounding..	28
3.3	Wenner arrangement for profiling	28
3.4	Schlumberger arrangement for profiling.. ..	28
3.5	Top view of terrameter SAS-300	33
3.6	Non polarizing electrodes	39
3.7	Block diagram of VLF-EM..	42
3.8	Block diagram of EM16 VLF-EM..	43
4.1	Particle size distribution of Bagurawa kaolin	49
4.2a	Topographic profile along Minjibir to Wasai..	52
4.2b	Gravel content along Minjibir to Wasai.. ..	52
4.2c	Coarse sand content along Minjibir to Wasai..	52
4.2d	Medium sand content along Minjibir to Wasai..	52
4.2e	Fine sand content along Minjibir to Wasai ..	53

		Page
4.2f	Silt content along Minjibir to Wasai	53
4.2g	Clay content along Minjibir to Wasai	53
4.2h	Porosity along Minjibir to Wasai..	53
4.3a	Topographic profile along dry river	54
4.3b	Gravel content along dry river	54
4.3c	Coarse sand content along dry river	54
4.3d	Medium sand content along dry river	54
4.3e	Fine sand content along dry river	55
4.3f	Silt content along dry river	55
4.3g	Clay content along dry river	55
4.3h	Porosity along dry river	55
4.4a	Topographic profile along Minjibir to Bagurawa	56
4.4b	Gravel content along Minjibir to Bagurawa ..	56
4.4c	Coarse sand content along Minjibir to Bagurawa	56
4.4d	Medium sand content along Minjibir to Bagurawa	56
4.4e	Fine sand content along Minjibir to Bagurawa	57
4.4f	Silt content along Minjibir to Bagurawa ..	57
4.4g	Clay content along Minjibir to Bagurawa ..	57
4.4h	Porosity along Minjibir to Bagurawa	57
4.5	Topographic map of the area surveyed showing height contours	69
5.1	Schlumberger profiling along dry river bed profile	74
5.2	Schlumberger profiling along Minjibir to Wasai profile	76
5.3	Schlumberger profiling along Minjibir to Bagurawa profile	77

		Page
5.4	Self-potential graphs along the profiles ..	79
5.5	The integrated S.P. graphs of the profiles..	81
5.6	A schematic sub-surface strata of the surveyed area	83
5.7	Very-low-frequency graphs along the profiles	85
5.8	The integrated V.L.F. graphs of the profiles	86
6.1	Layout of the grid	89
6.2	VES = 3N7	93
6.3	VES = 3N17	94
6.4	VES = 1N9	95
6.5	VES = 3N1	96
6.6	VES = 5N9	97
6.7	VES = 3N13	99
6.8	VES = 2N9	100
6.9a	Isoresistivity contoured map at AB/2=2m ..	104
6.9b	Isoresistivity contoured map at AB/2=3m ..	105
6.9c	Isoresistivity contoured map at AB/2=5m ..	106
6.9d	Isoresistivity contoured map at AB/2=8m ..	107
6.9e	Isoresistivity contoured map at AB/2=10m ..	108
6.9f	Isoresistivity contoured map at AB/2=12m ..	109
6.9g	Isoresistivity contoured map at AB/2=16m ..	110
6.9h	Isoresistivity contoured map at AB/2=20m ..	111
6.9i	Isoresistivity contoured map at AB/2=40m ..	112
6.9j	Isoresistivity contoured map at AB/2=80m ..	113
6.10	Cross-section of the surveyed area as deduced from the VES result	114

Page

6.11 Schematic diagram of the inferred sequence of geological history of surveyed area 116

6.12 Graph showing variation in resistivity relief with depth in the survey area 119

6.13 Graph showing the variation in maximum gradient with depth in the survey area.. .. 120

6.14 Graph showing the variation in mean radius with depth in the survey area 121

6.15 Graph showing the variation in area with depth in survey area 122

6.16 Estimated volume of high resistivity anomalous body 125

6.17 Wenner resistivity profiling in the east-west direction 127

6.18 Wenner resistivity profiling in the north-south direction 128

6.19 Map showing possible extent of kaolin deposit using Wenner resistivity profiling method .. 130

6.20 Self-potential data in east-west direction .. 133

6.21 Lateral extent of kaolin deposit by self-potential 134

6.22 Map showing extent of kaolin deposit and possible places for groundwater prospecting.. 136

6.23 Contour plot of the V.L.F. in-phase component data after applying Fraser's filtering.. .. 138

6.24 Cross-section of AB as deduced from V.L.F. in-phase component data.. 139

ABBREVIATIONS, GLOSSARIES AND SYMBOLS

A.C.	-	Alternating current
B.S.	-	British standard
D.C.	-	Direct current
E	-	East
N	-	North
S.P.	-	Self-potential
VES	-	Vertical electrical sounding
V.L.F.	-	Very-low-frequency
ϕ	-	Porosity
ρ	-	Resistivity
ρ_e	-	Apparent resistivity
mm	-	Milli-meter
m	-	Meter
km	-	Kilo-meter
mA	-	Milli-amperes
mV	-	Milli-volts
Ωm	-	Ohm-meter
m/s	-	Meter per second
kg/m^3	-	Kilogram per cubic meter
dB	-	Decibel
Hz	-	Hertz
KHz	-	Kilo-hertz

Chapter 1

INTRODUCTION

1.1 General:

Minerals constitute a major part of the raw materials and are of vital importance for the industrial production and economic growth of a country. The earlier methods for exploration of minerals were on the basis of visual examination of exposures and outcrops, supplemented by deep drilling. Currently with the rapid advancement in new exploration techniques, various geophysical methods. which are economical and less time consuming, are being used for these investigations.

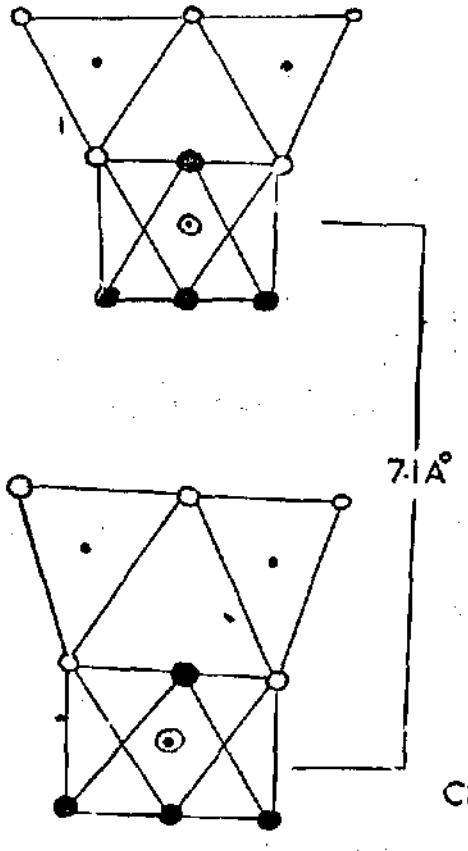
A geophysical survey helps to detect and locate subsurface geological structures, by means of measurements taken on the surface of the earth. The physical characteristics of the subsurface rocks sometimes differ in nature and this may show up in the form of anomalies in the observations on the ground surface.

In order to determine more accurately the exact location of a structure, several different techniques may be used concurrently in the same area. The results can then be interpreted more precisely, taking into consideration the geological information of the particular area. Thus in this survey for kaolin and groundwater, three geophysical techniques, resistivity, V.L.F. and S.P. were used.

1.2 Composition, Properties and uses of Kaolin:

Kaolin is a whitish clayey substance. It is mainly composed of kaolinite with small quantities of other clay minerals such as nacrite, dickite, and halloysite. Its composite formula is $Al_2Si_2O_5(OH)_4$. Crystallographically it is phyllosilicate, i.e., a silicate layer made up of two different sheets. The tetrahedral sheet has oxygen ions at the four tips and silicon ion at the centre and shares its four positive charges with four oxygen ions at the tips. The octahedral sheet has six tips, which are occupied by hydroxal or oxygen ions and their centre by aluminium ion. Together, they form one layer (Fig. 1.1).

Pure kaolin is a white powdery aggregate of minerals which consists principally of microcrystalline compounds approximating the normal kaolinites (Bateman, 1967). It is distinguished from other clays primarily by its whiteness, softness, ease of dispersion in water and other liquids, and is generally free from impurities particularly from compounds of iron and has negligible content of titanium and alkaline earths (Johnstone, 1961). Naturally occuring kaolin is seldom pure, the main impurities being fine-grained quartz or hydrous mica. In general, it has been found that it has a specific gravity of 2.60×10^3 kg/m^3, a fusion point of about 1,785°C and a refractive index of 1.56. Various workers have given different values with regard to its in-situ



• Si

⊙ Al_2

● OH

○ O

CRYSTALLO-CHEMICAL FORMULA

$Al_4Si_4O_{10}(OH)_8$

FIG. 1·1
SCHEMATIC STRUCTURE OF KAOLINITE
[AFTER DEGENS 1965]

density. Ebifegha (1977) has shown a dry density of 1.58 - 1.63 x 10^3 kg/m^3 for kaolin deposits near Kankara, in Katsina province, while Nkuesunam (1976) gave a wide range of 1.54 - 1.93 x 10^3 kg/m^3 for impure varieties at Tsanyawa, Kano State, Kirch (1968) and Johnstone (1961) found its specific gravity as 2.58 x 10^3 kg/m^3. According to Grimshaw (1971), the particle size of a high grade kaolin is about 0.001 mm. in diameter, though coarser varieties have also been found. As the particle size of all minerals present in pure kaolin is similar, it is difficult to deduce a mineralogical analysis of it with a good degree of certainty (Grimshaw, 1971). Kaolin is extensively used in a variety of ways in various industries all over the world. Its main use is in paper industry where it forms the filler constituent and replaces the fibre material which is expensive. It helps to flatten the paper, reduces expansion during printing and imparts better opacity and smoothness. The finer grades are deployed in coating the surface of the paper. Kaolin is also widely used in making ceramics. It has a limited use in the paint industry as a suspending agent in oil paints and as a pigment in distempers and water paints. In pharmaceuticals, it is used as medicine for the cure of diarrhoea among the babies. It acts as a filler in the manufacture of oil cloth, rubber and plastic and is used in conjuction with suitable binder to give weight to body cloth in textiles, as a catalyst in the petroleum industry and as a

colouring agent in the preparation of ultramine.

The largest producers of kaolin in the world are today U.K., U.S.A., Germany, Austria, India and Algeria.

1.3 Area of Survey:

The area of survey lies between 12^{o}-9' to 12^{o}-11' latitude and 8^{o}-37' to 8^{o}-40' longitude. The topography is generally flat. The approximate elevation is 480 m above sea level and the main drainage is provided by river Jakara, which is seasonal in nature (Faseke, 1977).

From inquiries at the Geological Survey Division at Kano, it was deduced that a reconnaissance survey of this area was carried out in July, 1977, by Mr. O.O. Faseke who had reported the existance of a kaolin deposit near Bagurawa in Minjibir Local Government. It is accessible by an all weather laterite road off the Kano-Gumel road.

The field work to explore kaolin deposits in this area commenced in September, 1982. The initial survey indicated the presence of some whitish boulders containing kaolin mineral at scattered places where wells had been dug and the subsoil had been heaped on the surface. On further search, a kaolin pit was located near Bagurawa. It is a very small village with few huts, about 3.2 km south-west of the Minjibir town Fig. 1.2. The existing

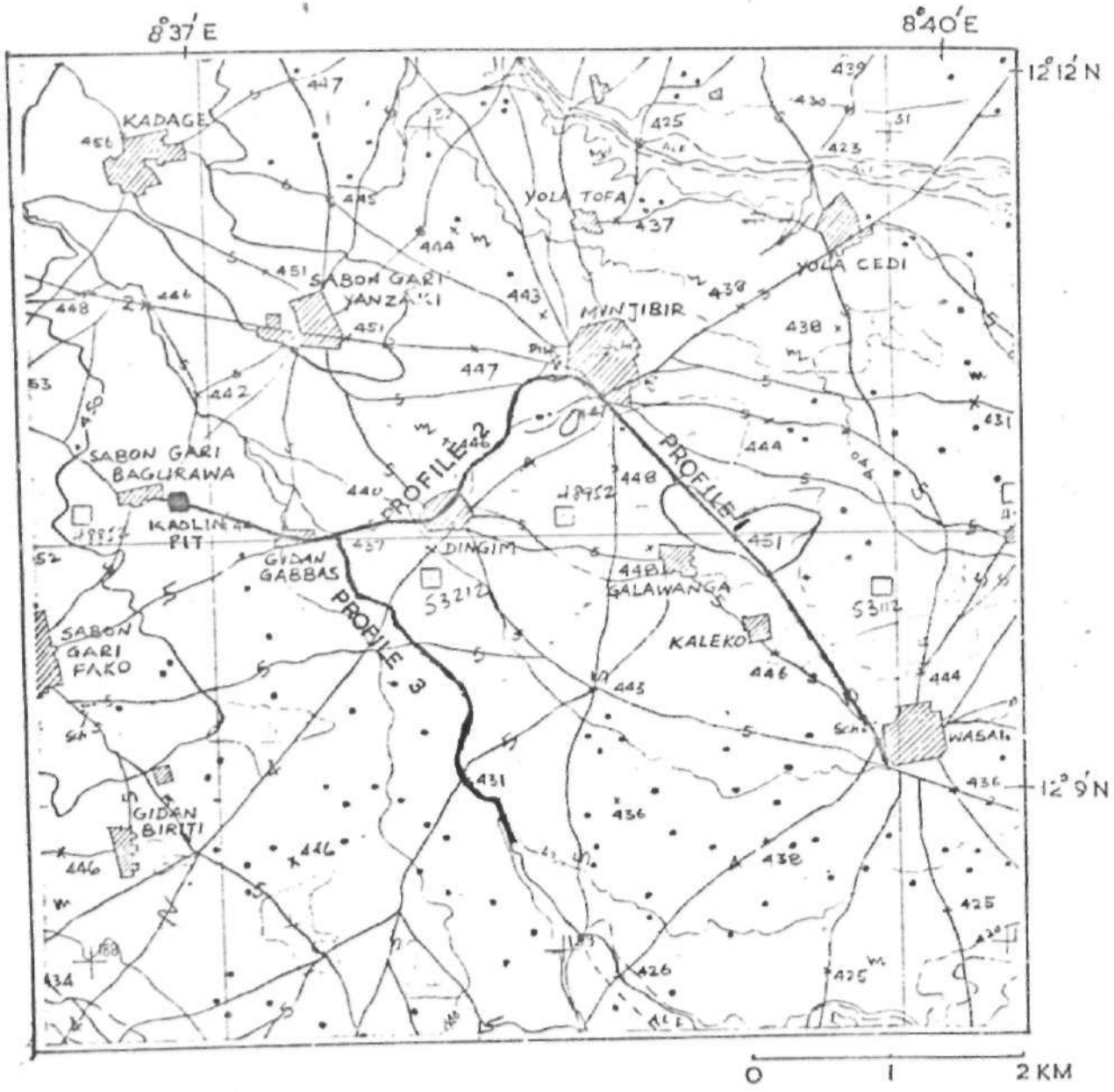


FIG. 1·2

MAP OF THE SURVEYED AREA
[COMPILED BY PHOTOSUR INC., CANADA, 1980].

pit is approximately circular, 32 m in diameter and 7 m in depth. Kaolin had often been extracted from the clay deposits by breaking and pulverising the partially weathered feldspar with the help of wooden battens and sieving off the impure coarser fraction for the past several years.

The surrounding area to this pit 200 x 400 m, was selected for geophysical survey to evaluate kaolin deposits, delineate the border outline and its approximate depth, and also to locate aquifer for ground water potentialities.

Besides this, three profiles were selected for a reconnaissance survey, as detailed below:

i) along the west side of the main road between Wasai and Minjibir, 2.8 km in length;

ii) along a narrow track from Minjibir to Bagurawa, 3.2 km in length; and

iii) along a dry stream bed, 2.4 km in length, which cuts across the Minjibir-Bagurawa track at 2.35 km.

The area under survey is shown in Fig. 1.2.

1.4 Choice of Methods:

A knowledge of geophysical parameters of different rock and soil types is essential to know which geophysical methods are most appropriate to be used.

Preliminary analysis is done by interpreting the geophysical data in relation with the published values for these parameters, alongwith laboratory measurements or any borehole information if available. The approximate ranges for the electric resistivity for various rock and soil types are shown in Fig. 1.3, while physical parameters of some rock materials are given in Table 1.1.

Table 1.1 indicates that there are significant contrasts in the resistivity values and seismic velocities for various rock types. These justify the adoption of the resistivity and seismic methods for identification and quantification of kaolin deposits in any given area. However, siesmic velocities could not be determined due to non-availability of suitable equipment.

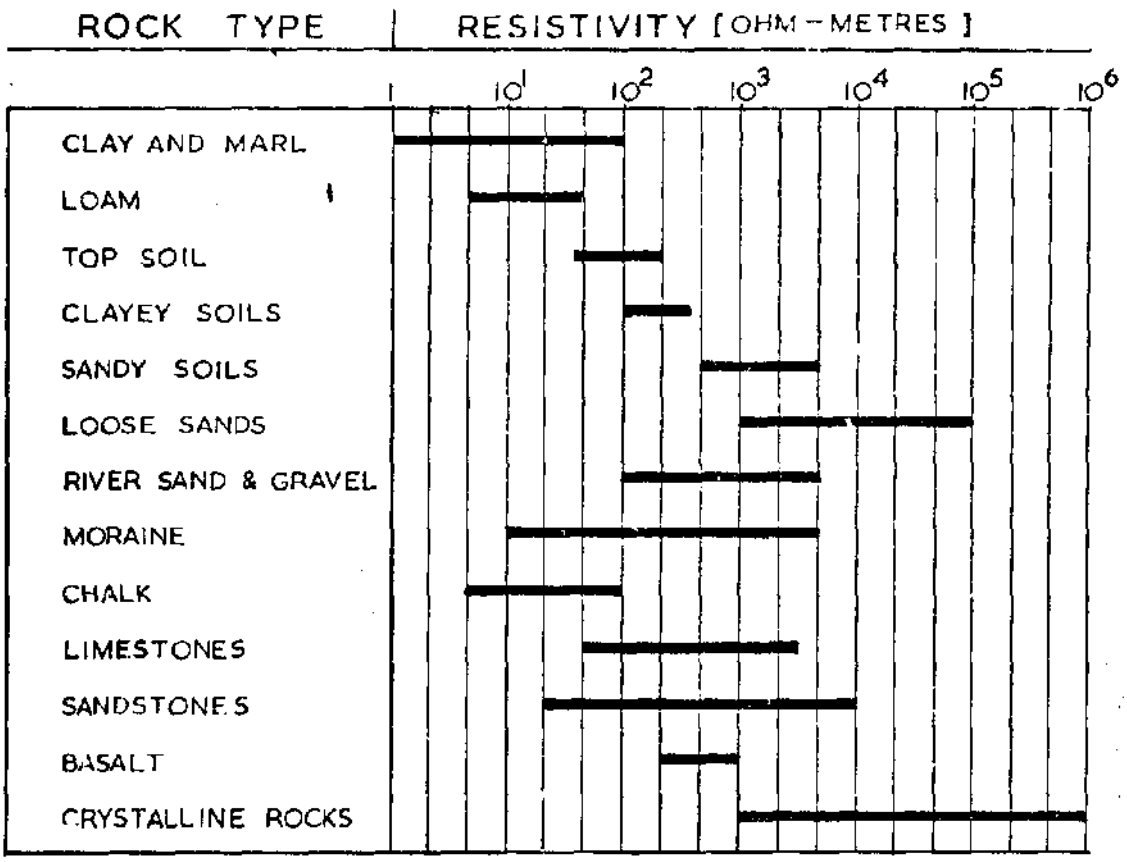


FIG. 1·3

APPROXIMATE RANGES FOR THE ELECTRIC RESISTIVITY OF ROCKS AND SOILS.
[ATLAS COPCO ABEM 1981]

TABLE 1.1

Physical Parameters Of Some Rock Materials.

Rock Type	Resistivity Range (Ωm)	Seismic Velocity (M/S)		Magnetic Suscep. ($\times 10^{-1}$)	Mean Density $\times 10^3$ Kg/m^3
		Dry Velocity	Wet Velocity		
Kaolin	1-120	915-1520	1380-1680	0.5	2.60
Clayey Earth Soil	10^2-4×10^2	110-305	1380-1680	-	1.70
Sands	10^2-10^4	300-460	1330-1680	1.0	1.50
Laterites	10^2-10^4	460-1220	1330-1680	1.5	2.00
Migmatites and Gneiss	10^3-10^6	3050-5490	1370-3050	1.0	2.70
Mica Schists	10^3-10^5	6400-7000	1380-1680	-	2.75

Compiled from Telford et al (1976), Keller (1966).

Chapter 2

GEOLOGY

2.1 General Geology:

The geologic formations in Nigeria can be divided into two broad groups, crystalline rocks and sedimentary rocks which occur in about equal proportions. Their distribution is shown in Fig. 2.1. The crystalline rocks are granites and gneisses, migmatities, pelitic schists and metaconglomerates, marbles and calcsilicate rocks, basic schists, amphibolites and basalts, quartzites and quartz schists, charnockites and fayalite granites. The sedimentary rock types are sandstones, shales and mudstones, limestones, siltstones, and other e.g. ironstones.

The crystalline rocks are further sub-divided into the following groups, depending on their age:

i) precambrian basement complex, which characteristically yields radiometric ages in excess of 500 million years (Grant, 1971), occupies about forty percent of the total surface area of Nigeria;

ii) younger granites, which are high level discordant intrusions in the basement complex, occupy about eight percent of the total surface area of Nigeria, (Bowden et al, 1976, Rahaman et al, 1977); and



FIG. 2·1

THE GEOLOGICAL FORMATIONS IN NIGERIA.
[TROPICAL SOILS OF NIGERIA IN ENGINEERING PRACTICE]
[1983]

iii) tertiary volcanics, which constitute only one percent of the total surface area of Nigeria, are restricted in occurrence to only eastern part of the country.

The sedimentary rocks can be found in seven major sedimentary basins in Nigeria. These are:

i) the Dahomey basin;
ii) the Niger Delta basin;
iii) the Anambra basin;
iv) the Benue trough;
v) the south-western part of the Chad basin;
vi) the Bida basin; and
vii) the south-western sector of the Iullemeden basin.

The rocks in these basins range in age from cretaceous to recent.

The geological map of the northern parts of Nigeria and extent of the Chad basin is shown in Fig. 2.2. Granitic rocks are the commonest crystalline rocks. The word 'granitic' is used in the broadest sense to cover all felsic rocks which may vary in composition from true granites to diorites.

2.2 Local Geology:

The area under investigation lies within Kano State

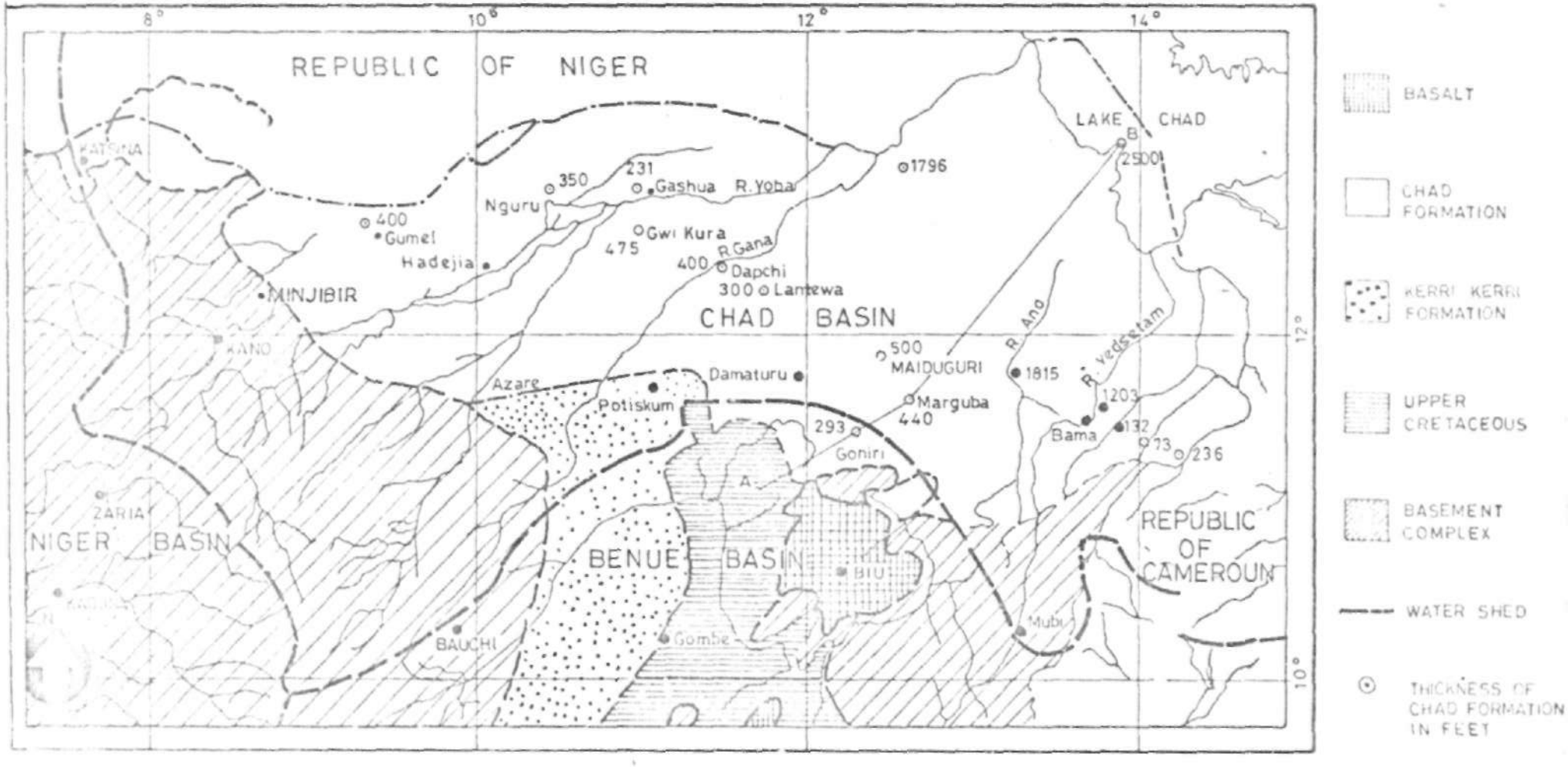


FIG. 2·2

GEOLOGICAL MAP OF NORTHERN NIGERIA.

[SOIL SURVEY AND MATERIALS REPORT. 1976]

which can be divided geologically into two groups, the undifferentiated basement complex in the south and south-west parts of the State which comprises of the older granites, syenite, gabbro, undifferentiated metasediments and the sands and clays of the Chad formation in the north and north-east of the State. The geological map of Kano State is shown in Fig. 2.3. The geology at a depth of 50 m is presented in Fig. 2.4.

The particular area of study lies completely within the undifferentiated basement complex. The area is low lying and virtually devoid of relief. There is hardly any exposure of outcrop except for a small laterite hardpan and some weathered outcrop close to the pit.

No geological map of this area has so far been published. From the few open pits that could be located in this area, it was observed that there is an overburden of loose sandy soil which is underlain by weathered basement consisting of clayey material and which is in turn underlain by unweathered basement complex. A borehole log and sub-soil lithological profile in the area is shown in Fig. 2.5.

The surface soils in the area formed as a result of weathering of these rocks are predominantly earthy to light brown friable porous sands and silty clays. At

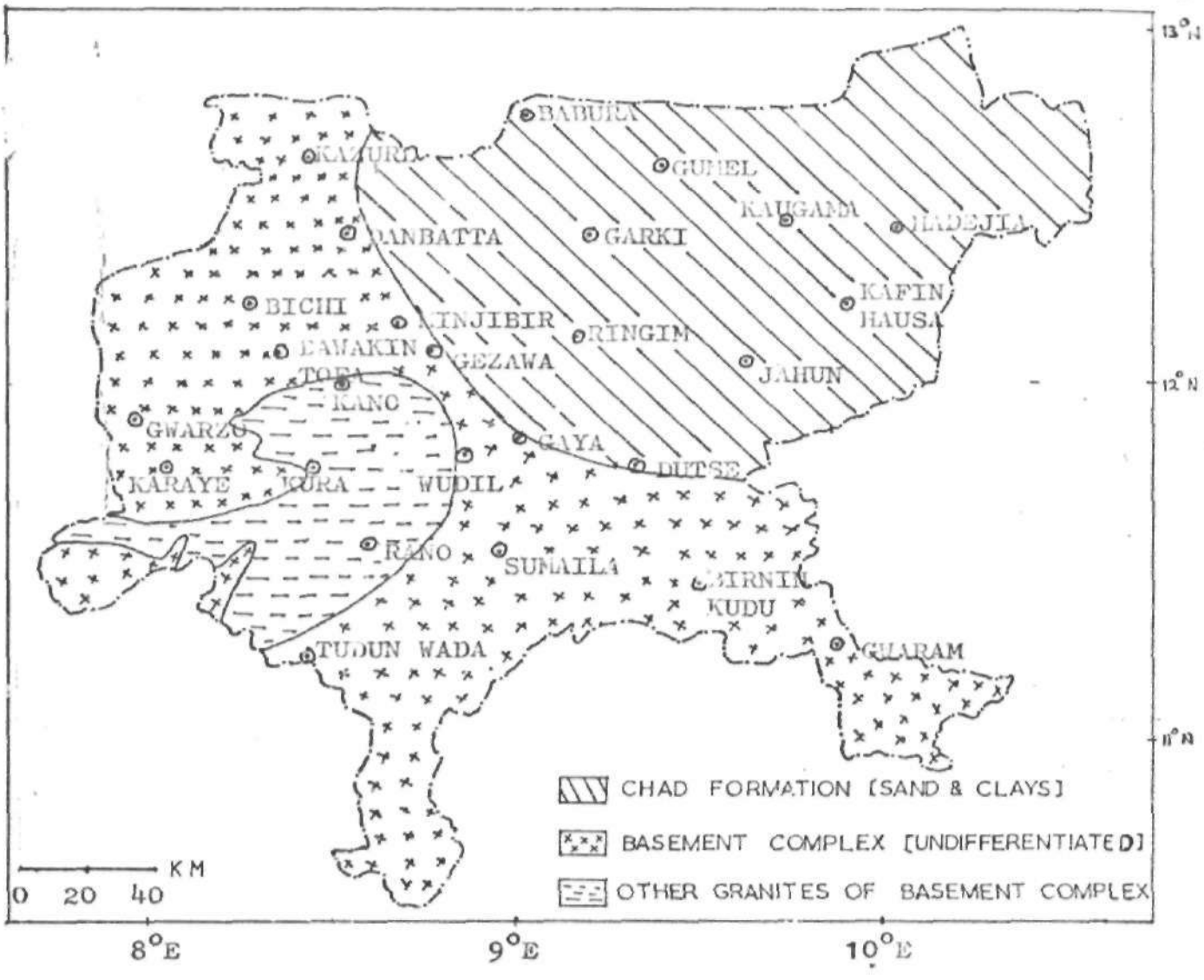


FIG. 2·3

GEOLOGICAL MAP OF KANO STATE.
[ADAPTED FROM KANO STATE]
[INTERGRATED RURAL DEVELOPMENT PROJECT 1979]

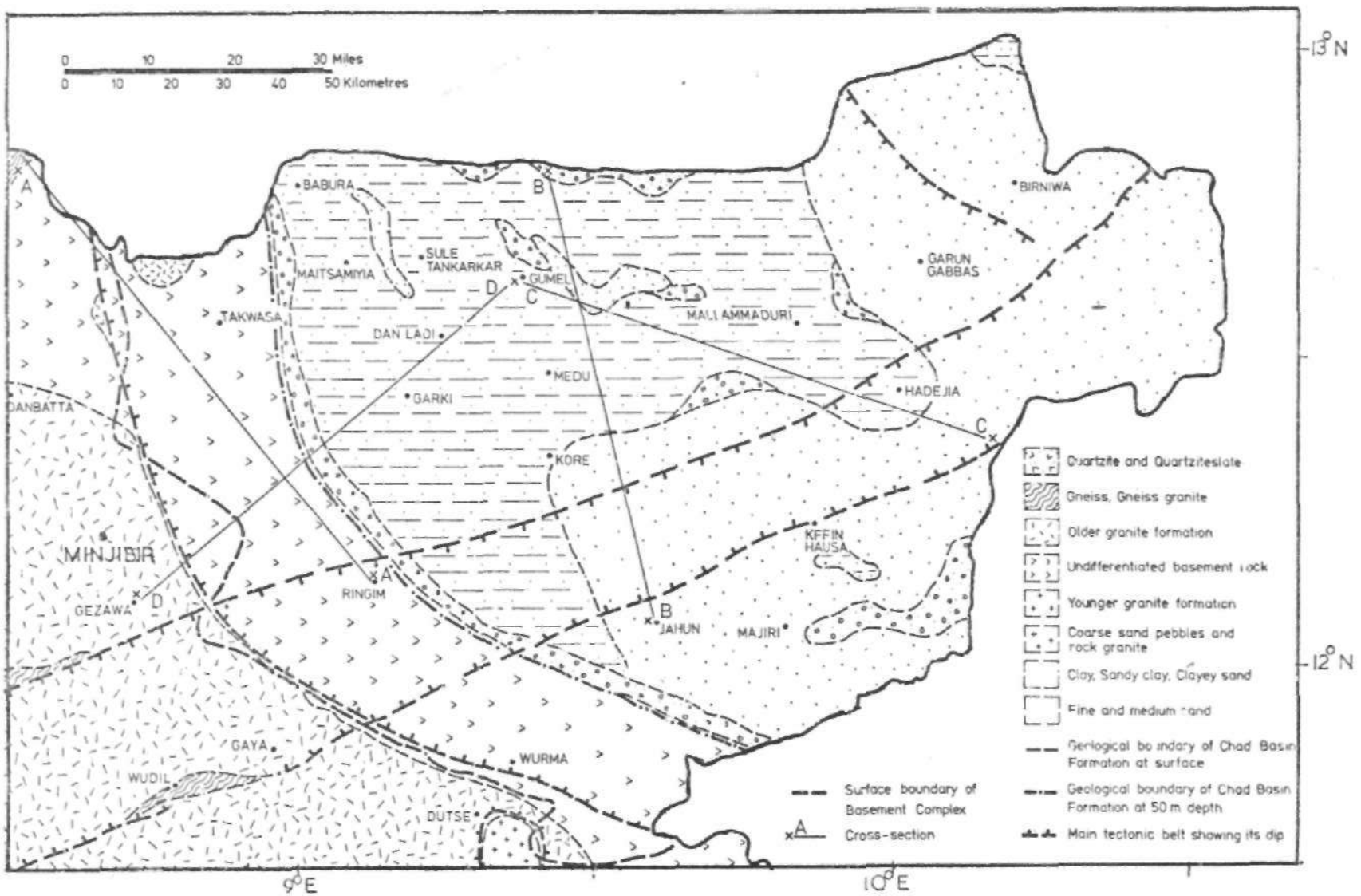


FIG. 2·4
GEOLOGICAL MAP OF KANO STATE AT A DEPTH OF 50 *m*
[KANO STATE INTEGRATED RURAL DEVELOPMENT PROJECT, 1979]

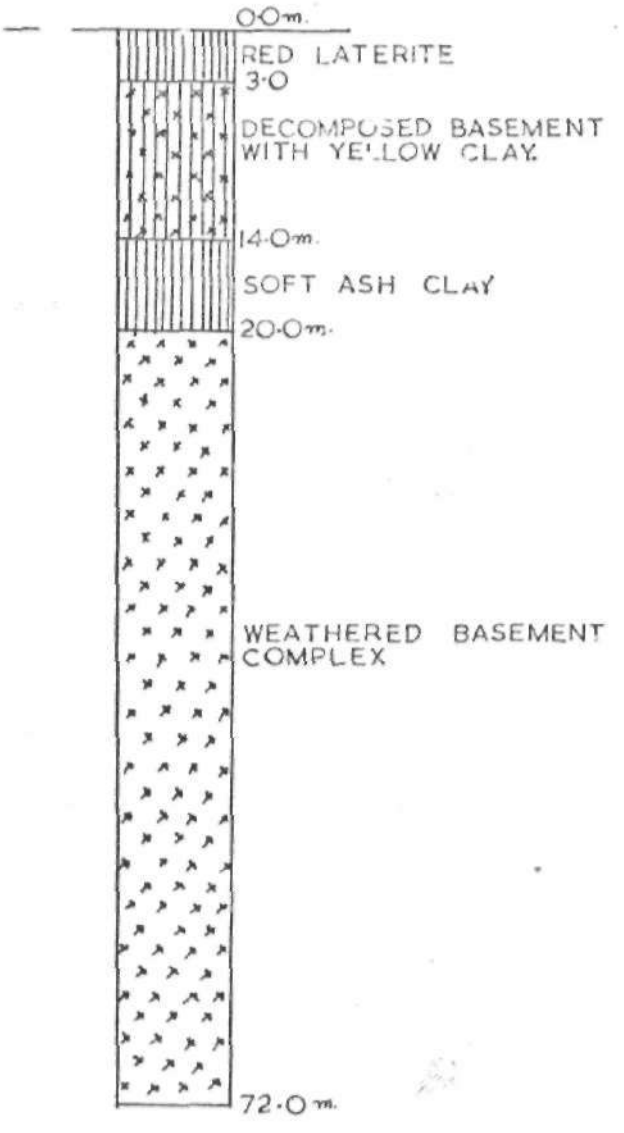


FIG. 2·5
LITHOLOGY OF BOREHOLE AT WASAI.
[SOURCE: FED. MIN. OF WATER RESOURCES KANO]
1983

places, laterite hardpan is encountered at shallow depths forming a "capping" to lateritic gravel that can extend to depths of as much as 3.0 m. The underlying gravels contain some cohesive material. These gravels formed from the porphyritic rocks (granites and gneisses) tend to form a matrix of stable minerals such as quartz and mica, in which is weathered feldspar. During weathering some constituents of the feldspar are leached away leaving a kaolin clay, with a porous, occasionally laminar structure. It is believed that iron bearing waters deposit oxides of iron in the pores of the clay, yielding a ferruginous gravel in which the large particles retain a resemblance to the rectangular shape of the parent feldspar crystals.

2.3 Soil Formations in Nigeria:

The Nigerian soils are often derived in place from the underlying rock. Their mineralogical and chemical analysis (Hoore, 1964; Ahn, 1970; Ojanuga and Lee, 1973; Ojanuga, 1979) have shown the following main inorganic components:

i) silicates which are mostly clay minerals such as kaolinite, halloysite, illite and montmorillonite; and

ii) oxides and hydroxides of iron and aluminium.

Kaolinite is the major clay mineral in Nigerian

soils. It is formed by the weathering of rocks containing most common rock forming minerals, olivines, pyroxenes, amphiboles, feldspars (Maignien, 1966) under moderately acidic and considerably leached environments.

The oxides of iron, heamatite and magnetite (Fe_2O_3) occur in soils of the tropics, while the hydroxide geothite (Fe_2OH) is a common soil constituent. Among oxides and hydroxides of aluminium, amorphous alumina hydrate and amorphous silica are present. Silicon occurs as the common oxide while quartz as the cryptocrystalthe oxide.

2.4 Laterite Deposits:

There are extensive deposits of laterites. These are the traditional materials for road and airfield construction. Laterites are yellowish to reddish brown materials consisting partly of spongy open textured pebbles which vary in colour from rusty red to liver colour of almost black, set in matrix of silty clay. The spongy coarse pebbles possess a vesicular structure. Based on this structure and its frequent association with basalt, it was first thought to be a volcanic rock. But later views regard the rock as the result of the sub-aerial decomposition in-situ of basalt, granite, quartzite, sandstone, schist etc., under a warm, humid and monsoonic climate. The former class of rocks is

especially prone to laterization or silica leaching. The process of laterization and hardening is due to:

i) dehydration of the hydroxides of iron and aluminium present;

ii) further oxidation of the high iron content of the material; and

iii) the precipitation of these oxides as cementing material.

The extent to which a residual soil has been laterized may be measured by its silica to sesquioxide ratio,

$$\frac{SiO_2}{Fe_2O_3 + Al_2O_3} .$$

Ratios less than 1.33 are indicative of true laterites, those between 1.33 and 2.00 of lateritic soils, and those greater than 2.00 of non-lateritic weathered soils.

2.5 Geology of Kaolin:

A small pit of kaolin exists near Bagurawa, 3.2 km in south-west direction of Minjibir town. The clay occurence lies within the undifferentiated basement complex in the area. The parent rock of the white clay is a coarse grained feldsparthic granite with phenocrystals of feldspar averaging 0.03 m in diameter (Fasoke, 1977). The gritty white clay is formed in-situ

by the chemical weathering of the feldspar of the host rock. Kaolin content of the rock, which is approximately 44 percent, appears to increase with depth which probably suggests the influence of hydrothermal fluid in the formation of the clay (Faseke, 1977). When the clay samples were air dried and subjected to firing at 1,150°C in a muffle furnace, the percentage linear shrinkage from plastic to air-dried state was 2.92 percent and from air-dried to burnt state was 2.45 percent. The colour before firing was dirty white and after firing it became pinkish white.

Chapter 3

METHODS OF SURVEY

3.1 Resistivity:

In most resistivity measurements, an electric current is introduced into the ground through two electrodes, and the potential difference is determined between the second pair of electrodes placed in line between them. Using the values for potential difference, the current applied and the electrode separation, the apparent resistivity of the non-homogeneous ground can be derived. The resistivity ρ of the material is expressed as the resistance R across a unit cube of the material. When current flows between two points of a conductor of cross-sectional area A, and distance d apart, then the resistance between these two points is given by the formula:

$$R = \frac{\rho d}{A} \qquad . \quad . \quad . \quad . \quad . \quad (1)$$

The two basic laws used in electrical resistivity survey are:

i) Ohms law $\vec{E} = \rho \vec{j}$ . . . . (2)

where $\vec{E}$ = potential gradient.

ρ = resistivity of the medium.

$\vec{j}$ = current density.

ii) Divergence condition $\nabla . \vec{j} = 0$ . . (3)

Combining equations (2) and (3)

$$\nabla\cdot\vec{j} = \frac{\nabla\cdot\vec{E}}{\rho} = -\frac{\nabla^2\vec{V}}{\rho} = 0 \quad . \quad . \quad . \quad (4)$$

Since the electric field is the gradient of a scalar potential and is given by

$$\vec{E} = -\nabla\vec{V} \quad . \quad . \quad . \quad . \quad . \quad . \quad (5)$$

Since for a homogeneous medium ρ is independent of co-ordinate axes, equation (4) becomes

$$\nabla^2\vec{V} = 0 \quad . \quad . \quad . \quad . \quad . \quad . \quad (6)$$

which is Laplace's equation. In spherical polar co-ordinates it is written as

$$\frac{\partial}{\partial r}\left(r^2\frac{\partial V}{\partial r}\right) + \frac{1}{r^2\sin\theta}\frac{\partial}{\partial\theta}\left(\sin\theta\frac{\partial V}{\partial\theta}\right) + \frac{1}{r^2\sin^2\theta}\frac{\partial^2 V}{\partial\phi^2} = 0 \quad . . (7)$$

Considering a single source of current and complete symmetry of current flow with respect to θ and ϕ direction, then the potential at any point is only a function of r.

$$\frac{\partial}{\partial r}\left(r^2\frac{\partial V}{\partial r}\right) = 0. \quad . \quad . \quad . \quad . \quad (8)$$

By integration, equation (8) has a solution of the form

$$V = -\frac{B}{r} + A. \quad . \quad . \quad . \quad . \quad . \quad (9)$$

where A and B are constants of integration.

Now as $r \to \infty$, $V \to 0$, $A = 0$

$$V = -(B/r) \quad . \quad . \quad . \quad . \quad . \quad . \quad (10)$$

The total current I flowing out of a semi infinite half space of radius r is given by

$$I = \int_s \vec{j}\,ds = \int_s (\vec{E}/\rho)\,ds \quad . \quad . \quad . \quad (11)$$

but $E = dV/dr = -(D/r^2)$ from equation (10)

Therefore $I = -\int(B/\rho r^2)ds$ . . (12)

where $ds = \sin\theta \, d\theta \, d\phi$ and by integrating eqn. (12)

$B = (\rho I/2\pi)$ . . . . . (13)

Let us consider a very large, semi-infinite solid mass with uniform resistivity ρ. Four electrodes are inserted into this material at position A, B, C and D, as shown in Fig. 3.1.

If I is the current which is passing through a point electrode placed on a flat, semi-infinite earth of resistivity ρ, the electric potential V at any point P at a distance r from the electrode is given by the equation

$$V = \frac{I\rho}{2\pi r} \quad . \quad . \quad . \quad . \quad . \quad . \quad (14)$$

In these measurements, there are always two current electrodes. One is positive through which the current enters into the ground and the other is negative through which it returns. The potential at electrode C resulting from the flow of current is calculated as

$$V_C = \frac{I\rho}{2\pi}\left(\frac{1}{r_1} - \frac{1}{r_2}\right) \quad . \quad . \quad . \quad (15)$$

Similarly, the potential at electrode D is calculated as

$$V_D = \frac{I\rho}{2\pi}\left(\frac{1}{r_3} - \frac{1}{r_4}\right) \quad . \quad . \quad . \quad (16)$$

The potential difference V (measured by the

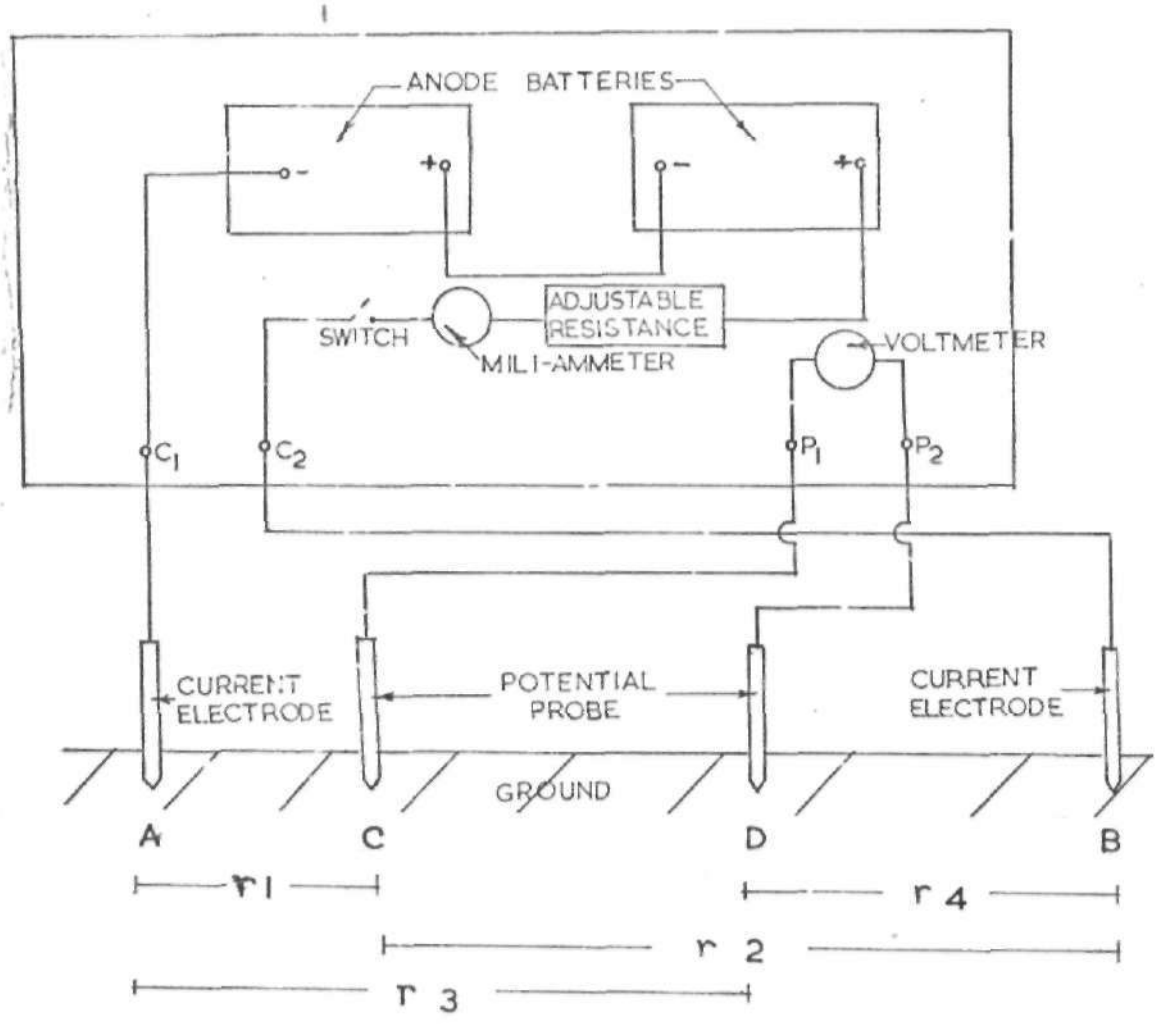


FIG. 3.1

SCHEME OF SIMPLE FIELD APPARATUS FOR RESISTIVITY MEASUREMENTS

[AFTER PARASNIS 1973]

voltmeter between C and D) is then equal to

$$V = V_C - V_D$$

$$= \frac{I\rho}{2\pi}\left(\frac{1}{r_1} - \frac{1}{r_2} - \frac{1}{r_3} + \frac{1}{r_4}\right)$$

or $V = (I\rho)/(2\pi K)$. . . . . (17)

Therefore $\rho = 2\pi VK/I$ . . . . . (18)

where $K = 1/\left(\frac{1}{r_1} - \frac{1}{r_2} - \frac{1}{r_3} + \frac{1}{r_4}\right)$

K is called geometric constant and depends upon the position of the electrodes.

For the vertical electrical sounding the Schlumberger arrangement given in Fig. 3.2 has been used. Here the configuration is symmetrically colinear. The apparent resistivity is calculated from the equation:

$$\rho_a = \frac{\pi L^2 R}{a} \quad . \quad . \quad . \quad . \quad . \quad . \quad (19)$$

where ρ_a = Schlumberger apparent resistivity;

L = half current electrode spacing;

a = potential electrode spacing; and

R = observed resistance.

For the Wenner profiling, the arrangement is given in Fig. 3.3. It uses four electrodes equally spaced along a straight line. The apparent resistivity is calculated from the equation:

$$\rho_a = 2\pi aR \quad . \quad . \quad . \quad . \quad . \quad . \quad (20)$$

where a = constant electrode separation; and

R = measured resistance.

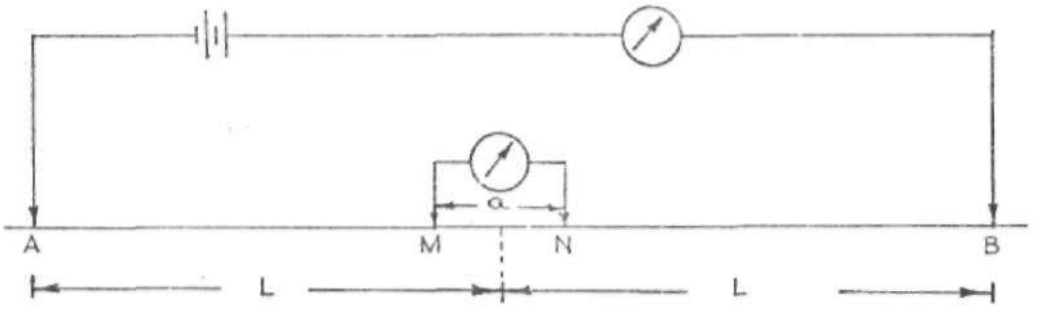


FIG. 3·2
SCHLUMBERGER ARRANGEMENT
FOR VERTICAL SOUNDING.

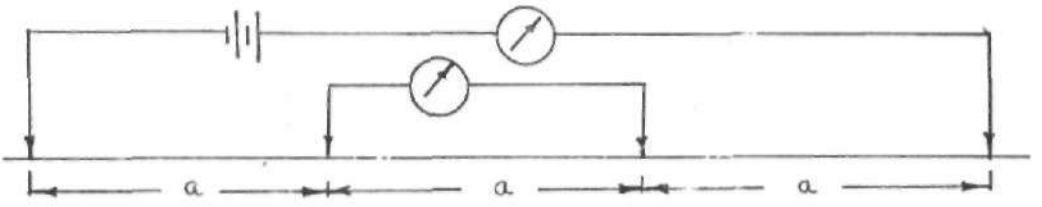


FIG. 3·3
WENNER ARRANGEMENT FOR PROFILING.

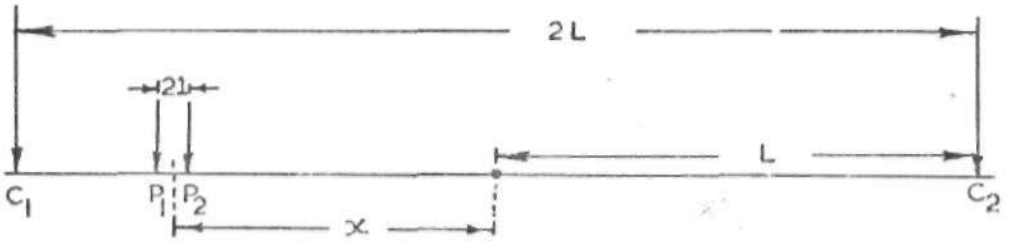


FIG. 3·4
SCHLUMBERGER ARRANGEMENT FOR PROFILING.

For Schlumberger profiling, the arrangement is given in Fig. 3.4. Here the two potential electrodes are moved between the two widely spaced current electrodes. The apparent resistivity is calculated from the equation;

$$\rho_a = \frac{\pi R(L^2 - x^2)^2}{2l(L^2 + x^2)} \quad . \quad . \quad . \quad . \quad (21)$$

where R = measured resistance;

l = half the potential spread;

L = half the total current spread; and

x = distance from the mid-point of the potential spread to the mid-point of the current spread.

There are four common approaches for interpreting VES. These are complete curve matching, partial curve matching, use of maximum and minimum points, and equivalent curve matching.

i) Complete curve matching involves the matching of the field curve with a set of computed master curves e.g. Rijkwaterstaat (1975). These master curves are prepared with dimensionless co-ordinates on logarthmic paper. The field results are plotted on a transparency and slided on the master curves until they coincide, keeping the respective co-ordinate axes parallel. The co-ordinates of the point of intersection on the field curve axes of the theoretical curve axis 1-1 are read off. These values corresponds to ρ_1, the true resistivity of top layer and h_1, thickness of top layer. The resistivity ratios given on the

master curve yield the values for the resistivity of the other layers and the parameter on each curve yields the ratio of the second layer to that of the first. Thus the resistivities and thicknesses may be obtained of the other layers.

ii) Partial curve matching involves matching small segments of field sounding curve with theoretical curves for the single overburden, usually starting with the shorter spacings and working towards the longer spacing. As each portion of the curve is interpreted, the layers in this portion are lumped to form a fictitious layer of resistivity ρ_f and thickness h_f. This lumped layer is used as a surface layer and the next portion of the field curve is interpreted in a similar way. Auxillary curves are drawn by assuming a number of values for h_2 and obtaining the corresponding set of ρ_f and h_f and these are matched to the field profile to get the best fit and hence the best values of h_f, and ρ_f and eventually ρ_3.

iii) By using maximum and minimum point with either H or K type curve, an interpretation can be made by noting the electrode spacing, L, for which the maximum or minimum apparent resistivity ρ_a is measured. Two curves are plotted. One of ρ_a/ρ_1 against ρ_2/ρ_1 for various ratios of h_2/h_1 and the second of L/h_1 against h_2/h for various ratios of ρ_2/ρ_1. As the value of ρ_a/ρ_1 and L/h_1 are known from the field curve, a horizontal line is drawn

across these two curves corresponding to these values. A set of possible value of ρ_2/ρ_1 and h_2/h_1 are then got from the two curves. These are plotted and their point of intersection corresponds to the value of h_2 and ρ_2.

iv) For equivalent curve matching, different sets of layering parameters provide the same sounding curve and these sets of conditions are said to be equivalent. Graphs may be constructed to show the ranges in layering parameters which are equivalent. Koefoed (1969) has developed a method based upon the properties of the raised kernel function, to determine equivalent cases.

The methods used were the complete curve matching and equivalent curve matching.

The basic equipments required to carry out a resistivity survey are:

i) a voltmeter;

ii) a milli-ammeter;

iii) measuring tapes;

iv) metallic electrodes;

v) a source of power supply; and

vi) properly insulated long wires.

A simple arrangement of these instruments for a resistivity survey (Parasnis, 1973) is shown in Fig. 3.1. However, the milli-ammeter, voltmeter and power supply

can be assembled together as one unit and made into a very sensitive and sophisticated instrument, which is easier and faster to handle in surveying.

The power supply can be either D.C. or low frequency A.C. The D.C. instruments are less frequently used because electrochemical and e.m.f. are produced between the metal electrodes and the ground, which introduce errors in the measurements. Besides this, the results are also affected by natural earth currents and these have to be taken care of. Griffiths and King (1965) have found that the earth currents tend to be unidirectional and can be eliminated if A.C. are used. What is essentially required is that the A.C. should have a low frequency. At higher frequencies, ground inductance and capacitance and more complex effects such as induced polarization become more pronounced and are not desirable.

In this work the Terrameter SAS-300, shown in Fig. 3.5, was used. It is a fully self-contained unit, which is very light in weight, portable and easy to handle and which operates on rechargeable batteries. The consecutive readings for $\Delta V/I$ are calculated by the instrument and digitally displayed in KΩ, Ω or mΩ, thus making it possible to extract the signal from natural and man-made noise. It measures signal voltages created by the transmitter signal current, while

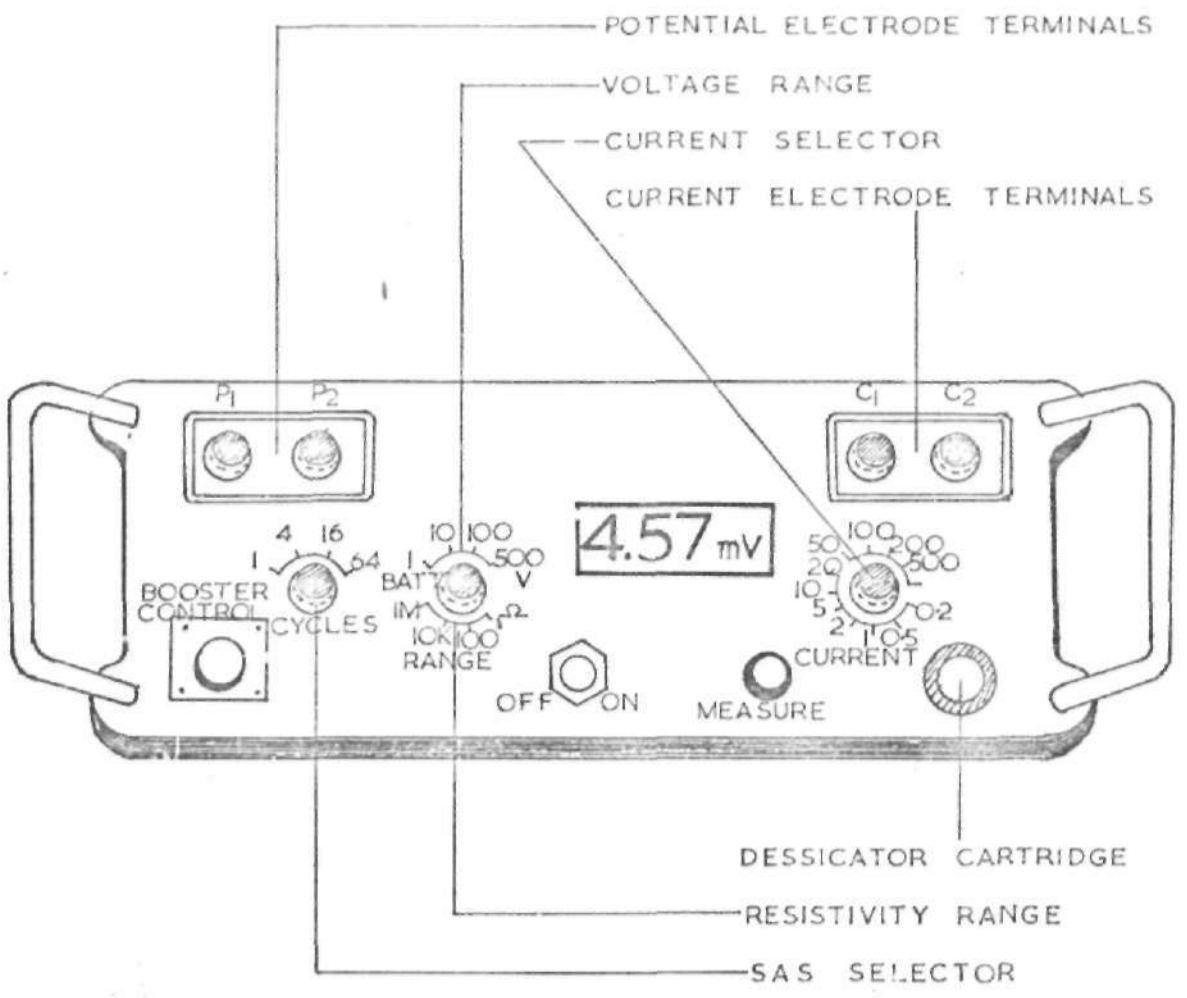


FIG. 3·5

TOP VIEW OF TERRAMETER SAS-300.

[ATLAS COPCO ABEM 1981]

rejecting both the D.C. voltages i.e., the self-potential and the noise.

Basically the instrument has three sub-units:

i) a micro processor for monitoring control and computation;

ii) an electrically isolated transmitter for the supply of defined regulated signal currents having a selectable current of 0.2, 0.5, 1.0, 2.0, 5.0, 10.0 and 20.0 mA; and

iii) a receiver for discrimination and measurement of voltages correlated with the transmitted signal current.

The electrodes were hammered 0.1 - 0.2 m deep into the ground. Since the ground was very dry, salt water was poured around the electrodes. The electrodes were re-hammered so as to improve contact with the soil. The electrodes were connected with wires through copper clamps soldered to one end of each of the electrode, while the other end of the wires were fixed to the appropriate terminal of the terrameter. The instrument was switched on to ascertain that the battery was well charged. For resistivity survey, the range switch was set at 1 Ω position, cycle switch in 4-position and current selector in 20 mA position. The power was switched on and measure button was pressed to take four readings which are displayed digitally. Warnings and information comprising

beeper signals and simple display codes given in the manual, (Atlas Copco), tells when to change parameters or to check circuits.

3.2 Self-Potential (S.P.):

The S.P. technique involves the measurement of the natural potential differences which usually exist between ary two points in the ground. These natural potential differences are set up as a result of electrochemical or mechanical activity between minerals and the solution with which they are in contact, in most cases it is underground water. When different portions of an ore body are in contact with solutions of different composition, chemical reactions take place. These result in different solution pressures along the respective areas of contact, giving rise to a potential difference which causes current flow in the ground (Dobrin, 1976). The potential difference range from a few millivolts to a few tens of millivolts.

They are classified into two categories, namely background and mineralization potentials. The background potential can be either positive or negative and range from a fraction of a millivolt to a few millivolts. It is created by fluid streaming, bioelectric activity in vegetation, varying electrolytic concentrations in groundwater and other geochemical actions (Telford, 1976).

The mineralization potential have maximum values of the order of a few hundred to several hundred millivolts and are almost exclusively negative. Their origin is still not fully understood, even though many theories have been suggested. The most reasonable and complete theory is that proposed by Sato and Mooney in 1960. They protulated that S.P. cannot be due to the oxidation of an ore body as such but to the difference in the oxidation capacity of the waters near the upper and the lower surface of an ore body. It may also be due to exchange of ionic and electronic charges which take place with the ore body serving to transport electrons from the lower surface to the upper until electrochemical equilibrium is reached.

Besides the background effects, there may be large local disturbances due to buried iron pipes, electrical earthings, chemical fertilizers, mine slags, topography, groundwater drainage etc., for which allowance must be made in the interpretation of S.P. anomalies (Parasnis, 1973).

The procedure used in the S.P. regional survey was the fixed base station method. This required keeping one electrode fixed at a base station while the other electrode, together with the cable reel and the terrameter was moved to different points.

The cable was laid and the electric potential of each point with respect to the base was read. The advantages of this layout are that the potential is measured continually with respect to a fixed point and small zero errors between the electrodes do not accumulate. Also the chances of discovering a weak S.P. anomaly which varies slowly with distance are greater.

When the cable length gets exhausted, a new base station is chosen, such that there is an overlapping of the last one or two stations and the new potentials are measured. If Δ_1, Δ_2, ----- are the potentials with respect to the first base and Δ_1', Δ_2', ----- those with respect to the new base, the mean of $\Delta_1 - \Delta_1'$, $\Delta_2 - \Delta_2'$, ---- gives the required differences Δ between the two bases which is added to all the measurements of the new base, after taking their polarity into consideration.

The apparatus required for S.P. are cables, electrodes and a voltmeter. The voltmeter should have a high impedance so that negligible current is drawn from the ground. The cables should be light in weight and well insulated. They are required for making connections between electrodes and the voltmeter. Instead of metallic electrodes which cause polarization, non-polarizeable electrodes are used. These are essentially made of a porous pot with a copper rod attached to the cover of the pot which is immersed in a

saturated solution of copper sulphate (with some crystals of $CuSo_4$ still lying at the bottom of the pot), see Fig. 3.6. The porous pot allows the solution to seep slowly into the ground.

The terrameter SAS-300 is used to measure the S.P. values or the natural D.C. potential. The input ranges are 1 V, 10 V, 100 V, 500 V with a precision of ± 0.00001 V (4 range) and a noise rejection > 95 dB at 50-60 Hz and 85 dB at 16-20 Hz (Atlas Copco ABEM, 1981).

3.3 Very Low Frequency (V.L.F.):

Powerful radio transmitters set up in different parts of the world radiate unmodulated carrier waves which have frequencies of 10-25 KHz. In geophysics these are very high frequencies but in radio technology this range is considered very low because usually their carrier frequencies are ten times this value. The V.L.F. technique makes use of signals from powerful military transmitters stationed in different parts of the world. The radiated waves from these transmitters contain both electric and magnetic components. These travel in three different modes and are known as skywaves, spacewaves and groundwaves. At long distances what is received are magnetic groundwaves and the skywaves which are guided by the ionsphere and earth's surface.

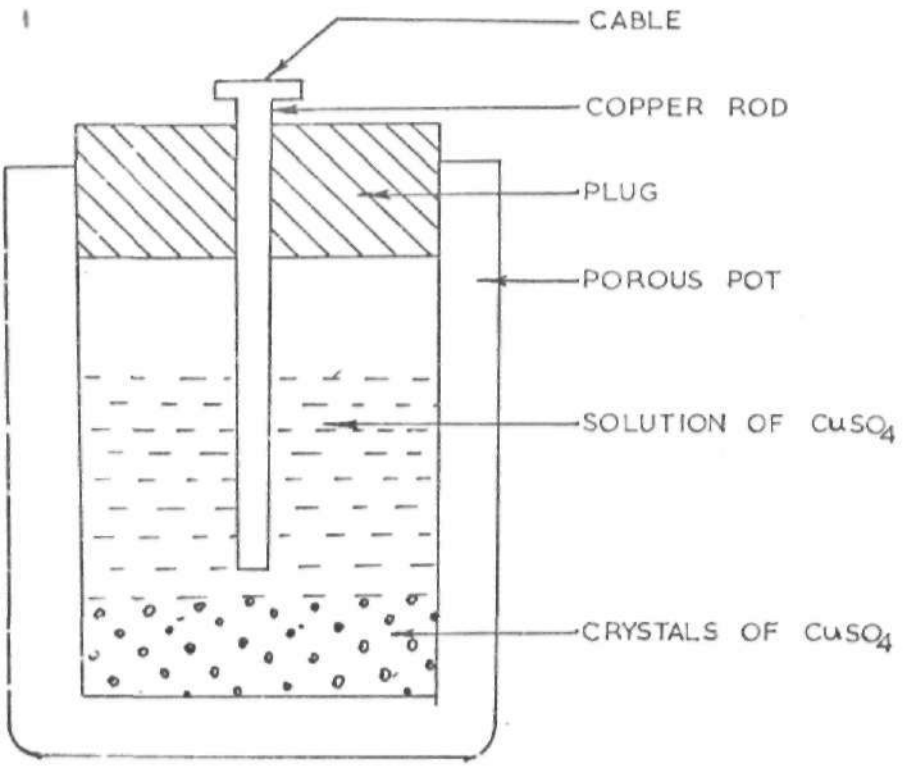


FIG. 3·6
NON–POLARIZING ELECTRODE

The antenna of V.L.F. transmitters is a long vertical wire through which an A.C. flows. It produces a magnetizing force in the space around it, the lines of which are concentric horizontal loops with centres at the antenna. As the primary magnetic fields encounter conductive bodies in the ground, secondary fields are set up. If the conductor has the strike parallel to the bearing of the V.L.F. station, it is cut by a maximum magnetic flux and an induced electric current flows. This produces a secondary magnetic field. However, if the strike is prependicular to the station, it will not be cut by the magnetic field. Consequently it will have no induced current and no secondary field will be produced. The secondary field tends to oppose the primary V.L.F. flux cutting the conductor. The total magnetic field which is horizontal far away from the conductor, is tilted out of the horizontal plane in its vicinity on both sides of the conductor, the presence of which is then detected by a receiver instrument.

V.L.F. anomalies tend to be clusttered and data has to be digitized and filtered. Fraser (1969) developed a technique of reducing the noise level and filtering and differentiating tilt angle profiles. These can be applied for rapid geological correlation and interpretation. According to him, for four consecutive data points M_1, M_2, M_3, M_4 for the in-phase component values, the plotted function is equal to $(M_3 + M_4) - (M_1 + M_2)$. This is

plotted mid-way between M_2 and M_3. The process is repeated on each profile until the data is exhausted. The cross overs and inflections are transformed into peaks (Fraser, 1969).

The EM-16,' V.L.F.-EM unit used (Figs. 3.7 and 3.8) is a sensitive receiver covering the frequency band of the V.L.F. transmitting stations (15-25 KHz). It is a compact case containing batteries and transmitter selector unit. The receiver has two receiving coils built into the instrument, one having normally vertical axis, while the other horizontal axis. The signal from the coil on the vertical axis is minimized by tilting the instrument. The tilt angle is calibrated in percentage. The remaining signal in this coil is then balanced out by a measured percentage of a signal from the other coil, after shifting by 90°. The V.L.F.-EM is nulled by audio tone. At this stage, the coil is normally parallel to the primary field. The two components measured are referred to as 'In-phase and Quad-phase'. The senstivity of the in-phase is $\pm$ 150 percent while that of the quad-phase is $\pm$ 40 percent. The different V.L.F. transmitters are shown in Table 3.1. The detailed procedure on the use of this instrument is given in the manual (Geonics Ltd., 1979).

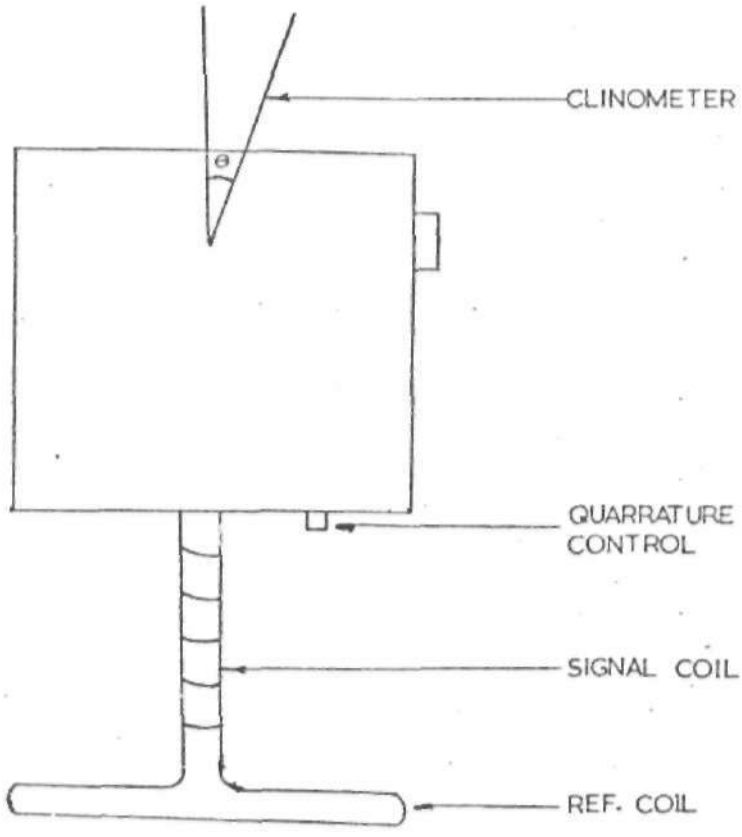


FIG. 3·7
BLOCK DIAGRAM OF VLF - EM

(NOT TO SCALE)

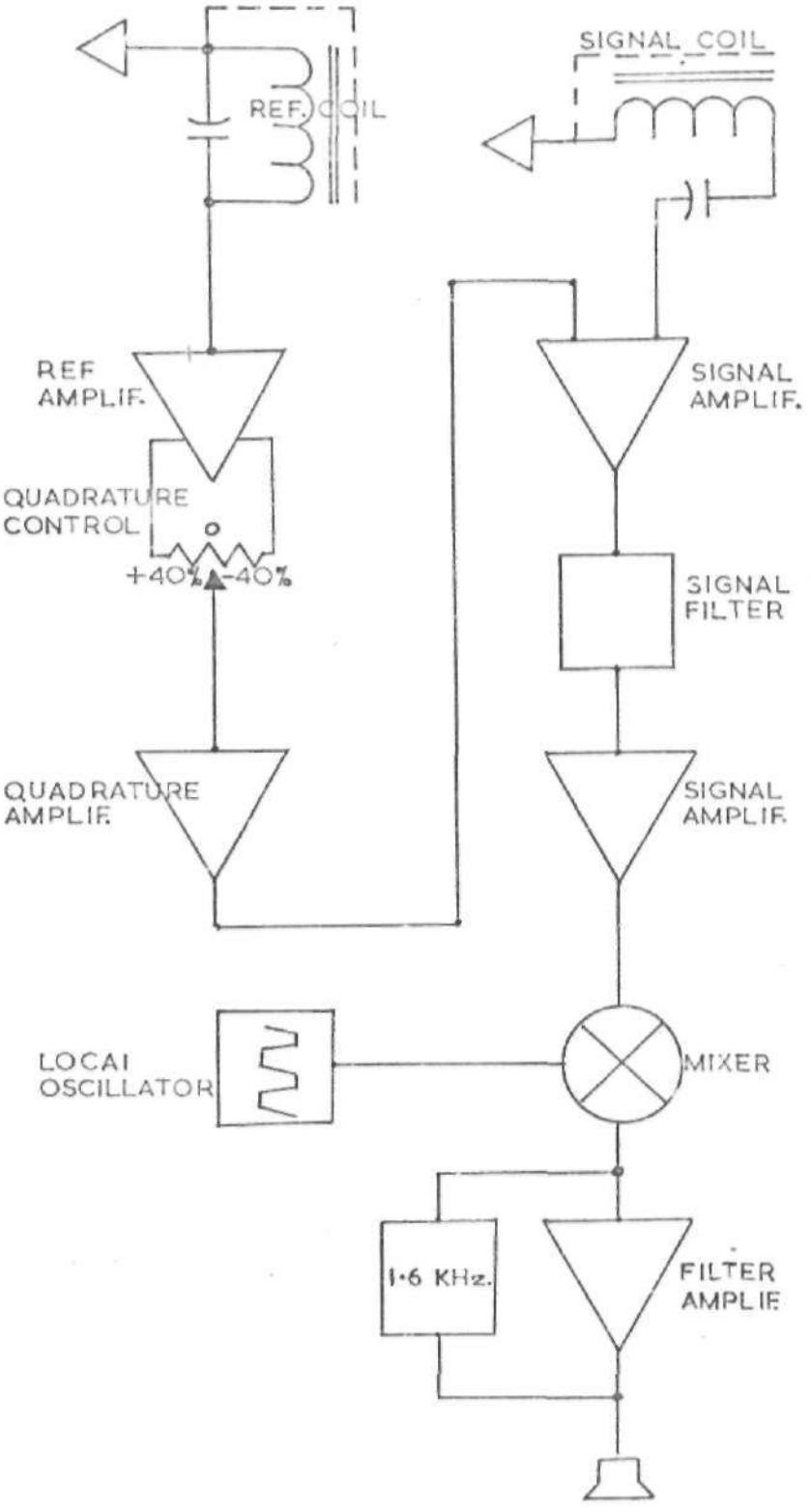


FIG. 3·8

BLOCK DIAGRAM OF EM16 VLF–EM

[GEONICS LTD.]

TABLE 3.1

Different Transmitting Stations

(After George, 1982)

Station	Location	Frequency in Khz.	Azimuth	Schedule
NAA	Cutler, main U.S.A.	17.8	113°	Off 1400 to 1800 GMT each Friday
GBR	Rugby, England	16.0	228°	-
FUo	Bordeuaux, France	15.1	53°	-
UMS	Moscow, USSR	17.1	-	-

Chapter 4

SOILS AND THEIR MECHANICAL ANALYSIS

4.1 Definition:

The soil in terms of geology can be defined as the weathered organic material on the surface, or topsoil. In engineering sense, it is considered to be any loose sedimentary deposit, such as gravel, sand, clay or a mixture of these materials.

4.2 Soil Classification:

There are several soil classification systems but the most widely accepted is the 'Unified System', proposed by Arthur Casagrande in 1952. It places soils into three divisions:

i) coarse grained;

ii) fine grained; and

iii) highly organic soils.

The coarse grained soils are those which have 50 percent or less material passing the No. 200 B.S. sieve and fine grained soils are those having more than 50 percent passing the No. 200 B.S. sieve. The highly organic soils can be identified by visual examination. This system recognises fifteen soil groups and uses names and letter symbols to distinguish between these groups. Each group is designated by two capital letters. Details about

this system are shown vide Table 4.1.

4.3 Soil Sampling Procedure:

Soil samples were taken at every 100 m along the two profiles, Wasai-Minjibir and dry stream section and at every 250 m along the third profile, the Minjibir-Bagurawa section due to transport difficulties. Both disturbed as well as undisturbed samples were collected, the former for mechanical analysis and the latter for dry density and porosity. The top 0.1 m of soil was scraped prior to sampling to remove grass roots and loose surface material. The disturbed samples were dug with a cutlass, put in a plastic bag and labelled. These represented a depth of 0.1 to 0.3 m. The undisturbed samples were taken with a core cutter, whose inner diameter is 0.0375 m and length 0.048 m, with constant volume ($\pi r^2 L$) of $5.3 \times 10^{-5} m^3$. The cutter was forced into the ground using a drop hammer, taking care that the sample was not compressed. The mould was dug out from the ground, both ends were made flush with a spatula so that the volume of core sample taken is equal to the volume of the cutter. The sample was taken out from the mould in a clean double plastic bag, labelled and sealed. The core sample represented a depth of 0.1 to 0.15 m. The samples were tested in the laboratory of the Ministry of Works and Transport, Kano State.

TABLE 4.1

Unified Soil Classification

(After Arthur Casagrande, 1952)

Major Divisions			Group Symbols	Typical Names
Coarse-grained Soils	Gravels	Clean Gravels	GW	Well-graded gravels, gravel-sand mixtures, little or no fines.
			GP	Poorly-graded gravels, gravel-sand mixtures, little or no fines.
		Gravel with Fines	GM	Silty gravels, gravel-sand-silt mixtures.
			GC	Clayey gravels, gravel-sand-clay mixtures.
	Sands	Clean Sands	SW	Well-graded sands, gravelly sands, little or no fines.
			SP	Poorly-graded sands, gravelly sands, little or no fines.
		Sands with Fines	SM	Silty sands, sand-silt mixtures.
			SC	Clayey sands, sand-clay mixtures.
Fine-grained Soils	Silt and Clays	Liquid limit less than fifty.	ML	Inorganic silts and very fine sands, rock flour, silty or clayey fine sands or clayey silts with slight plasticity.
			CL	Inorganic clays of low to medium plasticity, gravelly clays, sandy clays, silty clays, lean clays.
			OL	Organic silts and organic silty clays of low plasticity.
	Silt and Clays	Liquid limit greater than fifty.	MH	Inorganic silts, micaceous or diatomaceous fine sandy or silty soils, elastic silts.
			CH	Inorganic clays of high plasticity, fat clays.
			OH	Organic clays of medium to high plasticity, organic silts.
Highly Organic Soils.			Pt	Peat and other highly organic soils.

4.4 Laboratory Tests:

For mechanical analysis, 0.2 kg of the dry soil was weighed and put in a container to which sufficient quantity of water was added. The soil was rubbed with a rubber corked stirrer and the muddy water passed through No. 200 B.S. sieve. The process of rubbing, watering and washing was continued till the water passing out of the sieve was clear. The residue retained on the sieve was dried and its weight recorded. It was further sieved through a set of seven sieves, sizes 9.5 mm, 4.8 mm, No. 7, 14, 25, 72 and 200. The weight retained on each sieve was determined, and the percentage of the total sample passing through each of the sieves was calculated. This percentage was ploted on the sand and gravel fractions of a semilogarithmic chart as shown in Fig. 4.1. The various soil constituents as per B.S. 1377 are shown in Table 4.2.

The silt and clay fractions were determined from the fine analysis of the soil samples. The theory of fine analysis is based on Stokes law of settlement i.e. small spheres in a liquid settle at different rates according to the size of the sphere. The rate of sedimentation is determined from the rate of decrease in density of the upper part of the liquid as the largest particles settle out. A suspension of the particles is prepared and the density is measured at given intervals of time using a hydrometer. The percentage of silt and

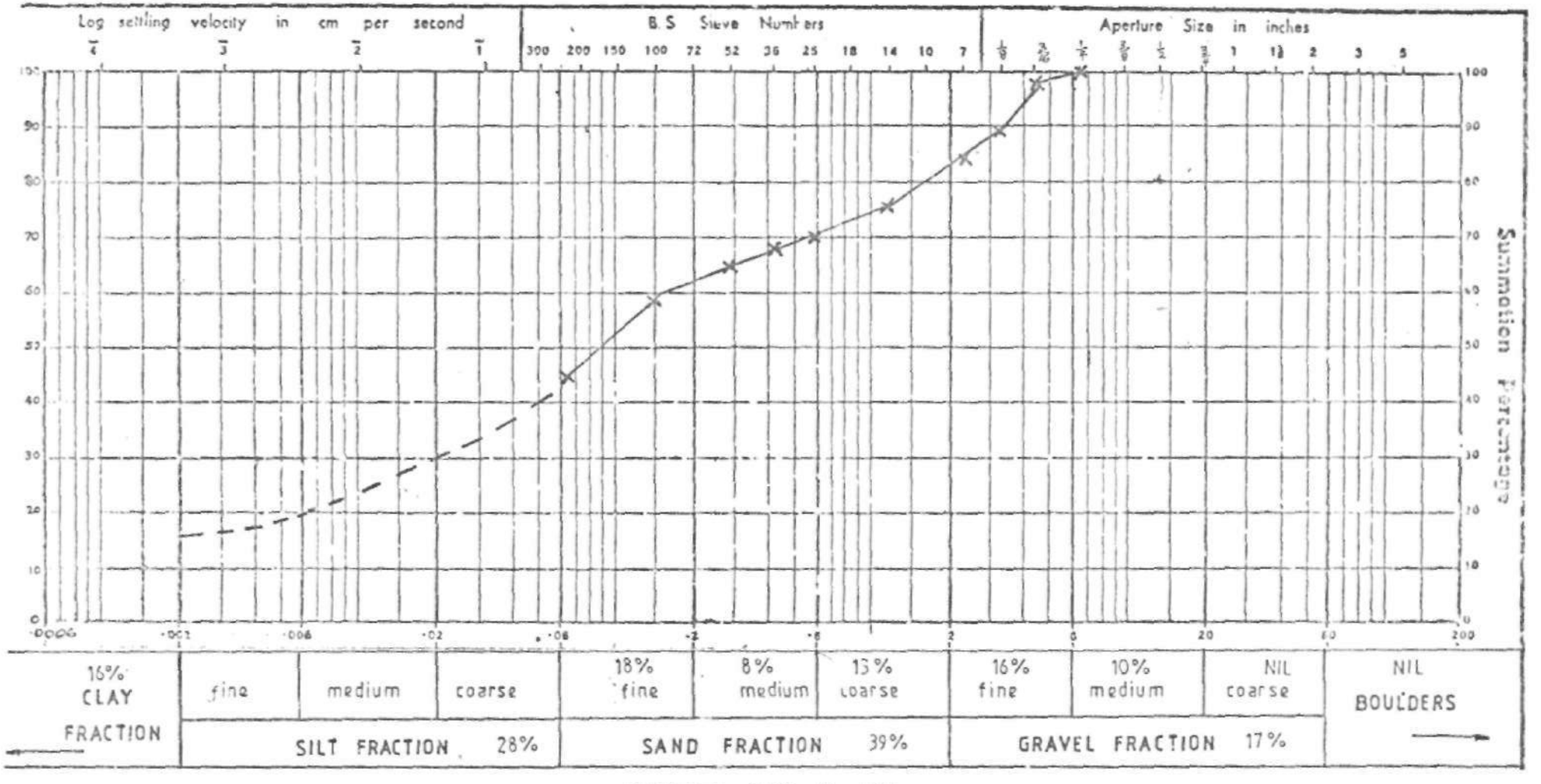


FIG. 4·1

PARTICLE SIZE DISTRIBUTION OF BAGURAWA KAOLIN

TABLE 4.2

Range of Particle Size of the Various Soil Constituents.

Type	Range of Particle Size in mm.
Cobbles	200 - 60
Coarse Gravel	60 - 20
Medium Gravel	20 - 6
Fine Gravel	6 - 2
Coarse Sand	2 - 0.6
Medium Sand	0.6 - 0.2
Fine Sand	0.2 - 0.06
Coarse Silt	0.06 - 0.02
Medium Silt	0.02 - 0.006
Fine Silt	0.006 - 0.002
Clay	Less than 0.002

clay fractions is then determined from the given charts.

For dry density, the entire core sample taken in a constant volume core cutter was dried, and weighed. The weight divided by volume gave the dry density. Porosity was calculated assuming its specific gravity as 2.65.

$$\text{Porosity } \phi = \frac{V - Vs}{V}$$

where Vs is given by weight of dry soil in the core cutter divided by its specific gravity.

4.5 Interpretation:

Histograms of soil constituents i.e. gravel, coarse sand, medium sand, fine sand, silt and clay fractions for the soil samples collected along these profiles were drawn, Figs. 4.2 to 4.4.

4.5.1 Minjibir-Wasai Section:

It would be seen that the fine sand is the most predominant followed by gravel fraction (Figs. 4.2e and 4.2b). Medium sand and silt are the next, (Figs. 4.2d and 4.2f), while the least is the coarse sand and clay (Figs. 4.2c and 4.2g). The presence of gravel shows that partial laterization of soils in that area is in process, though not consistent. The dry density varies between 1,470 and 2,070 kg/m^3 and the porosity between 21.9 to 44.5 percent.

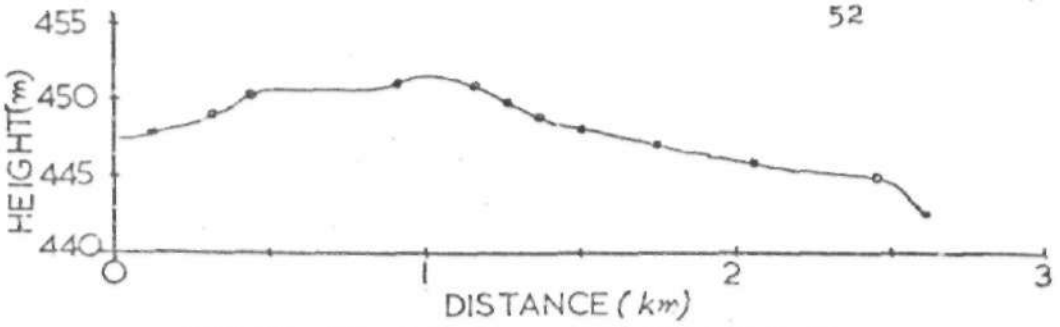


FIG. 4.2a TOPOGRAPHIC PROFILE ALONG MINJIBIR TO WASAI

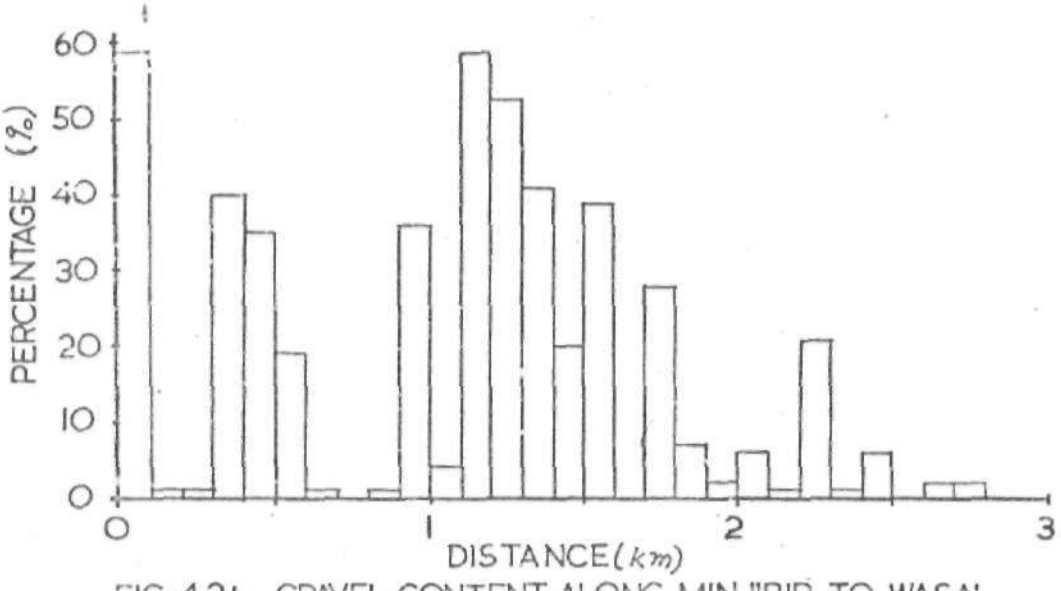


FIG. 4.2b GRAVEL CONTENT ALONG MINJIBIR TO WASAI

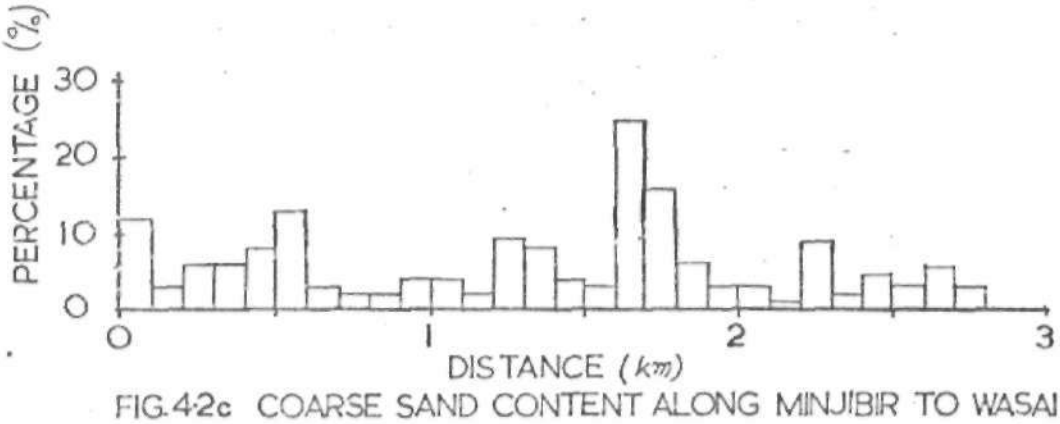


FIG. 4.2c COARSE SAND CONTENT ALONG MINJIBIR TO WASAI

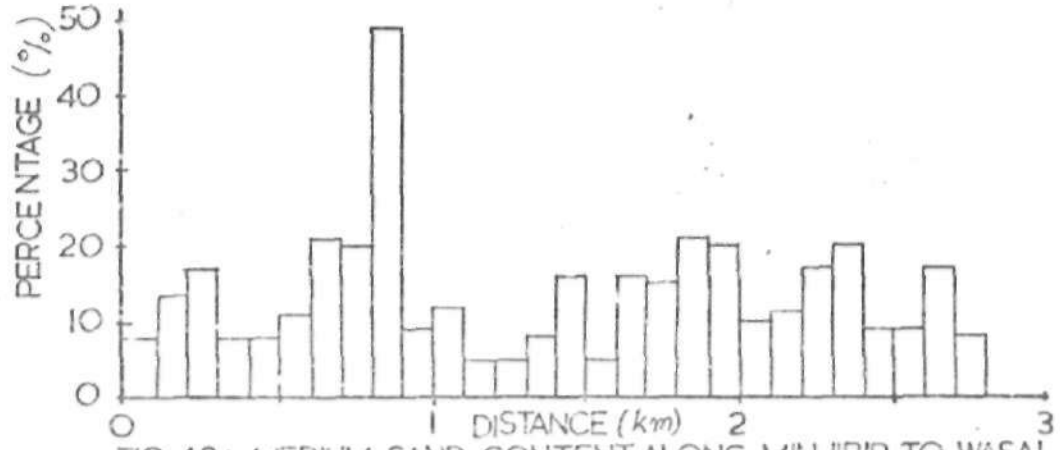


FIG. 4.2d MEDIUM SAND CONTENT ALONG MINJIBIR TO WASAI

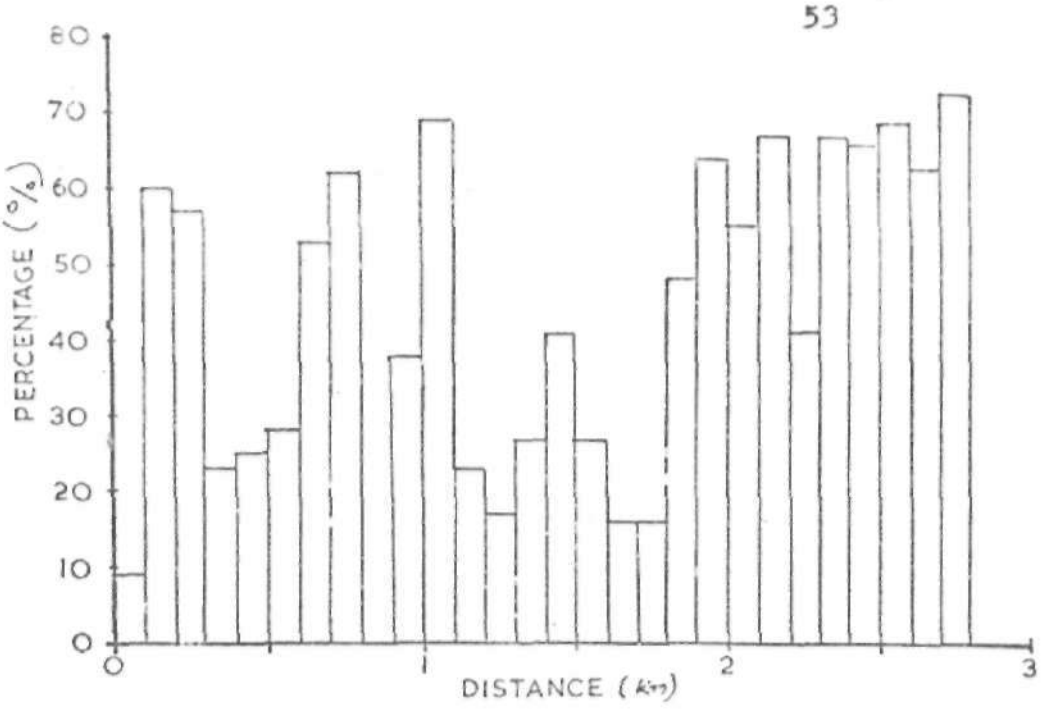


FIG.4·2e FINE SAND CONTENT ALONG MINJIBIR TO WASAI.

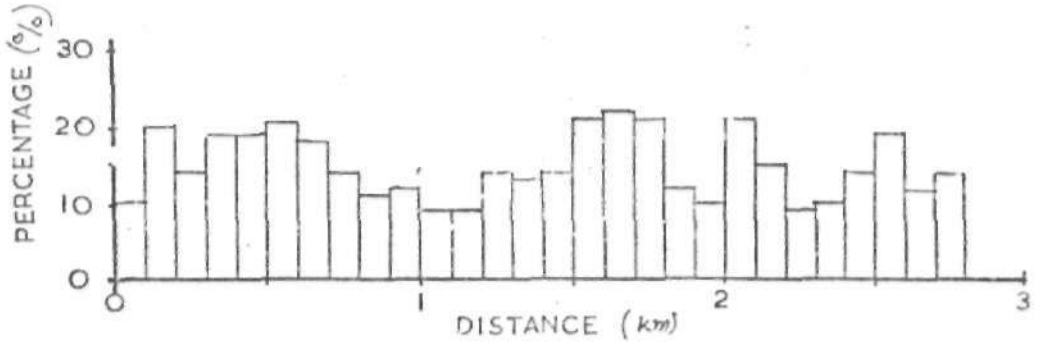


FIG.4·2f SILT CONTENT ALONG MINJIBIR TO WASAI.

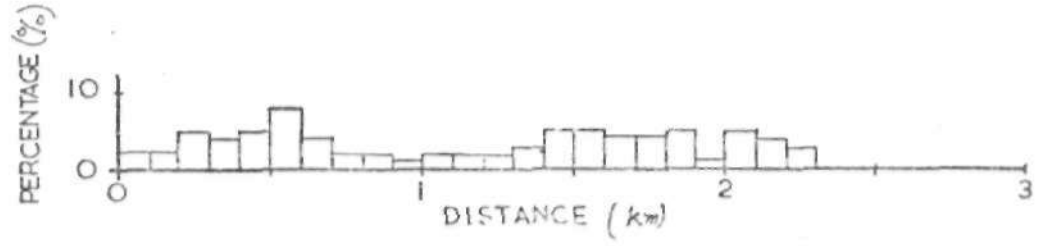


FIG.4·2g CLAY CONTENT ALONG MINJIBIR TO WASAI.

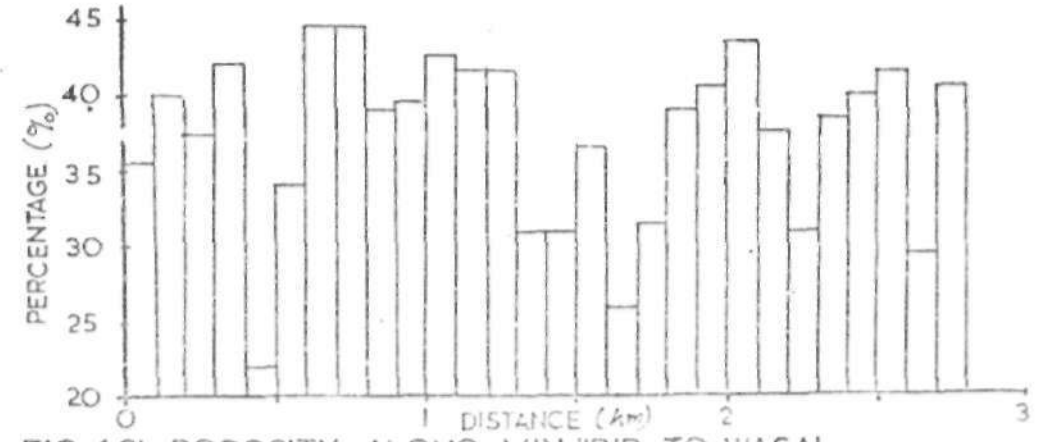


FIG.4·2h POROSITY ALONG MINJIBIR TO WASAI.

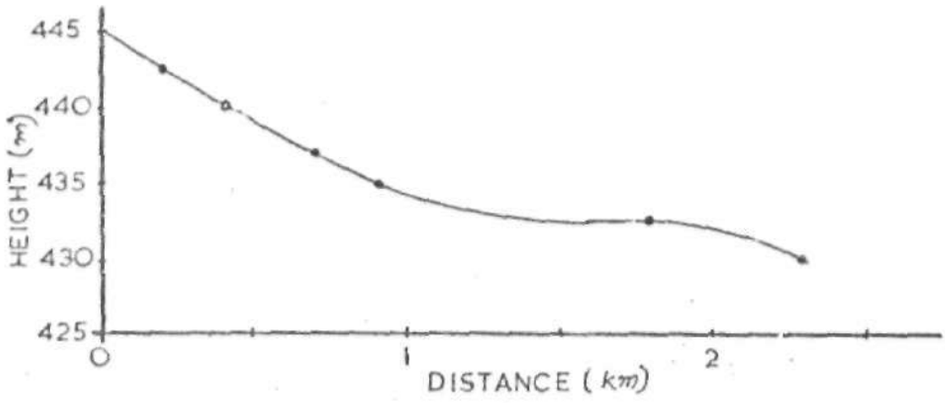


FIG. 4·3a TOPOGRAPHIC PROFILE ALONG DRY RIVER.

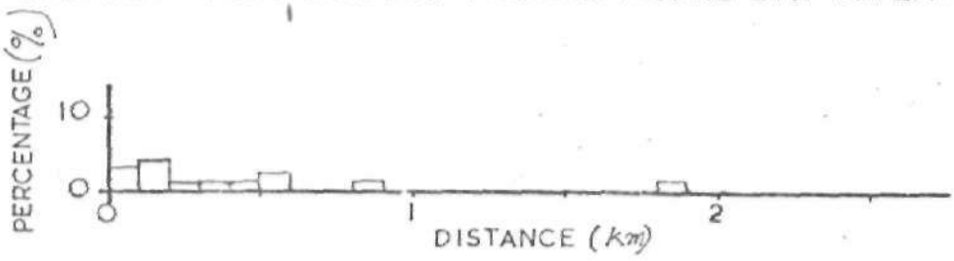


FIG. 4·3b GRAVEL CONTENT ALONG DRY RIVER.

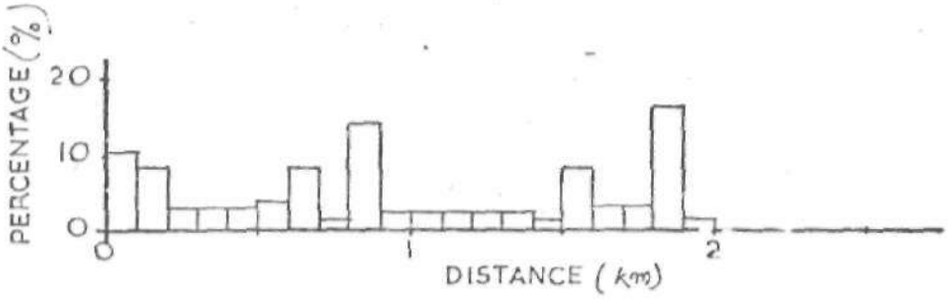


FIG. 4·3c COARSE SAND CONTENT ALONG DRY RIVER.

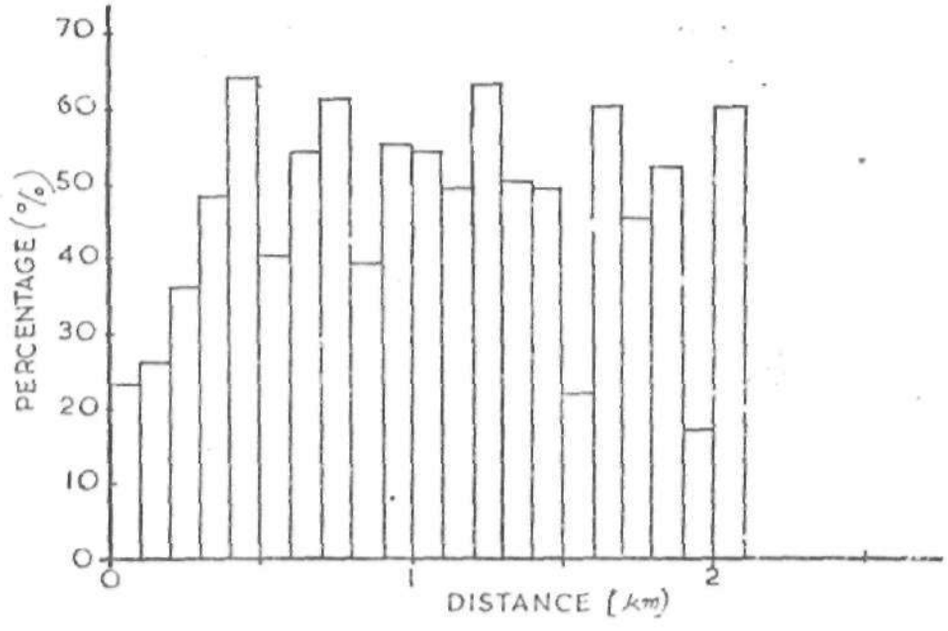


FIG. 4·3d MEDIUM SAND CONTENT ALONG DRY RIVER.

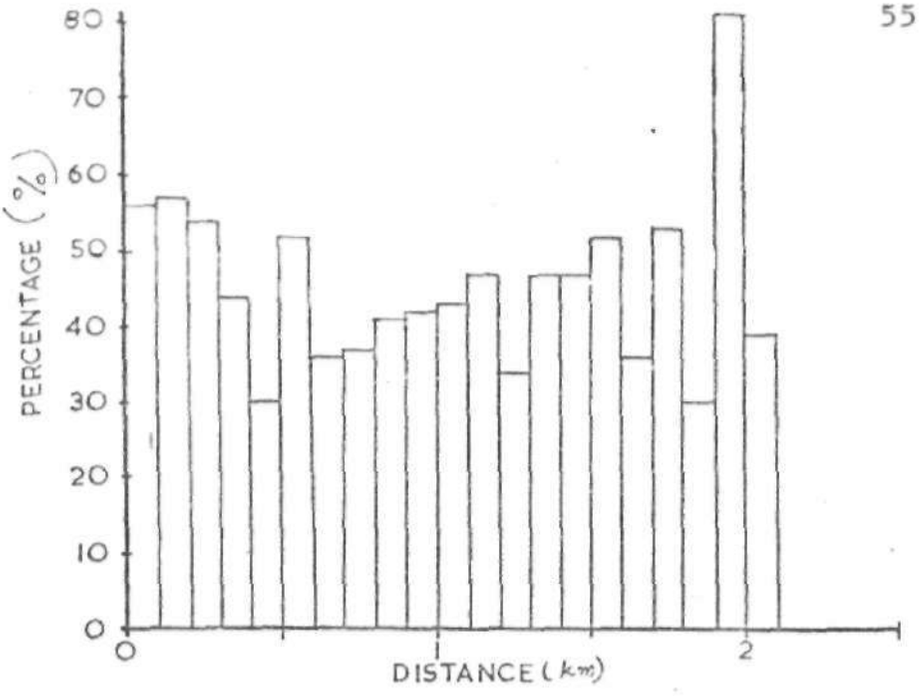


FIG. 4·3e FINE SAND CONTENT ALONG DRY RIVER.

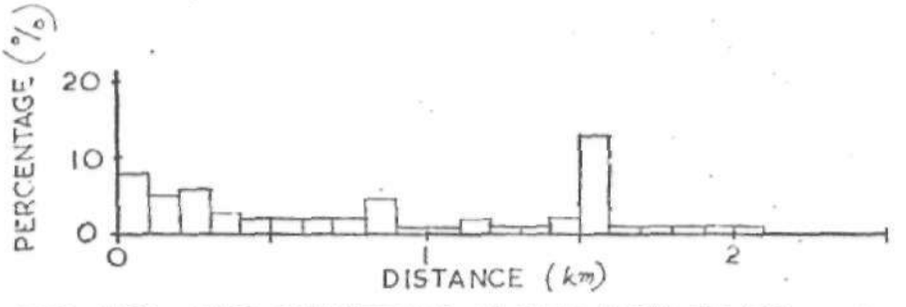


FIG. 4·3f SILT CONTENT ALONG DRY RIVER.

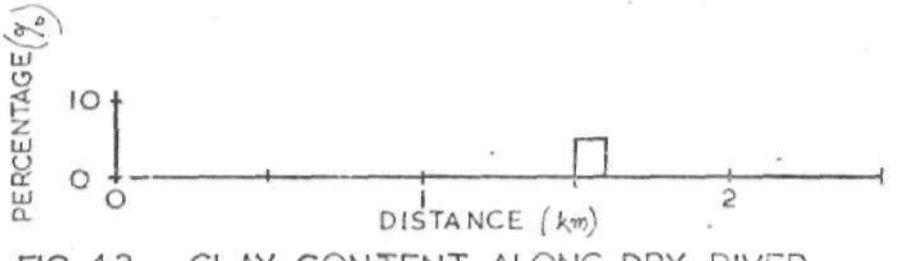


FIG. 4·3g CLAY CONTENT ALONG DRY RIVER.

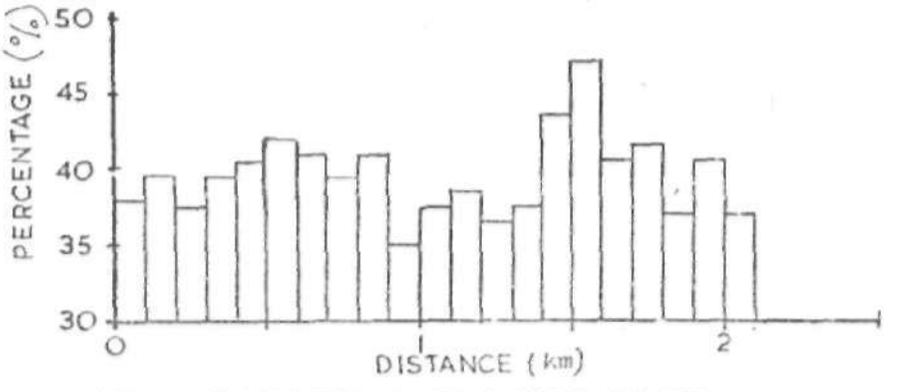


FIG. 4·3h POROSITY ALONG DRY RIVER.

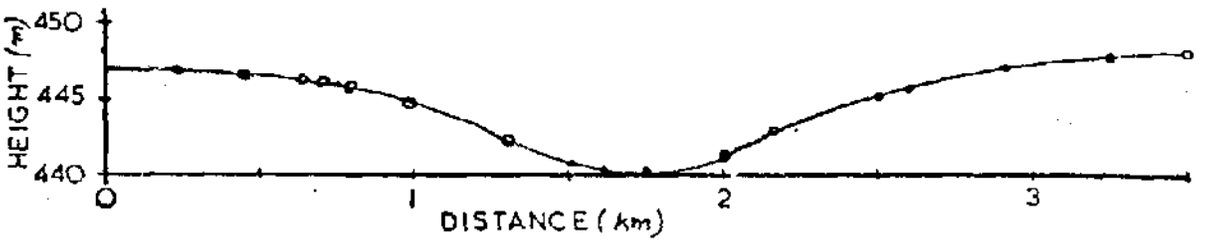


FIG. 4·4a TOPOGRAPHIC PROFILE ALONG MINJIBIR TO BAGURAWA.

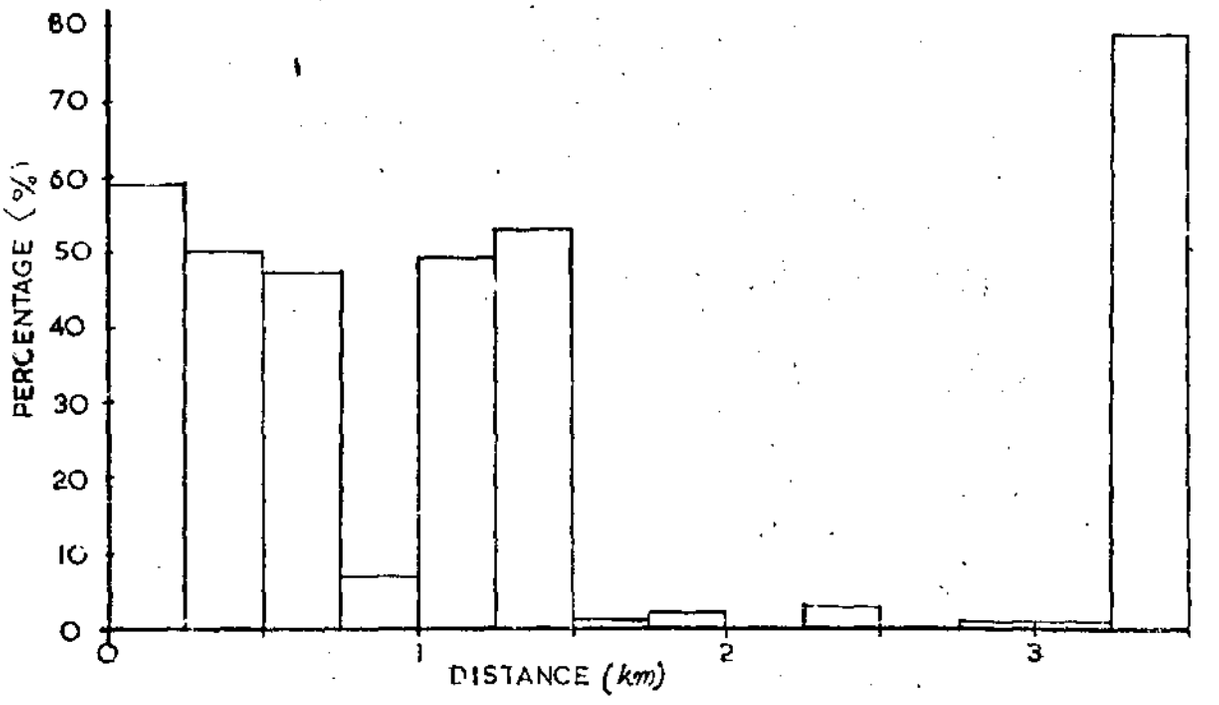


FIG. 4·4b GRAVEL CONTENT ALONG MINJIBIR TO BAGURAWA.

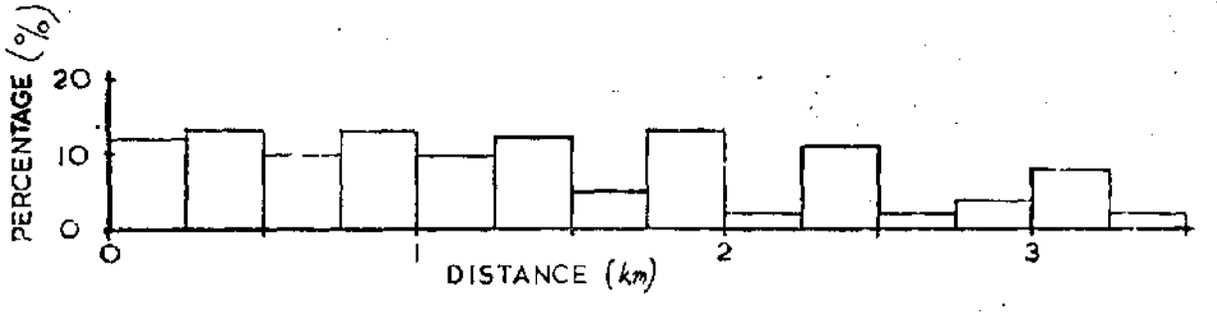


FIG. 4·4c COARSE SAND CONTENT ALONG MINJIBIR TO BAGURAWA.

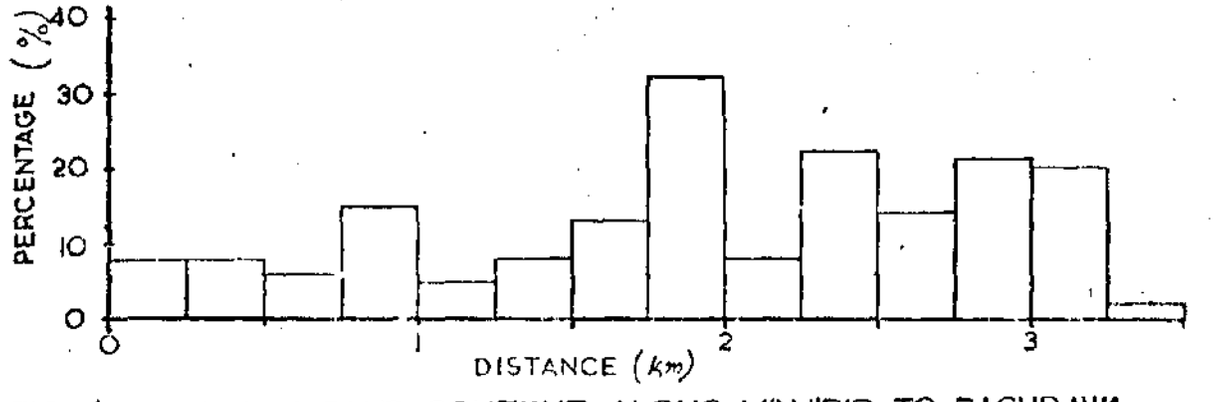


FIG. 4·4d MEDIUM SAND CONTENT ALONG MINJIBIR TO BAGURAWA.

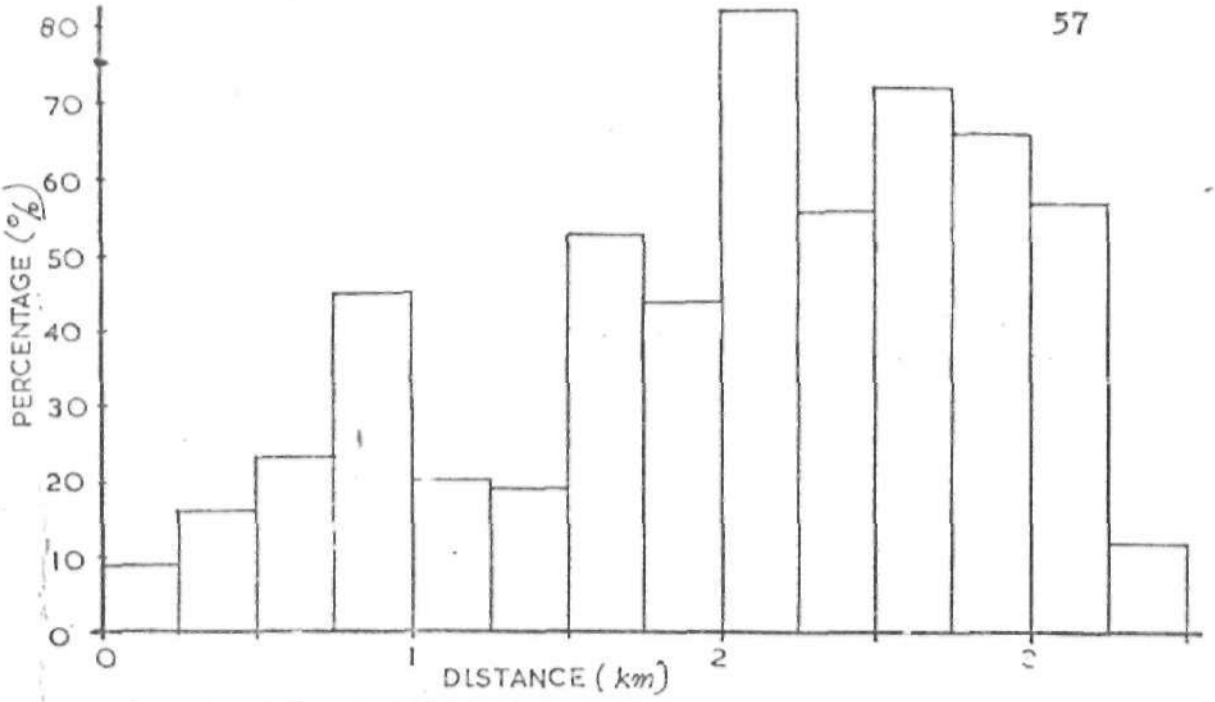


FIG. 4·4e FINE SAND CONTENT ALONG MINJIBIR TO BAGURAWA.

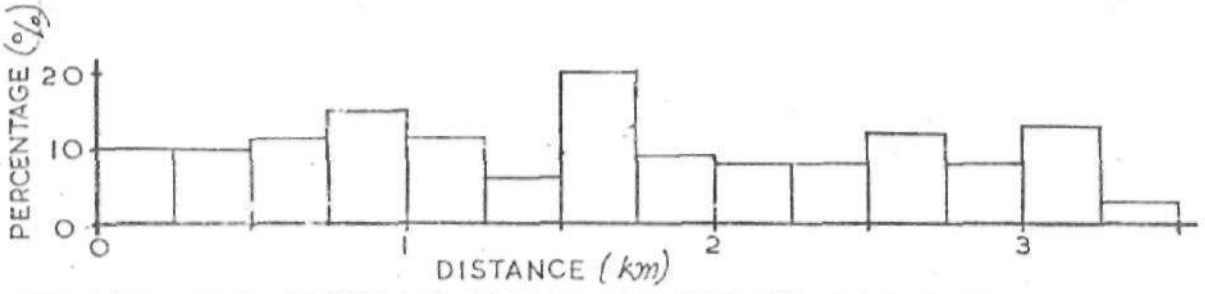


FIG. 4·4f SILT CONTENT ALONG MINJIBIR TO BAGURAWA.

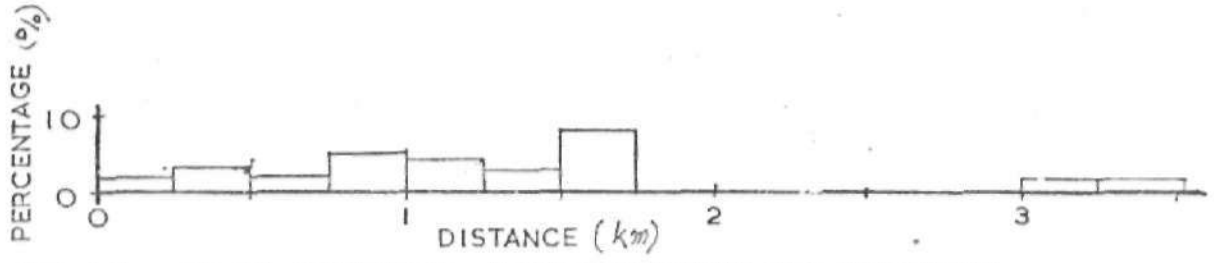


FIG. 4·4g CLAY CONTENT ALONG MINJIBIR TO BAGURAWA.

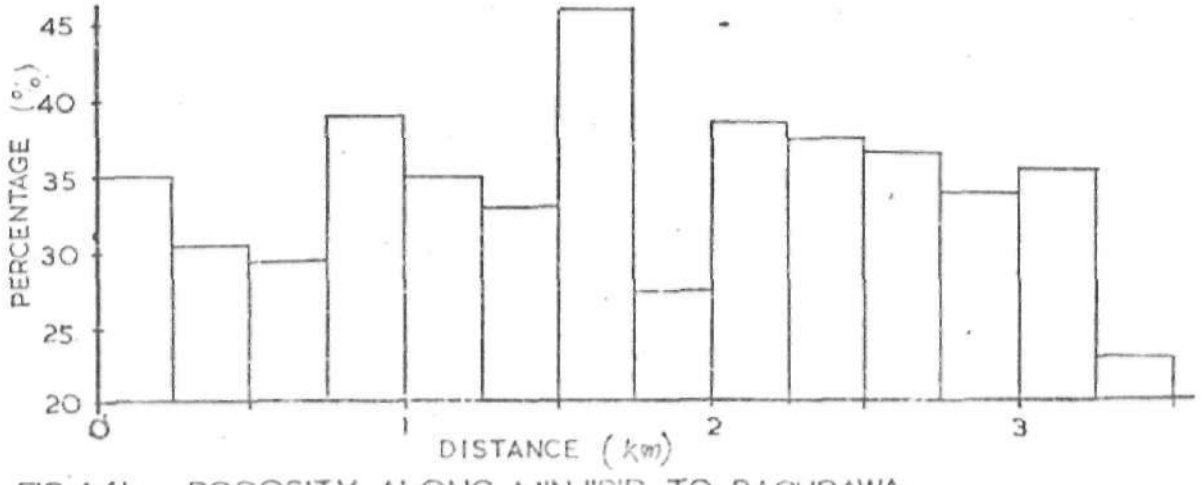


FIG. 4·4h POROSITY ALONG MINJIBIR TO BAGURAWA.

Assuming that the soils with a porosity of 35 percent and above are for water bearing zones, the histograms were analysed for the frequency of those fractions which are the highest and compared with porosity, for its value 35 percent and 37.5 percent respectively as given in Table 4.3. The analysis shows that fine sand and medium sand are the best for the water bearing zones.

4.5.2 Dry Stream Bed Section:

Histograms show that medium sand is the most prominent followed by fine sand (Figs. 4.3d and 4.3e). The other fractions i.e. gravel, coarse sand, clay and silt have very low content (Figs. 4.3b, 4.3c, 4.3g and 4.3f). Most of the soils are wind-blown fine sands with rounded to sub-rounded grains. The density of the soils varies between 1,500 to 1,720 kg/m^3 and porosity varies between 43.4 to 35.1 percent. The histogram analysis to find the most probable water bearing soil particles is shown in Table 4.3.

It would be seen from the analysis of both these profiles that in general, fine sand is the best for water bearing soils. For a porosity of 35 percent, Minjibir-Wasai section gives 77.8 percent for fine sand and dry stream bed section gives 100 percent. These values are 72.2 and 71.4 percent respectively for a porosity of 37.5 percent. Since these two profiles are almost parallel to

TABLE 4.3

Correlation of Porosity with Soil Constituents Along the Three Profiles.

SOIL CONSTITUENT	FREQUENCY OF PREDOMINANT SOIL CONSTITUENT			POROSITY ≥ 35 PERCENTAGE						POROSITY ≥ 37.5 PERCENTAGE					
				FREQUENCY			PERCENTAGE (%)			FREQUENCY			PERCENTAGE (%)		
	P_1	P_2	P_3	P_1	P_2	P_3	P_1	P_2	P_3	P_1	P_2	P_3	P_1	P_2	P_3
Gravel	8	6	-	5	2	-	-	40	-	3	-	-	37.5	-	-
Coarse Sand	1	-	-	-	-	-	-	-	-	-	-	-	-	-	-
Medium Sand	1	-	13	1	-	13	100	-	100	1	-	7	100	-	53.8
Fine Sand	18	8	7	14	6	7	77.8	75	100	13	4	5	72.2	50	71.4
Silt	-	-	-	-	-	-	-	-	-	-	-	-	-	-	-
Clay	-	-	-	-	-	-	-	-	-	-	-	-	-	-	-

P_1 represents profile-1 i.e. Minjibir to Wasai profile.

P_2 represents profile-2 i.e. Minjibir to Bagurawa profile.

P_3 represents profile-3 i.e. Along the dry river.

each other, it can be seen that the direction of the wind must be from north-west to south-east, i.e. from the dry river stream towards Minjibir-Wasai section.

4.5.3 Minjibir-Bagurawa Section:

This section is approximately along the strike of the host rock. The samples collected, fourteen in number, are also fewer than the samples collected from the other two sections. This profile is also dominated by fine sand, followed by gravel content (Figs. 4.4e and 4.4b). The remaining fractions are not very significant. The density varies from 1,430 to 2,040 kg/m^3 and porosity between 23 to 46 percent. An analysis showing the frequency of various fractions in the soil samples is given in Table 4.3, which further confirms that fine sand is the best water bearing zone.

The lithological description of the three profiles is given in Table 4.4, 4.5 and 4.6.

4.6 Comparative Study Between Topography And its Mechanical Analysis:

4.6.1 Correlation Coefficients between Two Different sets of Data:

The spot heights were extracted from the topographic map published by Photosur Inc. Montreal, Canada and

TABLE 4.4

Lithological Description of Soils Along Minjibir-Kazai Profile.

Sample No.	Distance km+m	Lithological Description	Soil Group
MW-0	0+000	Well-graded sandy laterite	GW
MW-1	0+100	Earthy brown silty sand, subrounded mostly quartz grain	SM
MW-2	0+200	Earthy brown silty sand, subangular quartz grains and rare black minerals	SM-SC
MW-3	0+300	Earthy brown sandy laterite, poorly assorted, quartz and granite nodules of laterite	GP
MW-4	0+400	Earthy brown sandy laterite, with some clay quartz grain and rare black minerals	GC
MW-5	0+500	Earthy brown clayey sand, subangular weathered feldspar, quartz & rare black minerals	SC
MW-6	0+600	Reddish brown silt sand, mostly quartz, subangular to subrounded	SM
MW-7	0+700	As above	SM
MW-8	0+800	Reddish brown well graded sand mostly quartz, subangular to subrounded grains	SW
MW-9	0+900	Earthy brown sandy laterite, mostly quartz, subangular to angular	GP

contd.

Table 4.4 contd.

Sample No.	Distance km+m	Lithological Description	Soil Group
MW-10	1+000	Earthy brown silty sand with traces of laterite nodules mostly quartz, subangular to angular	SM
MW-11	1+100	Reddish-brown sandy laterite, mostly quartz, subangular to angular grains	GP
MW-12	1+200	Earthy brown sandy laterite, quart and biotite, large nodules of laterite	GP
MW-13	1+300	Reddish brown well graded sand laterite quartz, rare black mineral subangular to angular grains	GW
MW-14	1+400	Reddish brown graded sand with little clay, subangular to angular grains, quartz black minerals	SC
MW-15	1+500	Reddish brown sand laterite with little clay, some quartz	GC
MW-16	1+600	Light brown graded sand subrounded to angular grains mostly quartz weathered feldspar, & rare black minerals	SW
MW-17	1+700	Little brown well graded laterite quartz, W.feldspar and rare black minerals	GW
MW-18	1+800	Light brown clayey sand, subrounded to angular grains, mostly quartz	SC

contd.

Table 4.4 contd.

Sample No.	Distance km+m	Lithological Description	Soil Group
MW-19	1+900	Earthy brown silty sand, subrounded to angular grains, mostly quartz	SM
MW-20	2+000	Earthy brown silty sand, subrounded subangular grains, quartz and feldspar	SM-SC
MW-21	2+100	Light brown silty sand, subrounded to subangular grains, mostly quartz	SM
MW-22	2+200	Earthy brown sandy laterite, subangular to angular grains, quartz, feldspar granite	GM-SM
MW-23	2+300	Light brown silty sand, subangular to angular grains, weathered feldspar and quartz	SM
MW-24	2+400	Earthy brown silty sand with laterite nodules, subangular to angular grains, quartz and rare black minerals	SM
MW-25	2+500	As above	SM
MW-26	2+600	Earthy brown silty sand with traces of laterite	SM
MW-27	2+700	As above	SM

N.B. The soil grouping has been based on Casagrandes soil classification system (1952).

TABLE 4.5

Lithological Description of Soils
Along Dry River Bed Profile.

Sample No.	Distance km+m	Lithological Description	Soil Group
R-0	0+000		
R-1	0+100	Light brown, fine to medium sand, subrounded grains	SM
R-2	0+200	As above	SM
R-3	0+300	As above	SW
R-4	0+400	As above	SP
R-5	0+500	As above	SM
R-6	0+600	As above	SP
R-7	0+700	As above	SP
R-8	0+800	Earthy brown, fine to medium sand, rounded to subrounded grains	SP
R-9	0+900	Light brown, fine to medium sand, well assorted quartz grains	SW
R-10	1+000	As above	SW
R-11	1+100	As above	SW
R-12	1+200	As above	SW
R-13	1+300	As above	SW
R-14	1+400	As above	SW

contd.

Table 4.5 contd.

Sample No.	Distance km+m	Lithological Description	Soil Group
R-15	1+500	Whitish silty sandy with some clay, subrounded to rounded grains, transparent quartz	SC
R-16	1+600	Whitish graded sand, subrounded to rounded transparent quartz grains	SW
R-17	1+700	Whitish silty sand, subrounded to rounded quartz grains	SM
R-18	1+800	Whitish brown, medium to fine sand, subrounded to rounded quartz & rare black minerals	SW
R-19	1+900	As above	SM
R-20	2+000	Light brown, medium to fine sand, well assorted rounded to subrounded grains	SW

N.B. The soil grouping has been based on Casagrande's soil classification system (1952).

TABLE 4.6

Lithological Description of Soils along Minjibir to Bagurawa Profile.

Sample No.	Distance km+m	Lithological Description	Soil Group
MB-0	0+000	Well graded sandy laterite	GW
MB-1	0+250	Earthy brown, sandy laterite with some granite	GC
MB-2	0+500	Earthy brown, sandy laterite with some quartz, angular to subangular grains	GW
MB-3	0+750	Reddish silty sand, poorly assorted subangular grains	SM
MB-4	1+000	Earthy brown, sandy laterite with clay and some quartz	GC
MB-5	1+250	Earthy brown, graded laterite with some quartz	GW
MB-6	1+500	Reddish brown, sandy clay, rounded to subrounded quartz grains	SC
MB-7	1+750	Earthy brown, graded sand, subangular to subrounded quartz grains	SW
MB-8	2+000	Light brown, silty sand, subrounded to rounded quartz grains	SM
MB-9	2+250	Whitish sand, very fine sub-rounded to rounded quartz grains	SM

contd.

Table 4.6 contd.

Sample No.	Distance km+m	Lithological Description	Soil Group
MB-10	2+500	Whitish sand, very fine subrounded to rounded quartz grains	SM
MB-11	2+750	Earthy brown, silty sand, rounded to subrounded quartz grains	SM
MB-12	3+000	As above	SM
MB-13	3+250	Earthy brown, laterite iron pan with cemented sand and quartz grains	GP

N.B. The soil grouping has been based on Casagrande's soil classification system (1952).

enlarged and then contoured at 2.5 m interval as shown in Fig. 4.5. A graph of heights of the three profiles was then constructed by using the contoured values (Figs. 4.2a, 4.3a, 4.4a). To correlate the readings of topography and the samples collected, since they are both surface features, we used the idea of multiple correlation coefficient R. Now supposing A is percentage of sample, and B is the height of the same place where the particular sample is collected, then the sum of the squares due to regression of A is given by:

$$SS_A = \sum A^2 - (\sum A)^2/n$$

and sum of squares due to regression of B is given by:

$$SS_B = \sum B^2 - (\sum B)^2/n$$

then the multiple correlation coefficient R is defined as

$$R = \sqrt{\frac{SS_A}{SS_B}} \quad \text{if } SS_A \leq SS_B$$

or $$R = \sqrt{\frac{SS_B}{SS_A}} \quad \text{if } SS_B \leq SS_A \text{ such that } R \leq |1|.$$

4.6.2 Results of Correlation:

The multiple correlation coefficient was found for the actual percentage of the samples and the actual height at each point, and this is shown in Table 4.7. It can be seen that there is a definate trend in pattern. From Table 4.7 it would be seen that the coarse sand and the silt gives the highest correlation with topography.

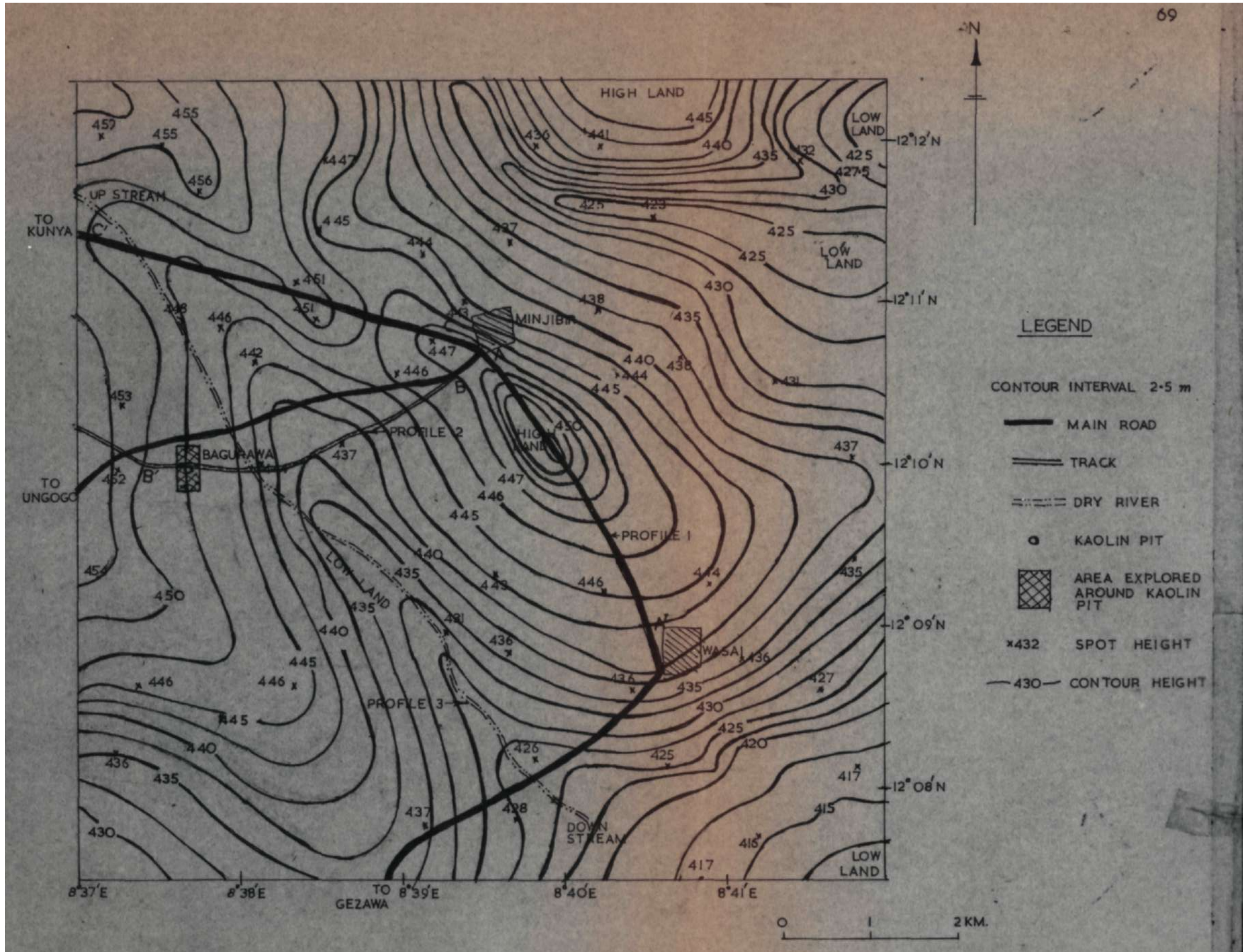


FIG. 4·5

TOPOGRAPHICAL MAP OF THE AREA SURVEYED SHOWING HEIGHT CONTOURS.

[SOURCE FOR SPOT HEIGHTS : PHOTOSUR INC., CANADA, 1980]

TABLE 4.7

Multiple Correlation Coefficient

Of Actual Data Points.

Soil Constituent	Multiple Correlation Coefficient		
	Minjibir-Wasai Profile	Dry River Bed Profile	Minjibir-Dagurawa Profile
Gravel	0.155	0.270	0.242
Coarse Sand	0.543	0.600	0.617
Medium Sand	0.375	0.273	0.374
Fine Sand	0.151	0.318	0.289
Silt	0.705	0.606	0.591
Clay	0.227	0.302	0.342

The high correlation coefficient for the coarse sand and silt would lead to the following conclusions:

i) There has been somehow severe interaction of weathering of these two types of soils which were predominant sometimes throughout a cycle of erosion.

ii) Since $R_{silt} > R_{coarse\ sand}$, it gives rise to the fact that the coarse sand layer is covered by the silt layer.

iii) Generally the weathering process has been carried out in such a way that it grooved the upper most layers to form low lands, while the weathered soils were deposited and accumlated to form high lands.

Chapter 5

REGIONAL SURVEY

A regional survey was carried out around Minjibir town to investigate the uppermost shallow structure and its stratigraphic sequence and also to try and determine the ground water potentials of any existing aquifer using the resistivity, S.P. and V.L.F. methods. Measurements were made along three long profiles shown in Fig. 1.2. These are:

i) along the main road from Minjibir to Wasai, (profile 1) covering a total distance of 2.8 km,

ii) along the main road from Minjibir to Bagurawa, (profile 2) a total distance of 3.2 km, and

iii) along the dry river bed, (profile 3) which cuts across the second profile at 2.35 km from Minjibir. The total distance surveyed was 2.4 km.

A base station was chosen at Minjibir which is at the junction of the first two profiles. For the third traverse, along the dry river bed, another base station was established at the start of the profile.

5.1 Resistivity Survey:

Profiling was done on the three traverses using the Schlumberger electrode arrangement shown in Fig. 3.4.

This method involves a very large (300 m) fixed separation of the current electrode with the potential pair moved between them at a fixed spacing of 50 m, subject to the limitation $(L - x) \geq 1$, where

L = half the current electrode distance,

l = half the potential electrode distance, and

x = the distance between the centre of the spread and the centre of the potential electrodes.

When the cable length was exhausted the electrodes were placed in such a way that there was an overlapping of one station. This procedure was carried out until the profile was completed.

5.1.1 Interpretation of Resistivity Profiling:

The apparent resistivity calculated using equation 21 of chapter 3 was plotted on a semi-log scale and the curve was smoothened visually. Only qualitative analysis has been carried out here. No quantitative analysis was carried out because only a broad study of the area was done. Variations in resistivity values were correlated with the observable geological exposures to get a general idea about the lateral and vertical extension of these exposures.

The resistivity profile along the dry river is shown in Fig. 5.1. From this figure it is noted that there are four peaks a, b, c and d having resistivity values of about 30,000 Ωm, 25,000 Ωm, 45,000 Ωm and 9,000 Ωm respectively. From the surface geology and the resistivity profiles there is an indication of five smaller buried channels cutting across the bank which might have opened up to form the present river. With

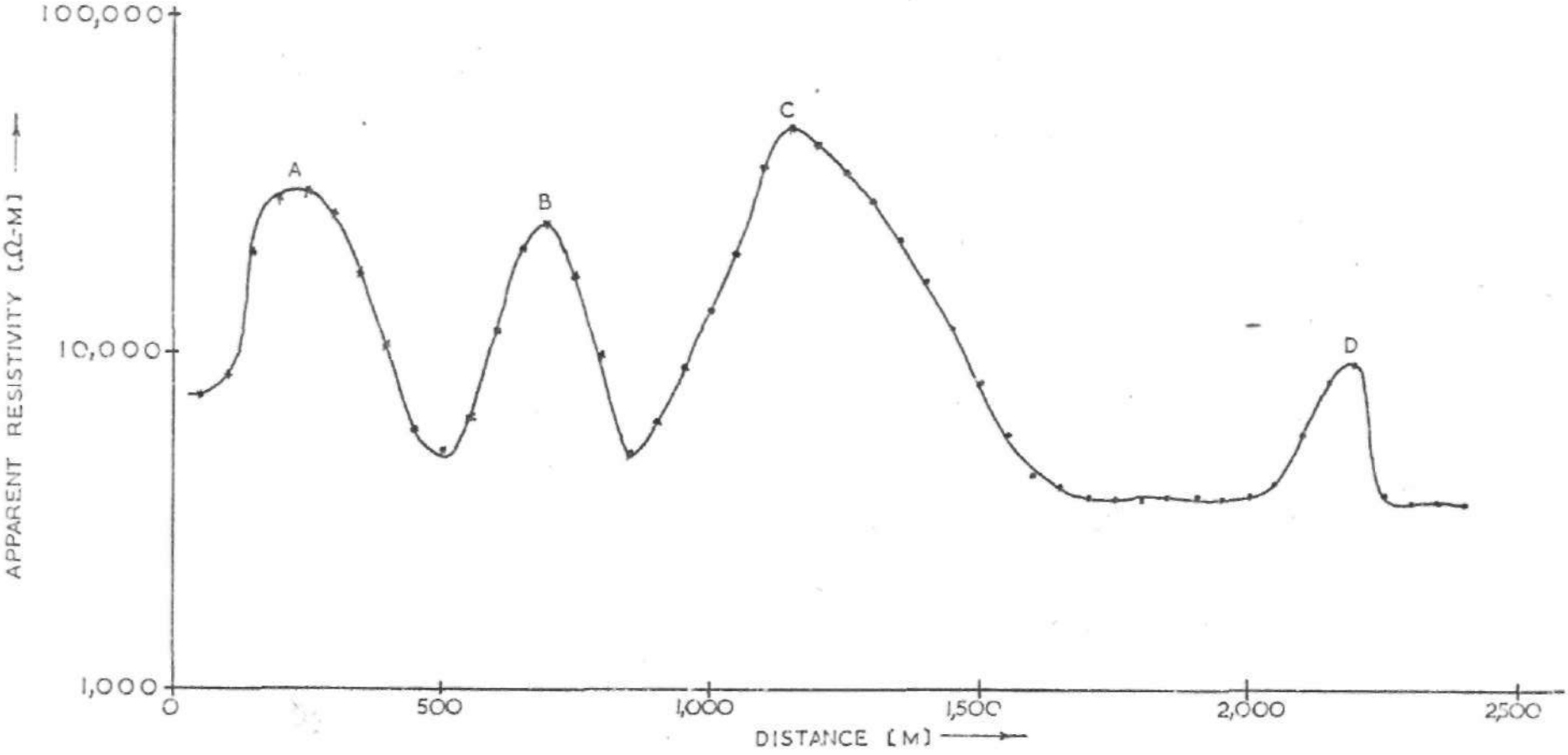


FIG. 5-1

SCHLUMBERGER PROFILILING ALONG DRY RIVER BED PROFILE WITH CURRENT ELECTRODE SPACING OF 300m AND POTENTIAL ELECTRODE SPACING OF 50 m

passage of time, the channels as well as the river dried up. Sediments such as alluvium were deposited on it. The shape of the contoured line on the topographic map for heights along the dry river bed, Fig. 4.5, gives an indication of the seepage system.

These buried channels should be very narrow and rather limited since these have not appeared along Minjibir to Wasai profile, Fig. 5.2. The only obvious anomaly in Fig. 5.2 is between 100 to 250 m from the Minjibir end of the profile where there is an appreciable drop in the resistivity value to 30 Ωm. This probably indicates the presence of trapped underground water to a depth less than 50 m. This is followed by gradual increase in the resistivity value, reaching upto a maximum of 4,000 Ωm at 1.5 km from Minjibir end and decreasing to about 400 Ωm at 2.4 km from Minjibir.

The Minjibir-Bagurawa profile, Fig. 5.3, shows two sharp peaks. The first one occurs at 1.4 km from Minjibir. It is as a result of laterite deposits which are even visible in that area. The second peak is at 2.4 km from Minjibir. It coincides with the crossing of the dry river and the value of 4,000 Ωm is similar to that obtained at the start of the dry river bed profile. The resistivity value at the start of Minjibir-Bagurawa profile is 2,750 Ωm and drops down to 250 Ωm at 200 m. From this place to 1.1 km, the resistivity value ranges

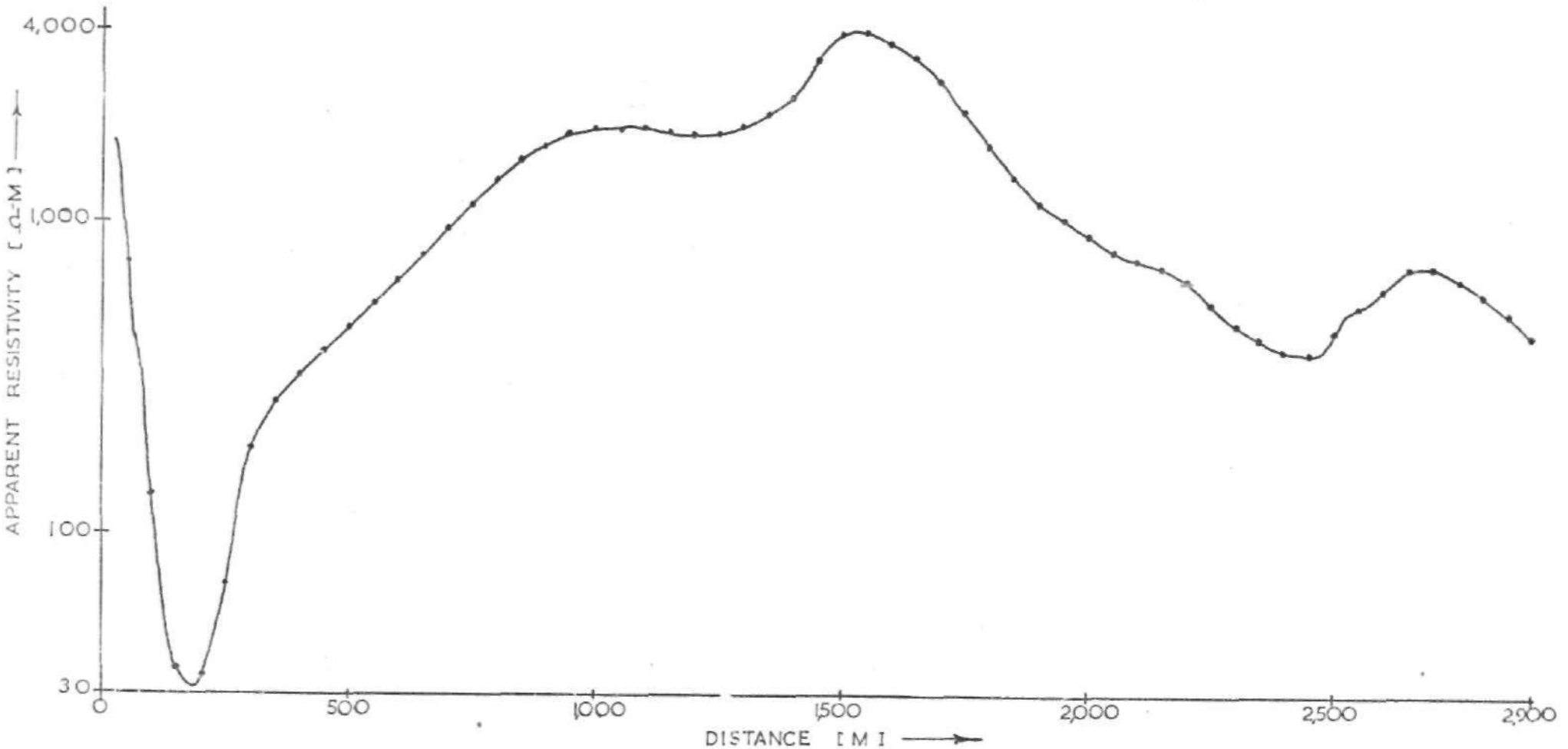


FIG. 5·2

SCHLUMBERGER PROFILING ALONG MINJIBIR TO WASAI PROFILE WITH CURRENT ELECTRODE SPACING OF 300 m AND POTENTIAL ELECTRODE SPACING OF 50 m

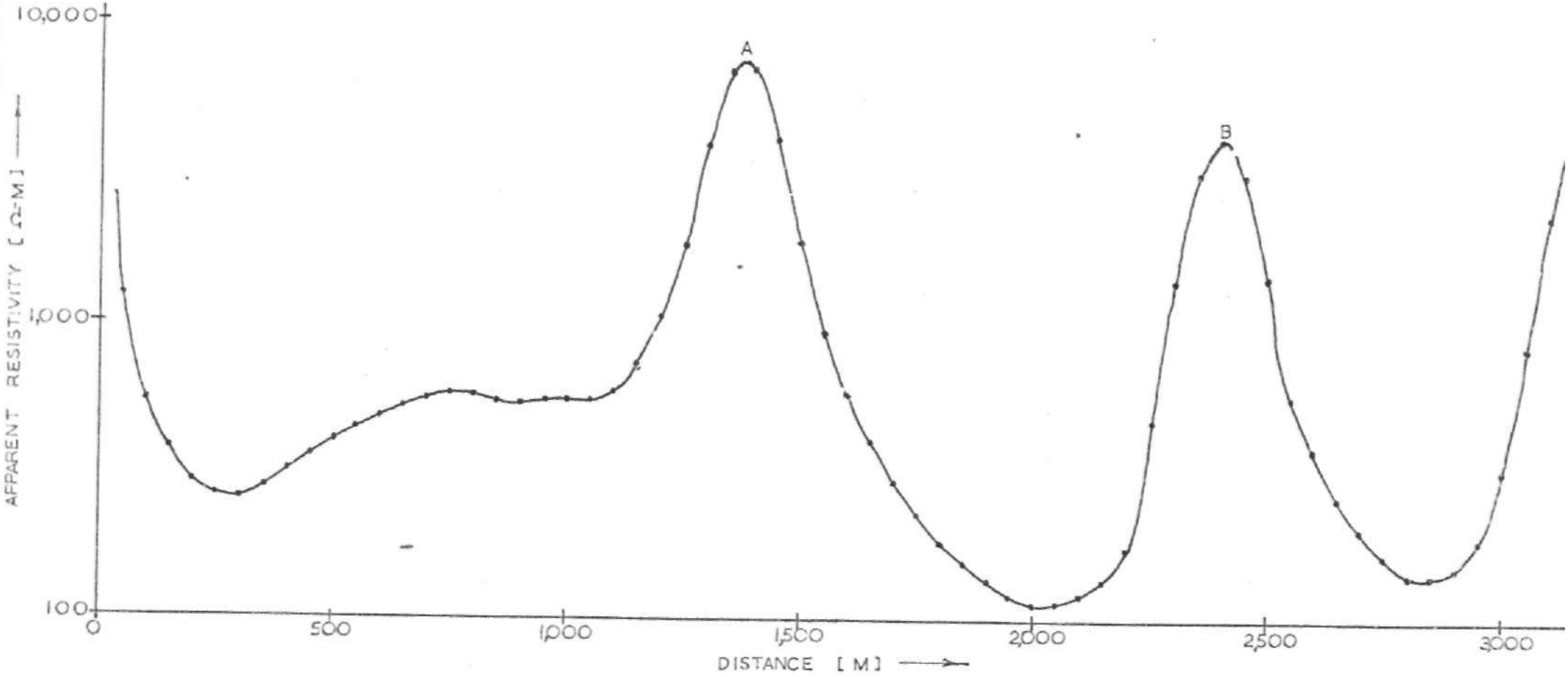


FIG. 5·3
SCHLUMBERGER PROFILING ALONG MINJIBIR TO BAGURAWA PROFILE
WITH CURRENT ELECTRODE SPACING OF 300m
AND POTENTIAL ELECTRODE SPACING OF 50m

between 250 to 600 Ωm. This indicates that there are possibly some traces of kaolin in that area. Its existance was even confirmed from visual examination of sub-soil samples taken from the wells along this stretch of the profile. At 2.0 km, the resistivity value of 120 Ωm is the least, which suggests that the area should be good for ground water prospecting. Also the depth of water table measured from the wells in this area around the village was the least compared to the rest of this profile. At 2.8 km, which is close to the pit, the resistivity value is about 150 Ωm and this is due to kaolin. The resistivity value starts rising at 3.0 km to a maximum of 10,000 Ωm. This may be attributed to deposits of laterite, which are even visible over the surface.

5.2 Self - Potential Survey:

The procedure used in the S.P. survey was the fixed base station method. This involves keeping one electrode fixed at one point while the other electrode alongwith the instrument is moved. The spacing was kept as 50 m between stations.

5.2.1 Interpretation of Regional Self-Potential Survey:

The three S.P. profiles are shown in Fig. 5.4. Along profile 1, the S.P. values are negative as well as positive and range between +200 to -275 mV. Along

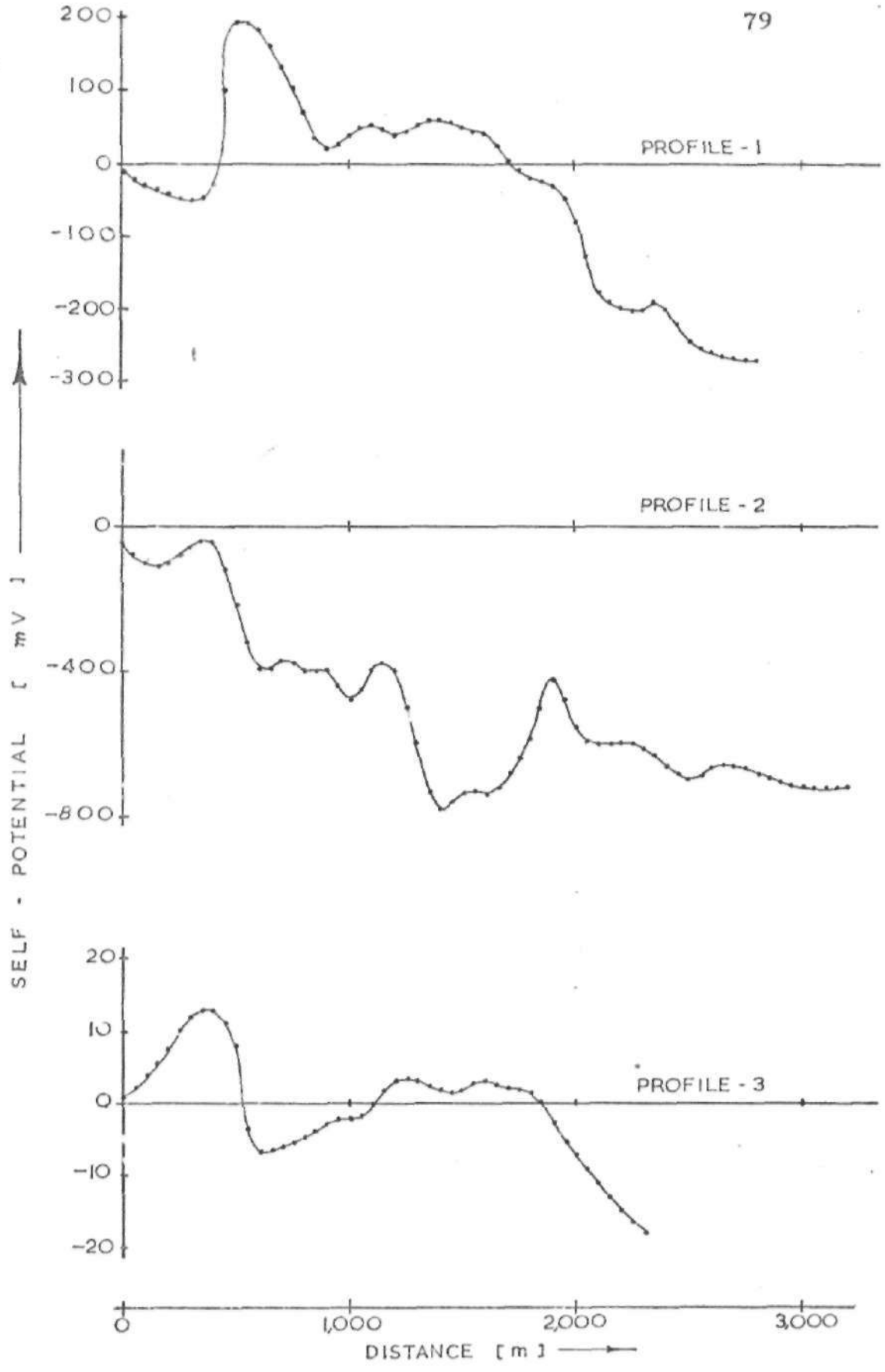


FIG. 5-4

SELF-POTENTIAL GRAPHS ALONG THE PROFILES.

profile 2, these values are all negative and range between -50 to -800 mV. Along profile 3, these values are both negative and positive and range between +13 to -17 mV.

The integrated figure of the three S.P. profiles is shown in Fig. 5.5. Profiles 1 and 3 are more or less parallel to each other. It would be seen from Fig. 5.5 that S.P. value is negative along AB and A'B', positive along BC and B'C' and becomes negative after C and C', in case of both these profiles. It may therefore be deduced that the structure of the sub-surface can be extended from profile 3 to profile 1. As the maximum positive S.P. values between BC and B'C' are obtained in the middle of both these profiles and has minimum negative S.P. value on both sides, it could be said that this is a shallow synclinal basin like structure filled with recent alluvial sediments. This basin is most likely an aquifer for ground-water. The flanks of this basin represented by negative S.P. values for profiles 1 and 3 are exposed closer to the ground surface and hence are considered very good for ground-water prospecting. The basin is striking in the north-east to south-west direction. The profile 2, Minjibir to Bagurawa, shows only negative values which is probably due to the reason that it is along the strike, while the other two profiles are prependicular to it.

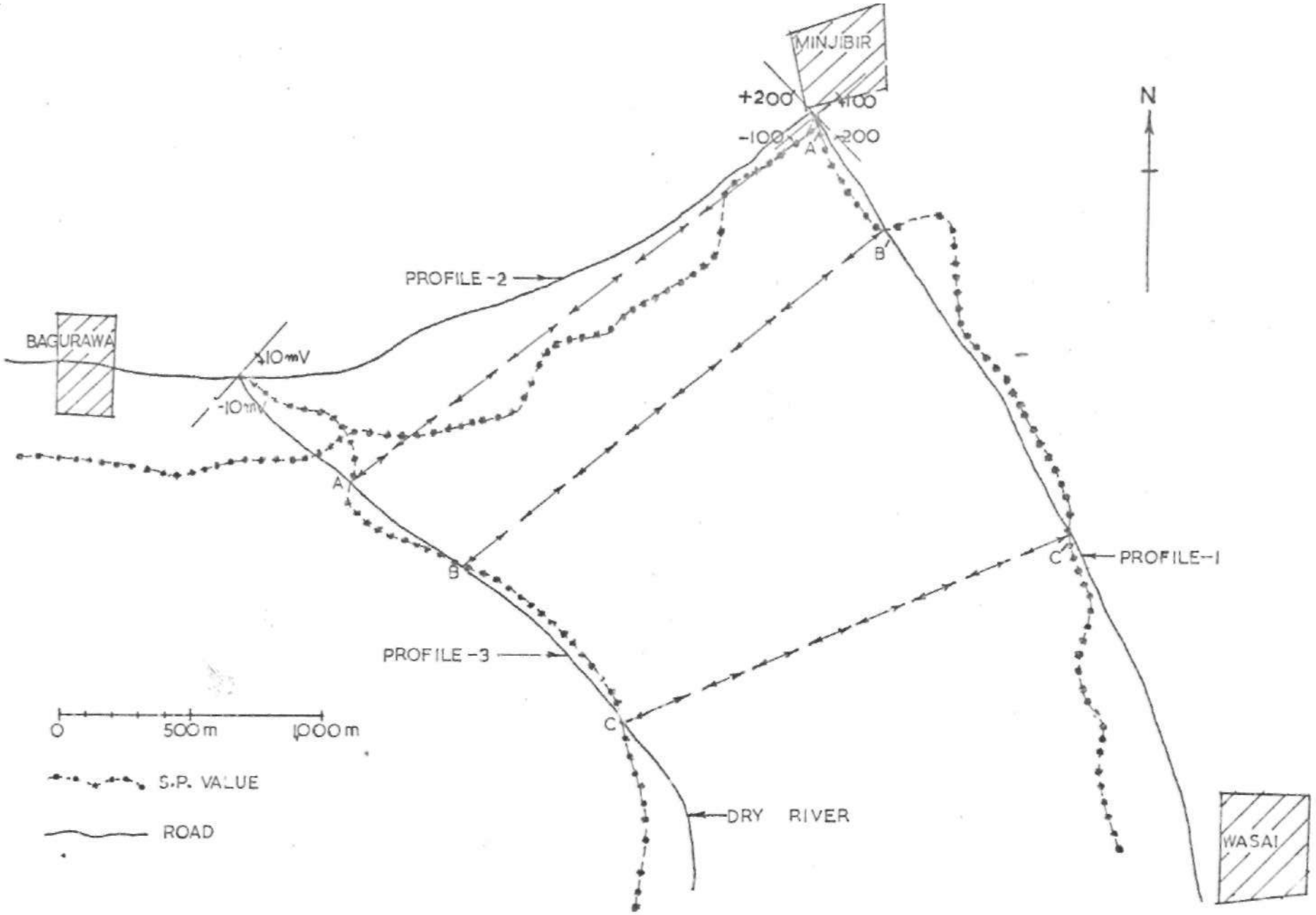


FIG. 5·5

THE INTEGRATED S.P. GRAPHS OF THE PROFILES

With this S.P. survey, in the absence of detailed work, nothing specific can be said about the depth and thickness of the alluvial aquifer. The probable schematic sub-surface cross-section of this area, as deduced from the qualitative interpretation of the S.P. data is shown in Fig. 5.6.

5.3 Very Low Frequency Survey:

As discussed in chapter 3, at very large distances the magnetic field lines are at right angles to the station direction. In view of this, the orientation of the survey lines was selected approximately parallel to the traverse direction, that is, approximately perpendicular to the expected strike of a conductor. This was done by turning the instrument sideways until the signal was minimum. A transmitter station of GBR, F = 16 KHz, was selected. Readings were taken along the three profiles at 150 m spacing.

The exact position at which the noise level is minimum cannot be known precisely when taking readings for the quad and in-phase components. George (1976) stated that an error in the range of 20-35 percent may be introduced in the measurement if a station having $\pm 45^{\circ}$ to the direction of the strike line is selected for the target body, even though it is stated in the manual that a variation of $\pm 45^{\circ}$ may not have any significant effect.

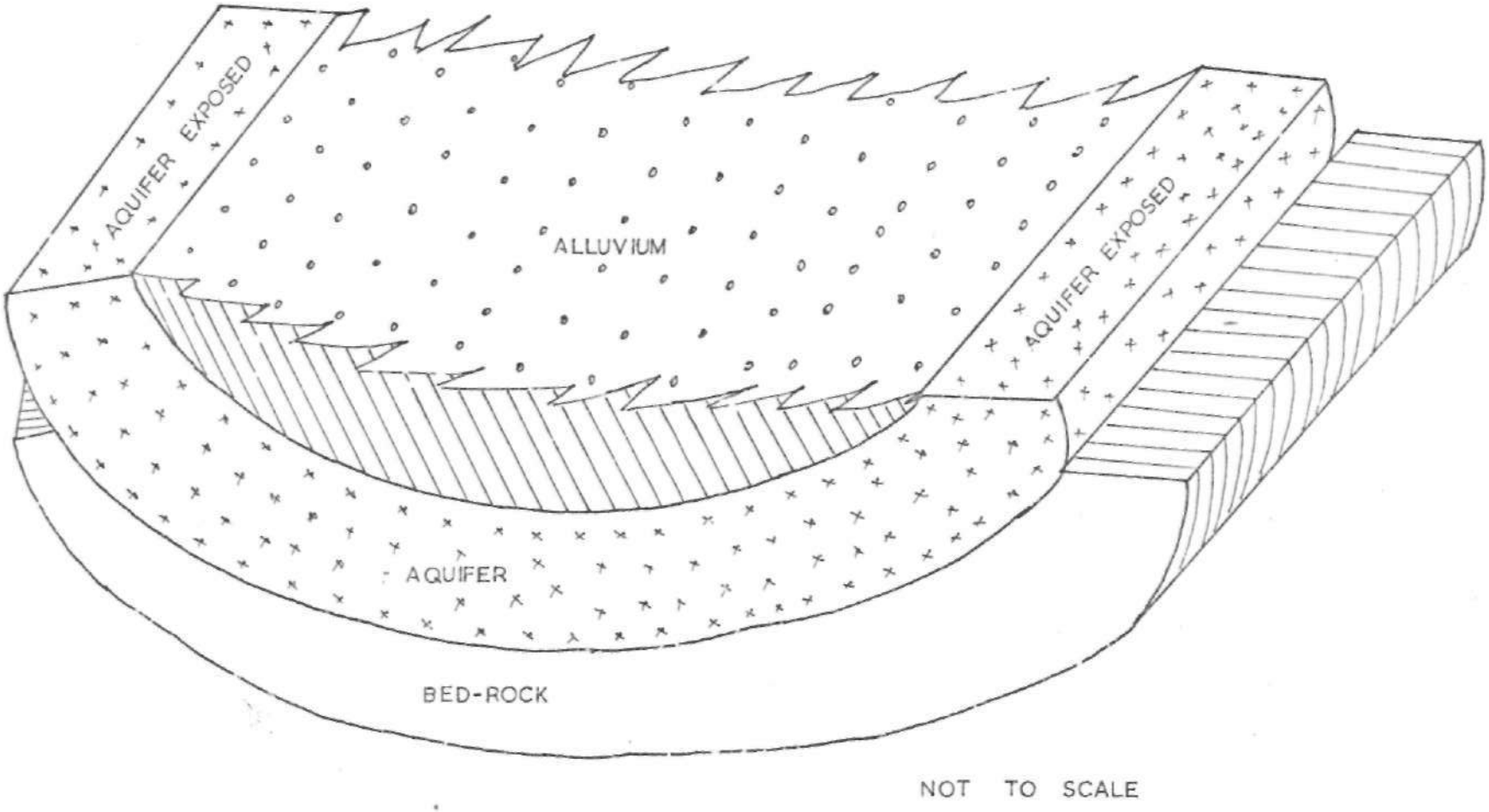


FIG. 5·6

A SCHEMATIC SUB-SURFACE STRATA OF THE SURVEYED AREA.

5.3.1 Interpretation of Regional V.L.F. Survey:

These are mainly qualitative though some theoretical work is currently being done (Ronka, 1969). Field data are often distorted by geological noise because of the very high transmitted frequencies involved. Topographic effects also contribute to errors in the data. In view of these, Fraser's filtering process was applied to the data as explained in chapter 3. The final result is shown in Fig. 5.7 in respect of all the three profiles.

It would be seen that in case of profile 1, the quad value ranges between +96 to -109 and the in-phase value between +86 to -94. There are two distinct cross-over points as indicated by A' and B'. For profile 2, the quad value ranges between +68 to -80 and the in-phase value between +30 to -30. There are five cross-over points as indicated by A, B, C, D and E. For profile 3, the quad value ranges between +58 to -50 and in-phase value between +78 to -39. There are two distinct cross-over points as indicated by A" and B".

The cross-over points indicate different layers of the sub-surface. The V.L.F. graphs are drawn in Fig. 5.8. The overall structure deduced from the V.L.F. survey is similar to that shown in Fig. 5.6. The two cross-over points on profile 1 can therefore be extended to profile 3. The structure of the region is in agreement with the S.P. survey where the basin extends in the north-east to

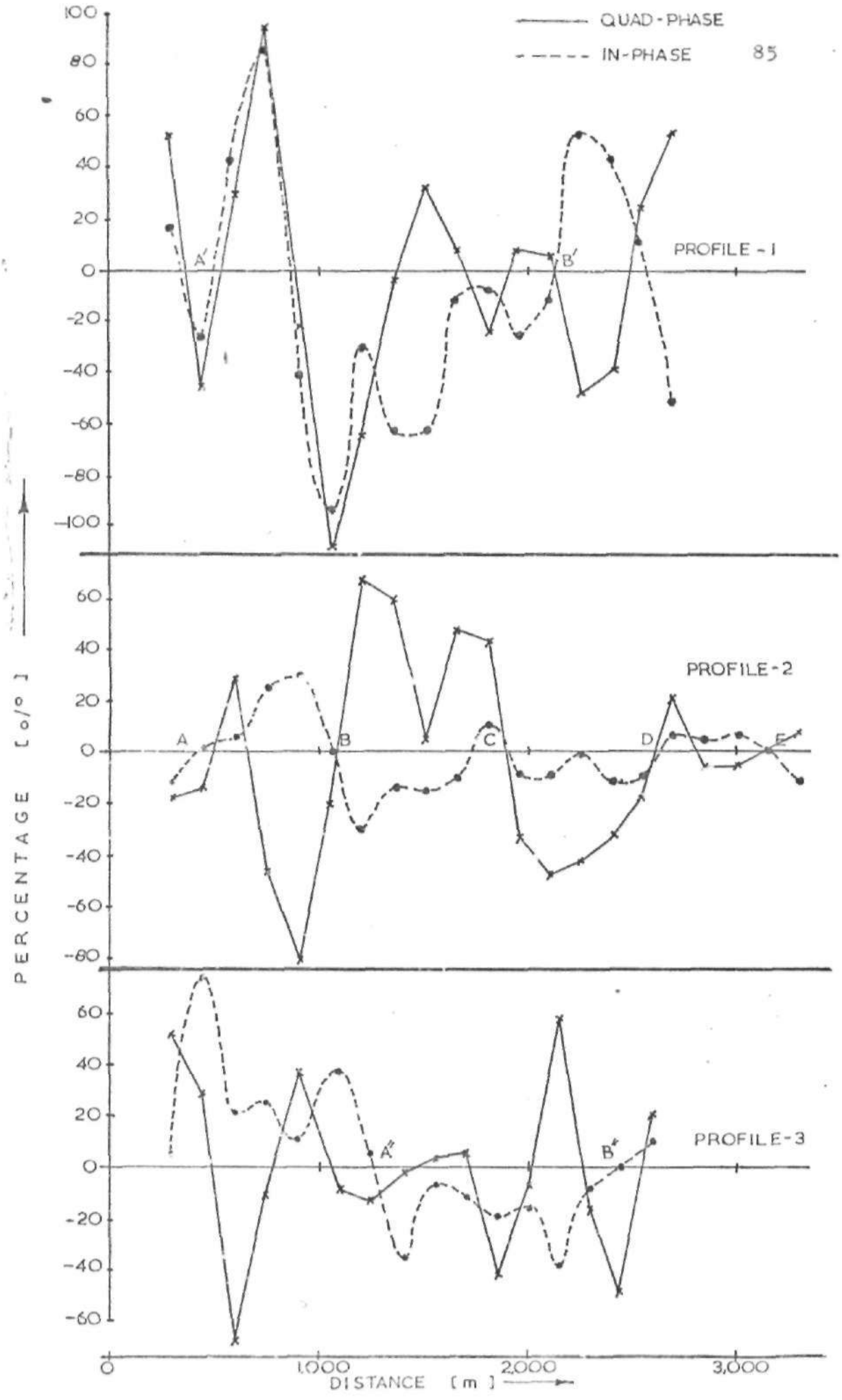


FIG. 5·7
VERY-LOW-FREQUENCY GRAPHS ALONG THE PROFILES.

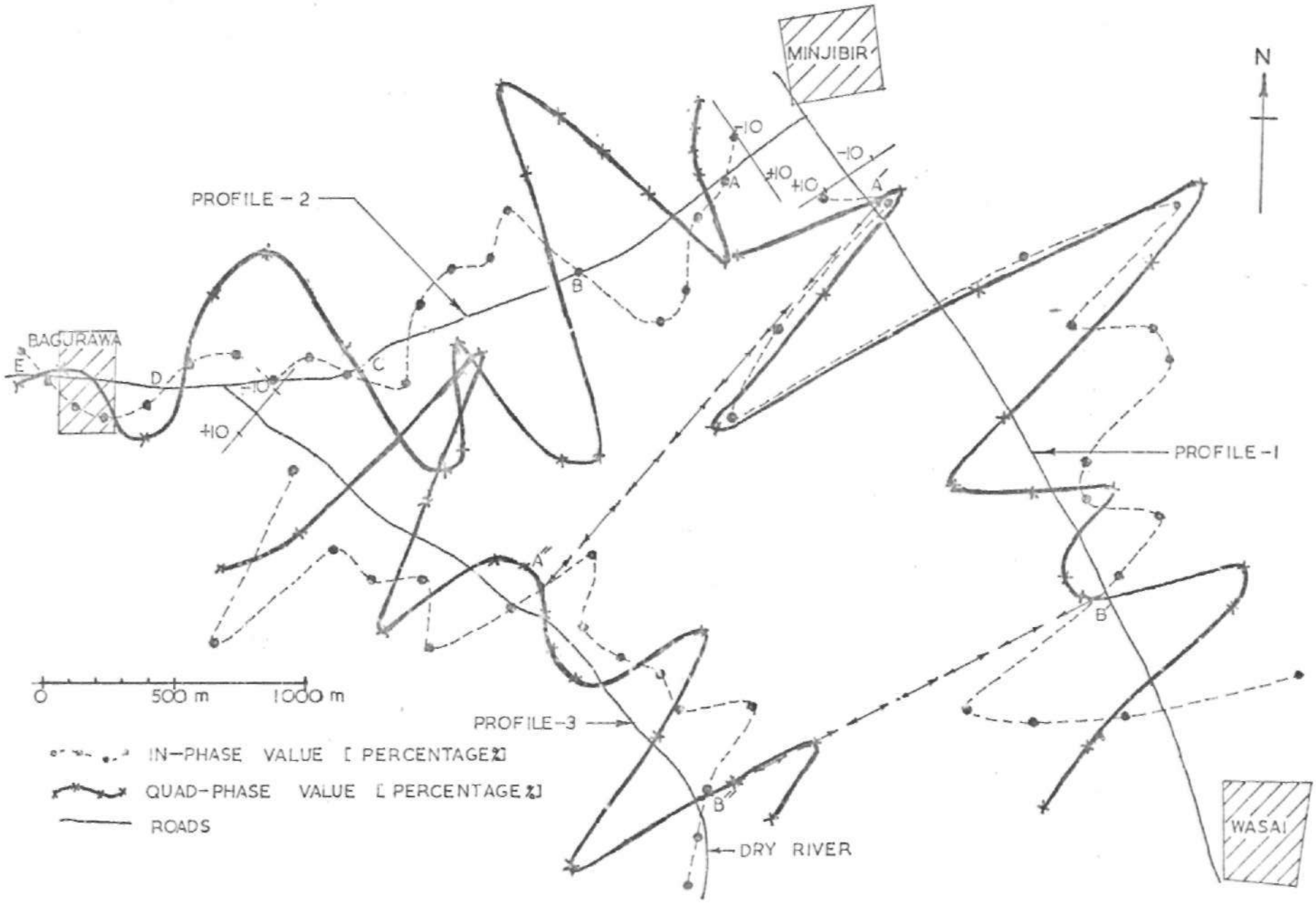


FIG. 5.8

THE INTEGRATED V.L.F. GRAPHS OF THE PROFILES.

south-west direction. On the basis of the structure obtained from S.P. curves and examples given in the V.L.F. manual (Geonics Ltd.), it could be concluded that strong negative in-phase value shown between the points A'B' and A"B" represent a shallow basin which is filled with recent sediments. The basin like layer is likely to be an aquifer for ground water. The layer underlying the basin which shows strong positive in-phase is most probably the bedrock.

The second profile, Minjibir to Bagurawa, is possibly along the strike as deduced from S.P. survey. The cross-over points give an indication of the contact points of different media. These are generally in agreement with sudden variations in the resistivity survey, Fig. 5.3. The first cross-over point A obtained at 500 m in V.L.F. survey could be correlated with the corresponding increase in resistivity value from 250 Ωm to 750 Ωm. Likewise, the cross-over point B at 1.05 km correlates with the sharp increase in resistivity value from 750 Ωm to 8,000 Ωm. The cross-over point C lies between the two peaks of resistivity value, as in Fig. 5.3. The cross-over point D at 2.55 km correlates with the sharp decrease in resistivity value from 4,000 Ωm to 150 Ωm, while the last cross-over point E at 3.15 km correlates with an increase in resistivity value from 200 Ωm to 9,000 Ωm.

Chapter 6

DETAILED INVESTIGATION OF THE AREA AROUND THE KAOLIN PIT AND ITS INTERPRETATION.

6.1 Field Configuration:

For investigation of the area surrounding the kaolin pit, a square grid as shown in Fig. 6.1 was employed around it. Five profiles 400 m each, running in the north-south direction and nine cross profiles, 200 m each in length were laid. The spacing between each profile was kept as 50 m and stations were placed at 25 m intervals along the profiles.

6.2 Resistivity Survey:

The aim of the resistivity survey was to delineate resistivity boundaries and estimate the lateral and vertical extent of the kaolin deposit. Terrameter SAS-300 and a set of copper electrodes was used for this survey. Salt water was poured into the ground around the electrodes for better contact between the electrode and the ground.

6.3 Vertical Electrical Soundings:

Resistivity soundings provide information on the variation in sub-surface conditions with the depth, that

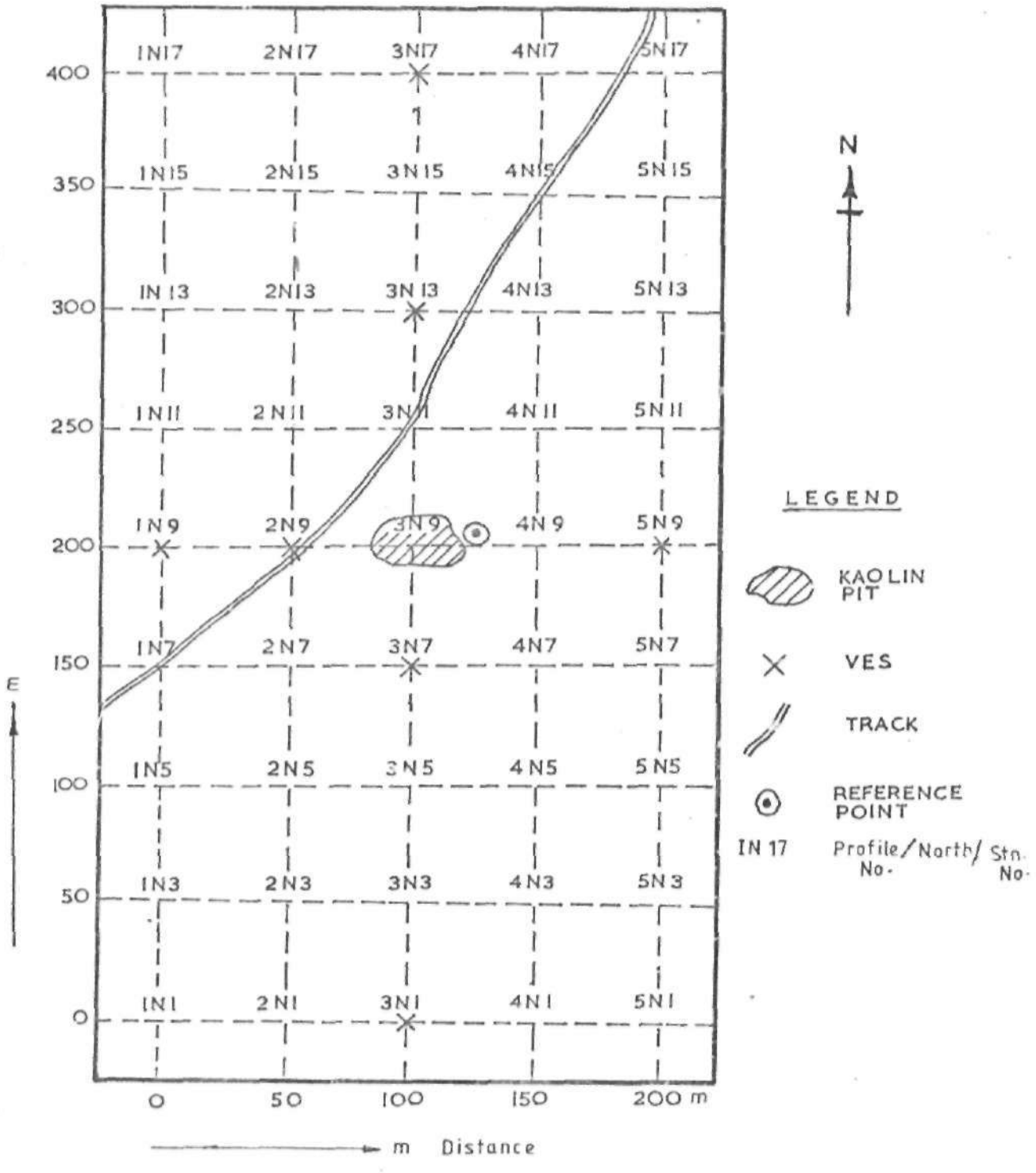


FIG. 6·1

LAYOUT OF THE GRID.

is the individual thicknesses and true resistivities of the various conducting zones. The technique is based on the fact that the fraction of the electric current injected into the ground penetrating below any particular depth increases with an increased separation of the current electrodes. In the sounding procedure, the centre or the mid-point of the electrode spread remains at one point while the electrode spacing is increased from one reading to the next. The spread is always symmetrical from the centre position. The system used in this investigation is the Schlumberger arrangement shown in Fig. 3.2. In this, the two potential electrodes are closely placed midway between the two widely spaced current electrodes.

A total of seven Schlumberger vertical electrical soundings (VES) were carried out around the pit, Fig. 6.1. The current electrode spacing AB/2 ranged from 2 to 100 m for four VES and from 2 to 200 m for three VES, while the potential electrode MN ranged between 1 to 7 m.

6.3.1 Interpretation of the Vertical Electrical Soundings Conducted around the Kaolin Pit:

The apparent resistivity ρ_a was calculated from the field data using equation 19 in chapter 3. It was plotted against the half current spacing on a transparent log-log scale. These field curves were matched against standard master curves (Rijkswaterstaat, 1975) until a good fit was obtained. The sounding curves thus obtained

were mostly of the H-type ($\rho_1 > \rho_2 < \rho_3$). The apparent resistivities and thicknesses of the different layers were calculated from the parameters of the matched curves. Four out of the seven VES gave a good match.

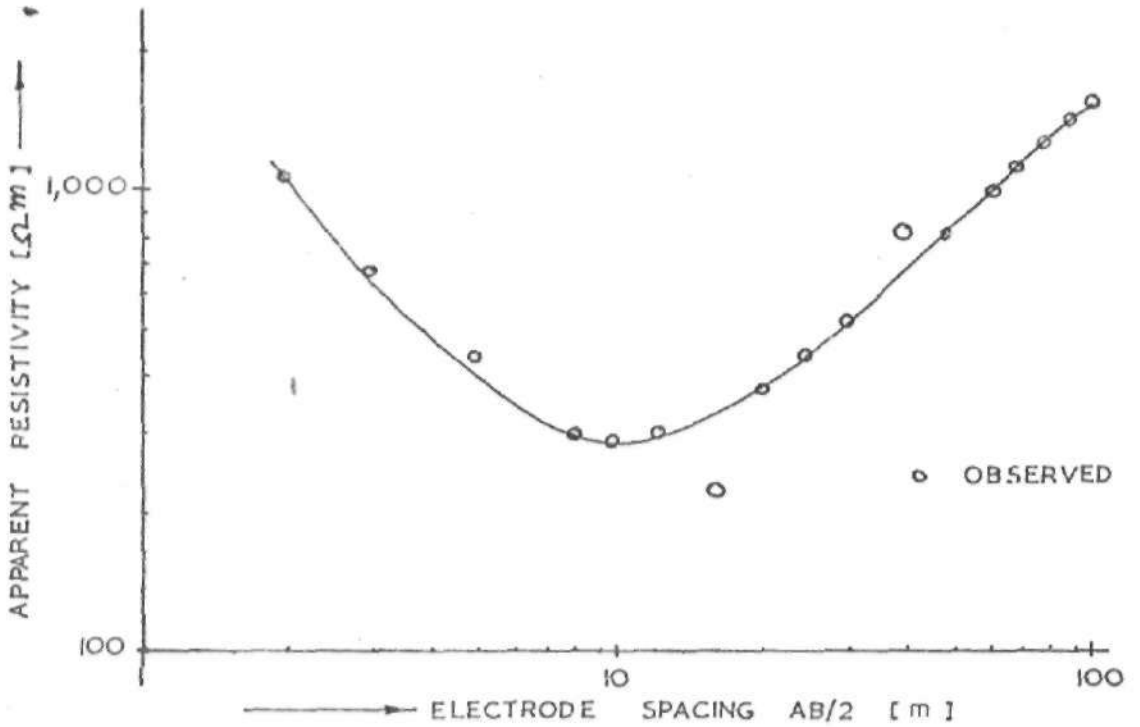
A summary of the estimated values of the thicknesses and resistivities of the layers of four matched curves is given in Table 6.1. All these curves are of the H-type with three layers, Figs. 6.2, 6.3, 6.4 and 6.5. The first layer in all the cases has a shallow thickness which ranges from 1.1 to 1.7 m with an average of 1.4 m. Its resistivity value ranges from 600 to 1,175 Ωm. This layer consists of sandy soil as indicated by the mechanical analysis results obtained for the top soil samples from that area. The second layer is the least resistive of the three and has a depth ranging from 11.4 to 21.7 m. The wide variation in the depth values suggests that this layer is probably of shallow syncline shape, striking in the north-east to south-west direction. Its resistivity values range from 100 to 235 Ωm. This layer could consist of clay material which possibly is kaolinitic. The best possible locations for kaolin deposits could be at VES 3N17 and VES 1N9. The third layer is the most resistive of the three layers and resistivity value is between 2,400 to 25,000 Ωm. This could be crystalline basement rock.

At VES 5N9, Fig. 6.6, the points are much scattered

TABLE 6.1

Resistivity Values and Thicknesses of the Layers at the Sounding Points.

SOUNDING POINT	NUMBER OF LAYERS	RESISTIVITY (Ωm)			THICKNESS (m)				KOEFOED COEFF. C	TYPE OF CURVE
		LAYER 1	LAYER 2	LAYER 3	LAYER 1	LAYER 2				
						LOW	BEST	HIGH		
1N9	3	820	164	2,400	1.4	15.0	17.4	19.8	2,556	H
3N1	3	600	200	15,000	1.7	20.1	21.7	23.3	1,628	H
3N7	3	1,175	235	11,750	1.4	10.1	11.4	12.7	570	H
3N17	3	1,000	100	25,000	1.1	11.1	13.1	15.1	3,275	H



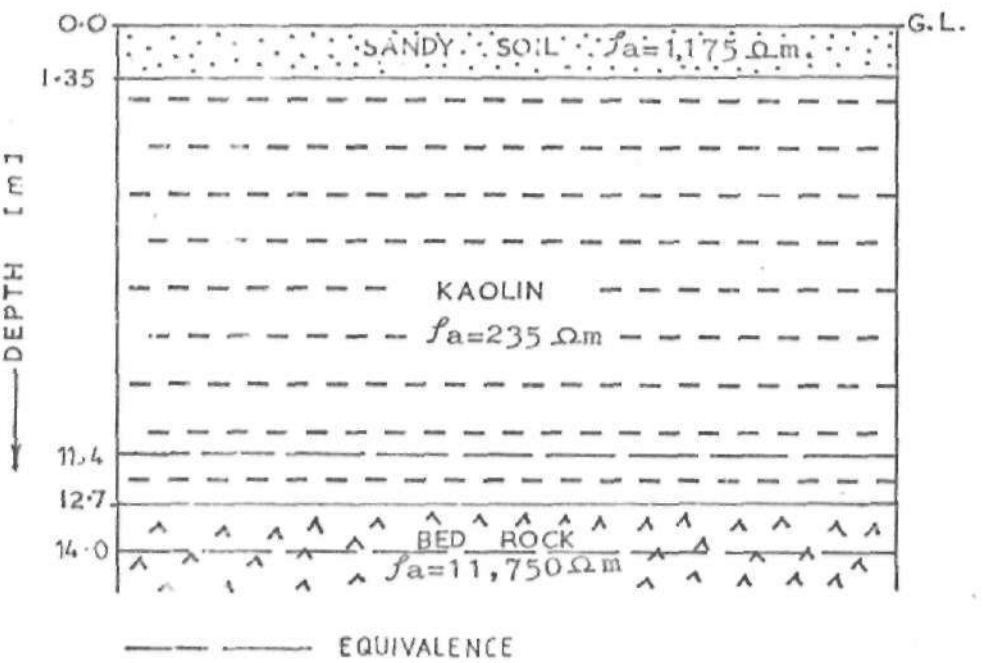
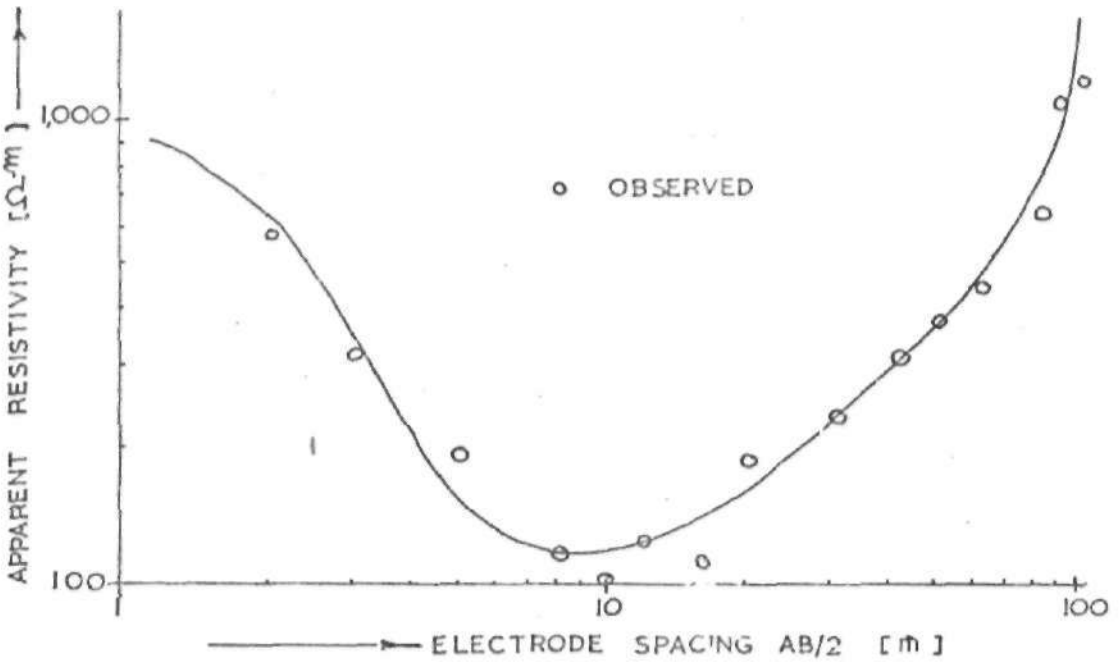


FIG. 6·2

VES 3N7.



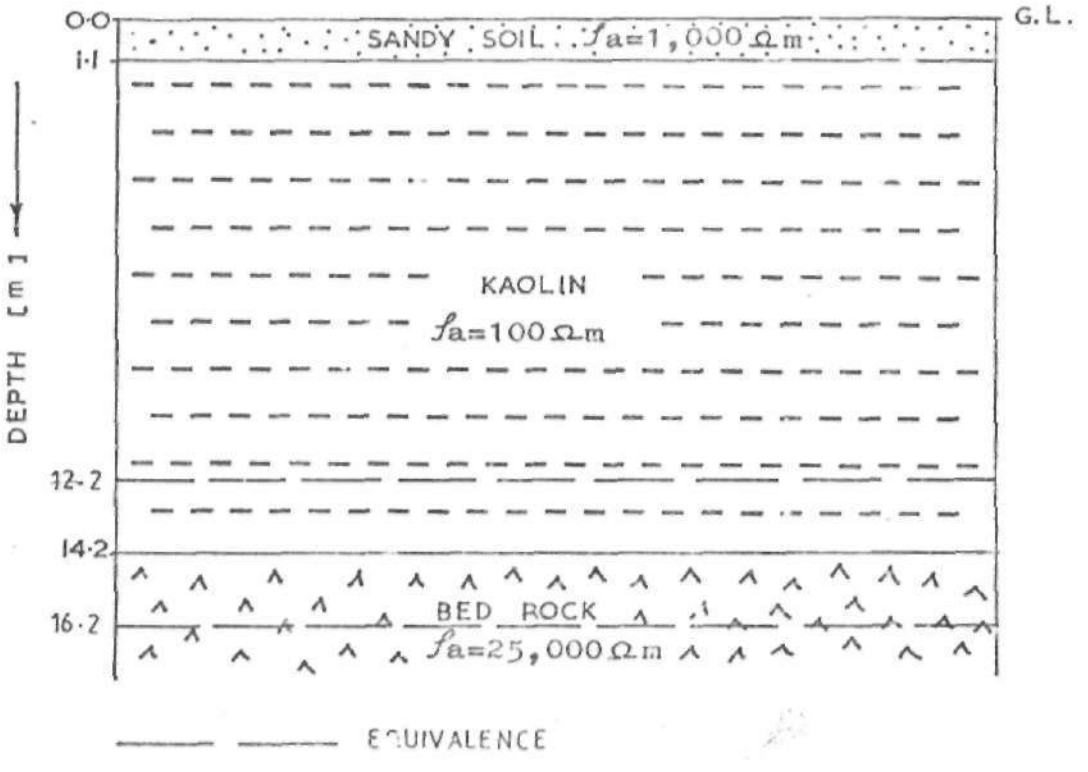
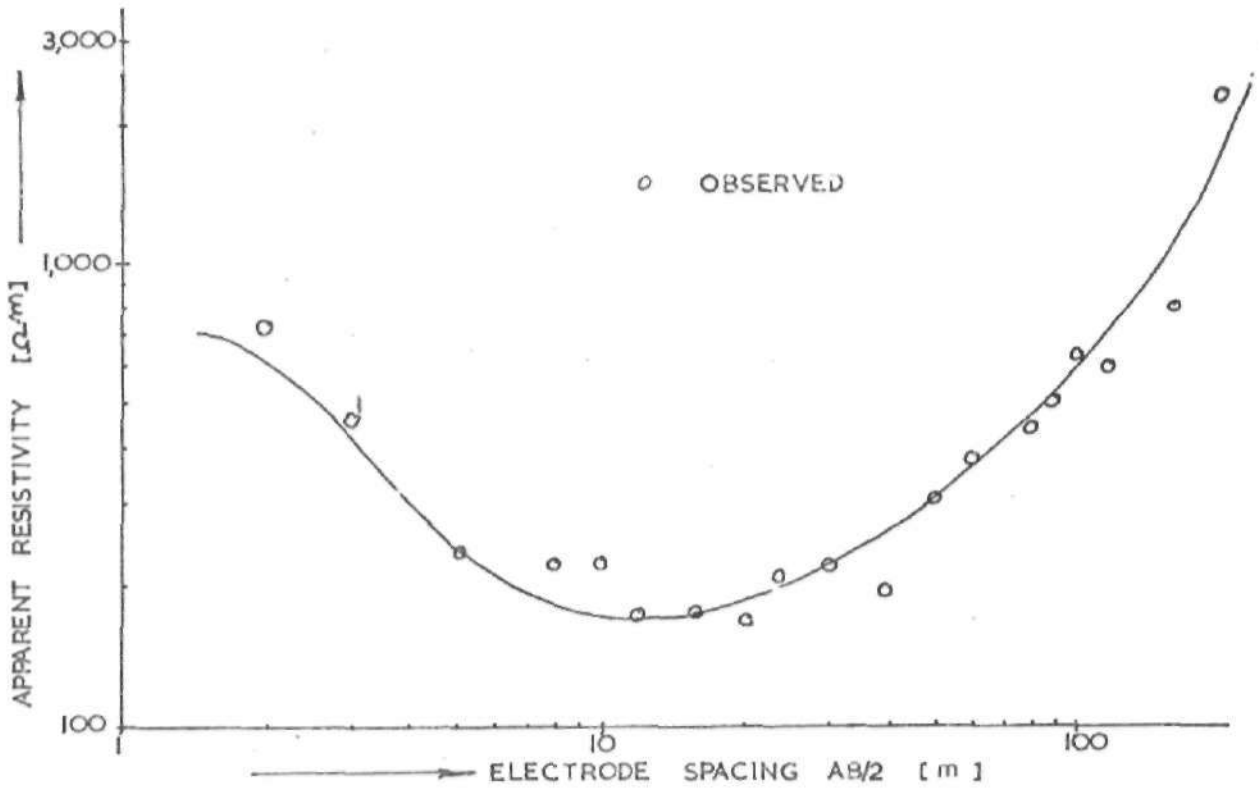


FIG. 6·3

VES 3N17.



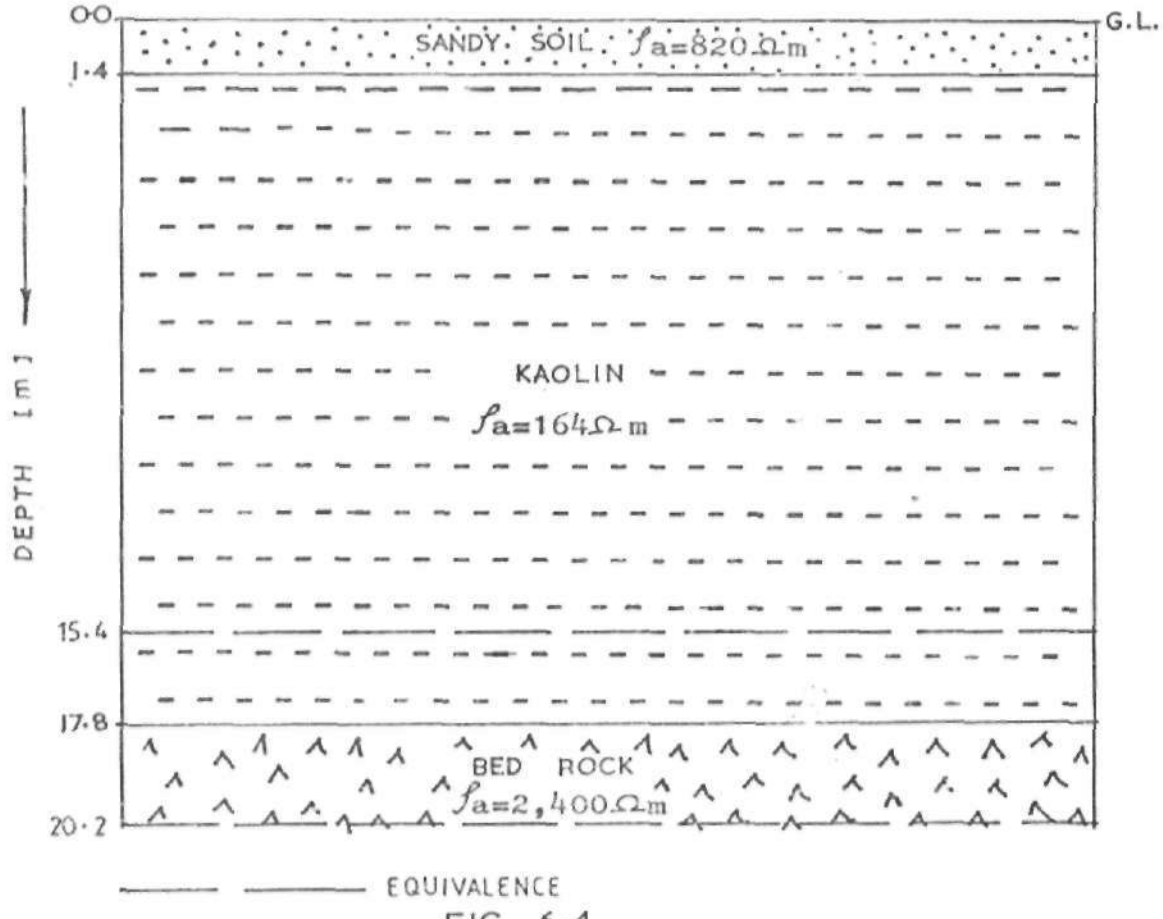
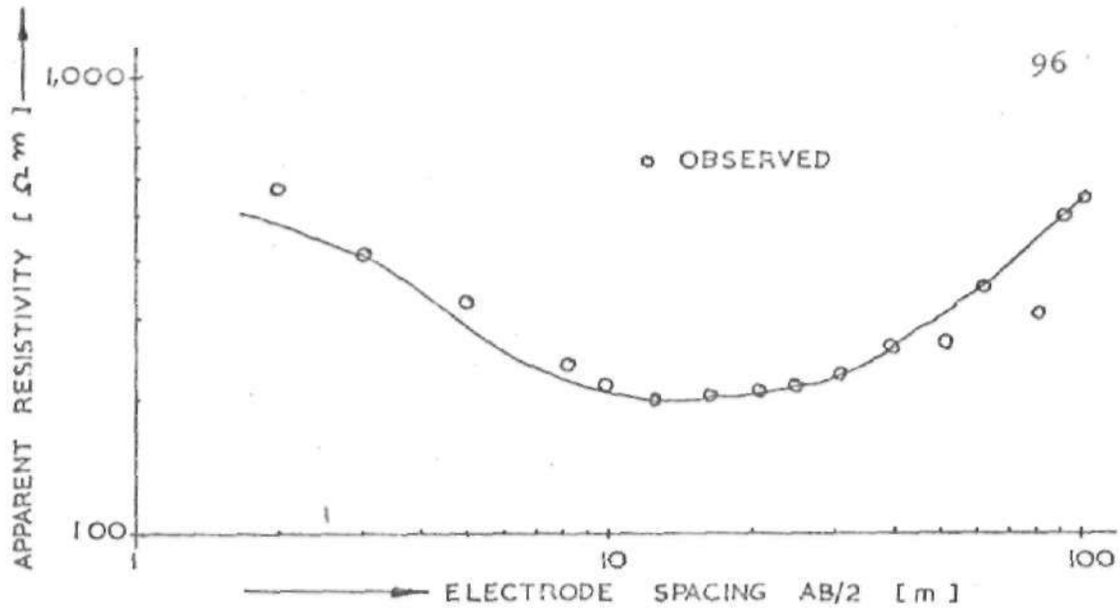


FIG. 6·4

VES IN9.



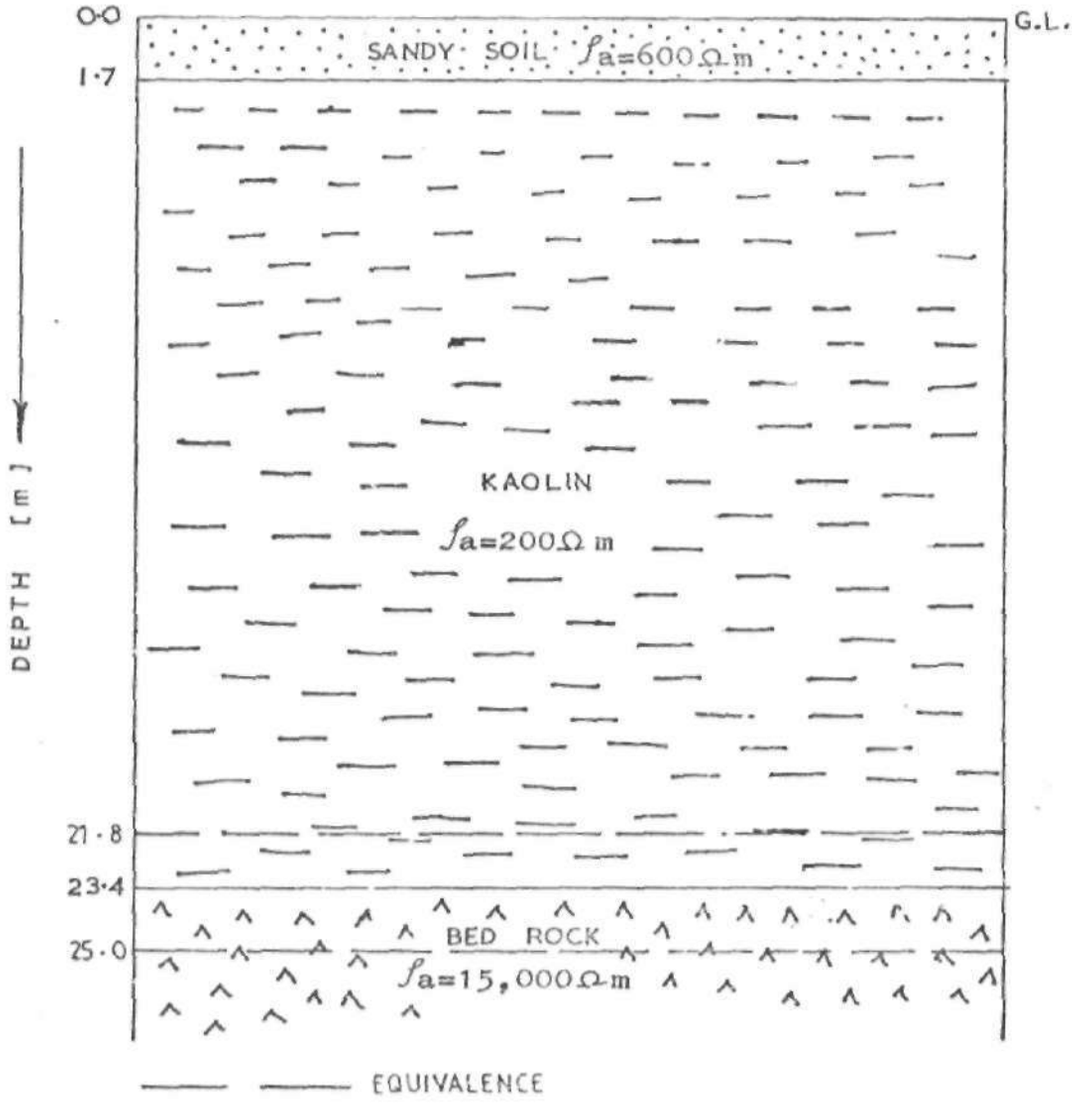


FIG. 6·5

VES 3NI.

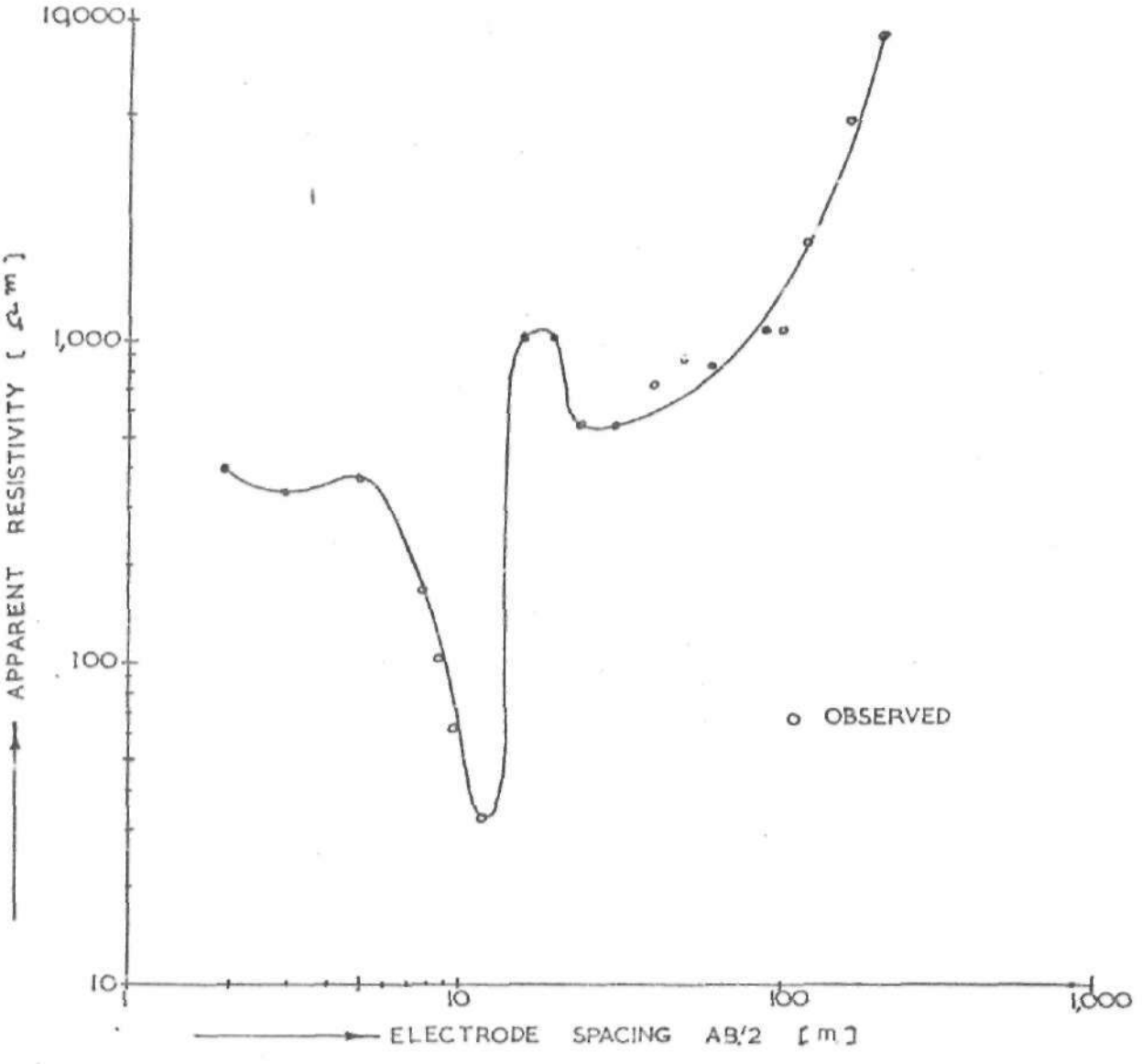


FIG. 6·6

VES 5N9.

for any accurate quantitative interpretation. The least resistive layer indicated on this profile with an approximate value of 20 to 30 Ω.m could also be associated with kaolin deposits.

Vertical soundings carried out at places of abnormally high resistivity upto 10^6 Ω.m (VES 3N13 and VES 2N9), Fig. 6.7 and 6.8, show a high degree of scatter in the data for any reasonable quantitative interpretation. It could be attributed to strong lateral heterogeneity at these locations.

6.3.2 Coefficient of Correlation and Equivalence:

The coefficient of correlation of both the actual and observed matched VES points was determined. This denotes the relationship between two random variables. High positive correlation denotes that the observed points follow closely the actual points. High negative correlation denotes that the observed points have a slope opposite to that of the actual points. For zero correlation there is no relationship between the two sets of points.

Correlation coefficient R is calculated by the formula:

$$R = \frac{n\sum_{i=1}^{n} x_i y_i - \left(\sum_{i=1}^{n} x_i\right)\left(\sum_{i=1}^{n} y_i\right)}{\sqrt{\left(n\sum_{i=1}^{n} x_i^2 - \left(\sum_{i=1}^{n} x_i\right)^2\right)\left(n\sum_{i=1}^{n} y_i^2 - \left(\sum_{i=1}^{n} y_i\right)^2\right)}}$$

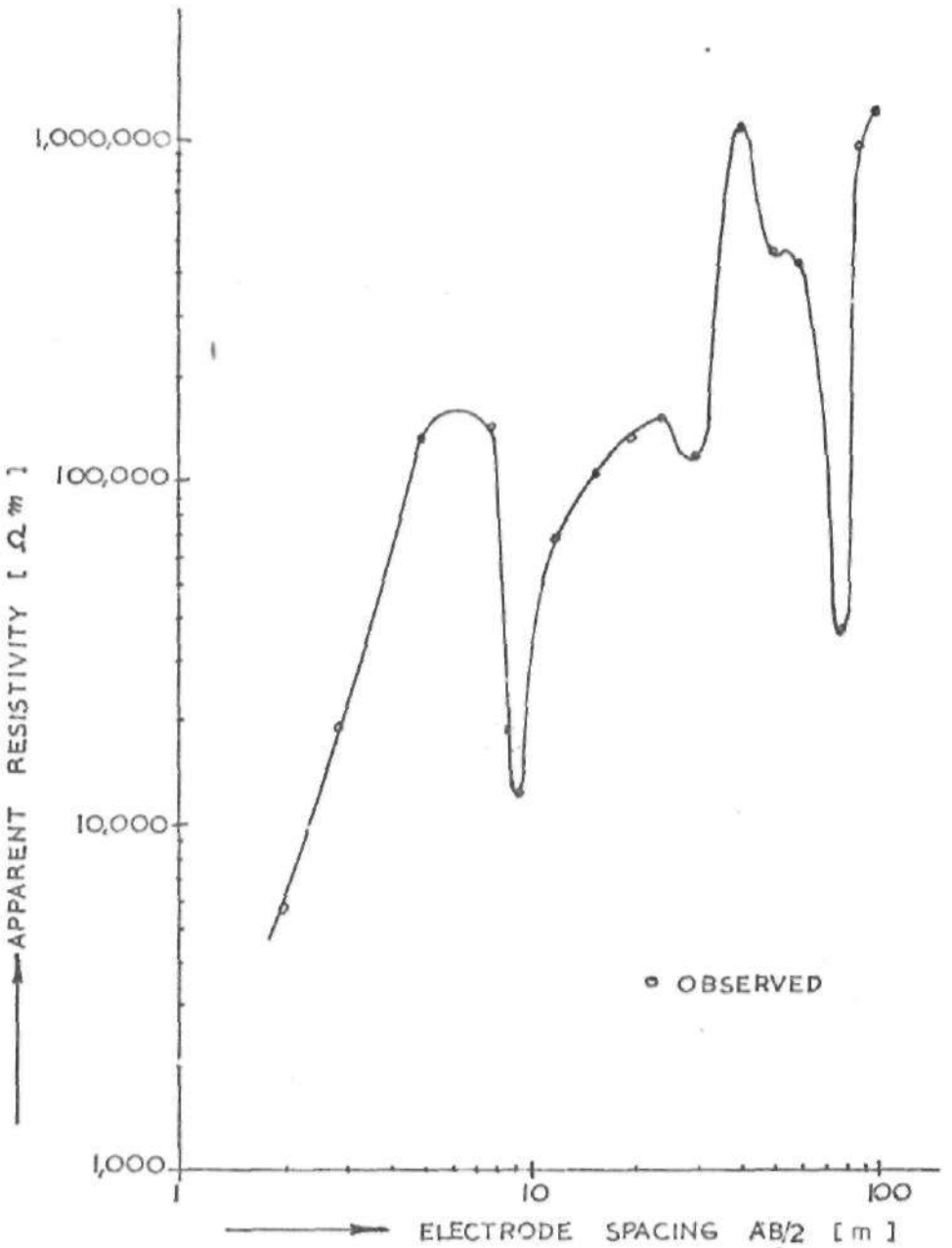


FIG. 6·7

VES 3N13

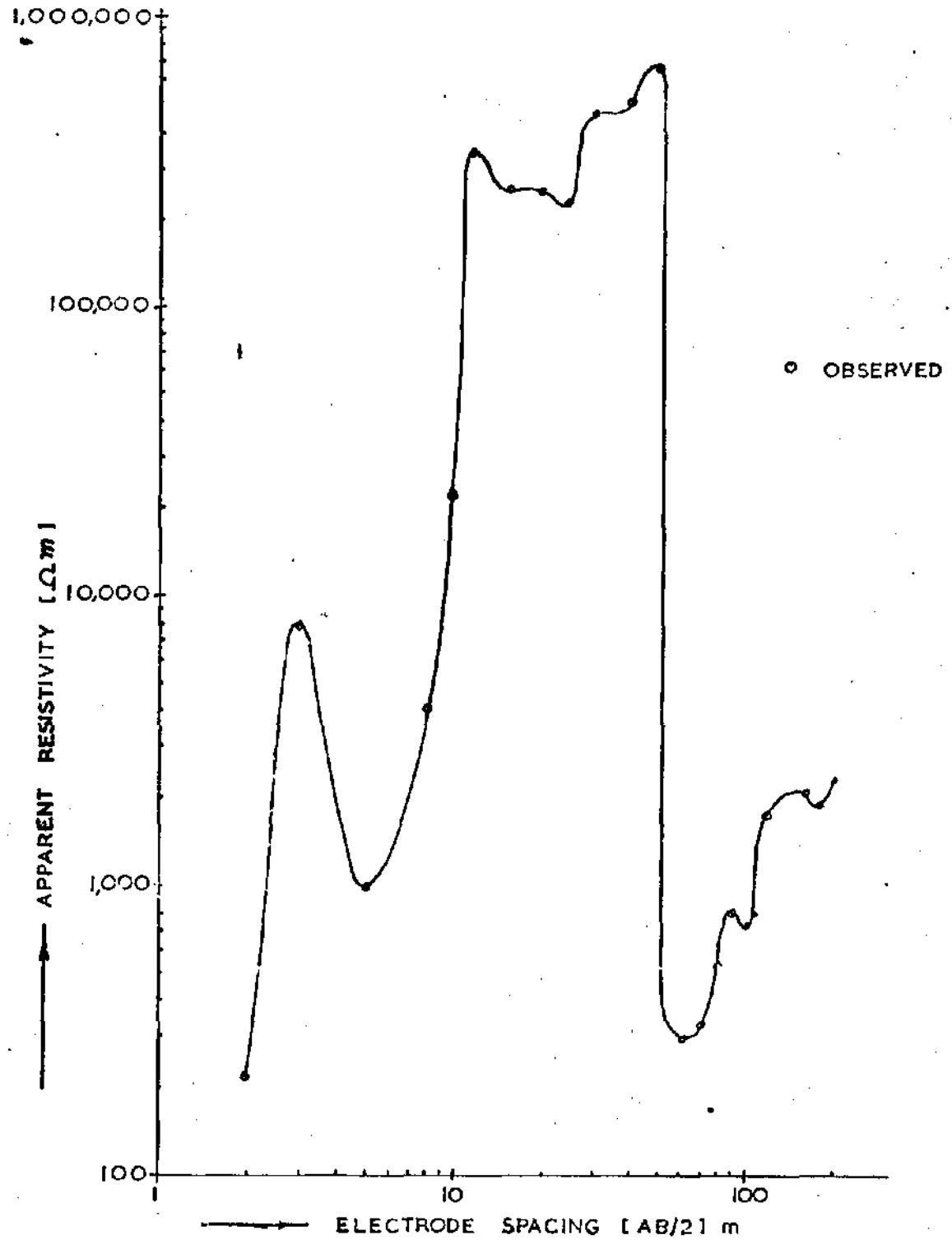


FIG. 6·8

VES 2N9.

where x and y are two variables.

The correlation coefficient values are given in Table 6.2. It would be observed that there is a very good correlation between the observed and actual points. The best correlation is at VES 3N7, followed by VES 1N9. The lowest correlation is at VES 3N1.

The equivalence problem arises where different layering configurations may give rise to identical field curves. H-type of curves are practically equivalent within certain limits if the ratio of thickness to apparent resistivity remains constant. Koefoed (1969) has developed a method based upon the properties of the raised Kernal function, K, a graphical method for determination of equivalent cases. He defined equivalence as given by the condition when the coefficient of the first order term must have a fixed value, which he denoted 'C'. The value of d_2/C corresponding to $\rho_2/\rho_3 = K$ could be found out from the graph for the determination of equivalent cases when $\rho_2/\rho_3 < 1$ (Koefoed, 1969). The value of Koefoed coefficient 'C' has been deduced for each VES using the appropriate combination of d_2, ρ_2, and ρ_3 values obtained and is given in Table 6.1.

To check the limits of equivalence for a given layer, arbitrary values of d_2' and ρ_2', whose quotient were equivalent to the best theoretical computed constants

TABLE 6.2

Correlation Coefficient of Actual and Observed VES Points.

VES	Correlation Coefficient
1N9	+ 0.99
3N17	+ 0.97
3N7	+ 0.99
3N1	+ 0.94

were substituted in h_2/ρ_2 to give a new set of theoretical curves that fitted the field curves. The thickness of the conductive layer was thus estimated by taking the value that gave the best theoretical fit. Some of the curves can give a unique solution to h_2/ρ_2, while others have a wide range.

6.3.3 Geological Deduction for area surrounding the Kaolin Pit from Isoresistivity Contours:

The apparent resistivity values calculated for certain similar depths for the seven different VES locations were plotted on the grid pattern. The AB/2 values chosen were 2, 3, 5, 8, 10, 12, 16, 20, 40 and 80 m. The resistivity values at these depths were contoured and are shown in Figs. 6.9a to 6.9j. A sub-surface section running from north to south cutting across the middle of the grid was drawn. It shows variation in resistivity with depth up to 20 m, Fig. 6.10.

From the diagram it would be seen that the region can be divided into four major sections with their resistivity values as follows:

ρ_1 = 1-200 Ω-m

ρ_2 = 200-500 Ωm

ρ_3 = 500-1,000 Ωm

ρ_4 = 10^3-10^6 Ωm

Referring to Fig. 6.10, the possible geological

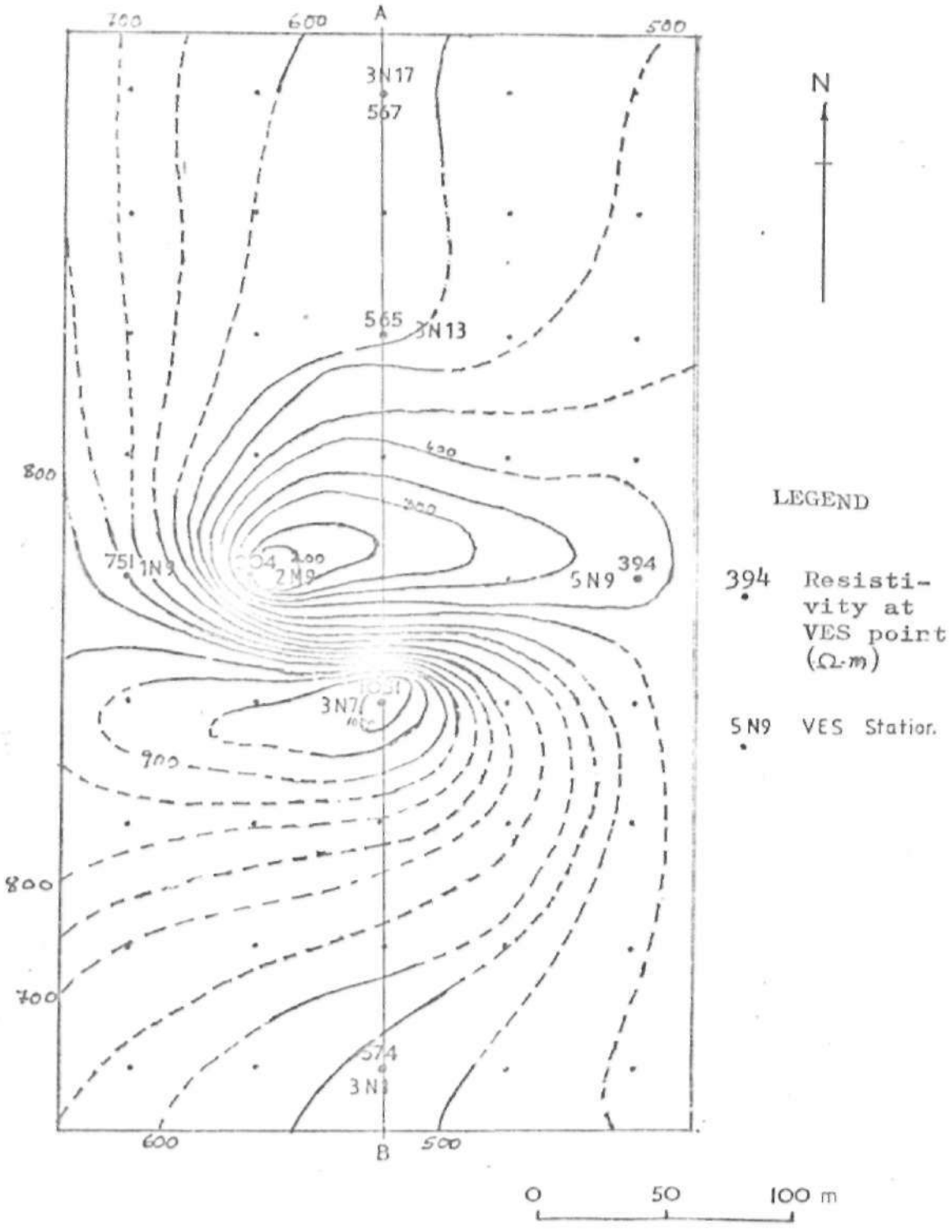


FIG. 6·9a

ISORESISTIVITY CONTOURED MAP AT AB/2 = 2 m

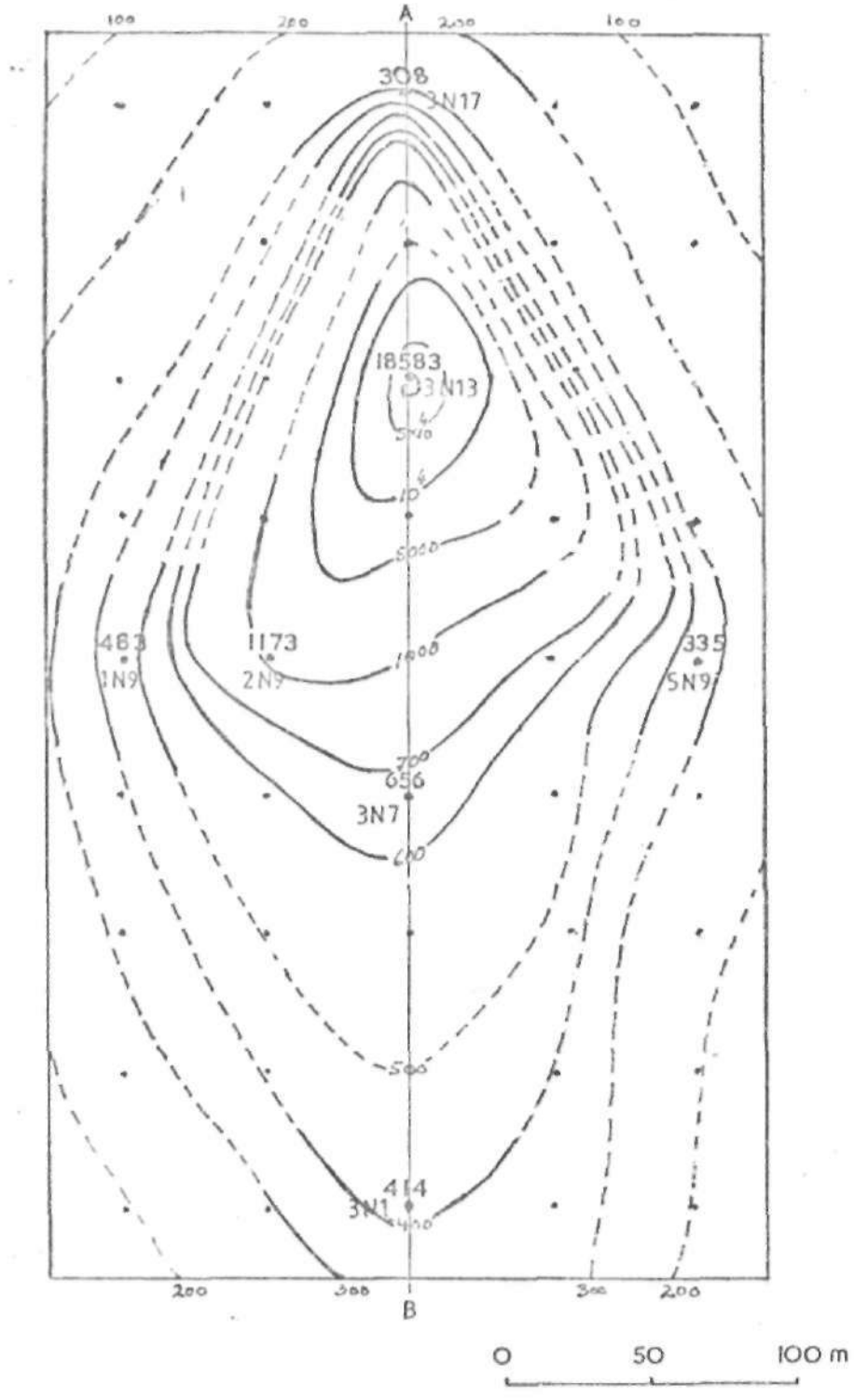


FIG. 6·9b.

ISORESISTIVITY CONTOURED MAP AT AB/2=3m

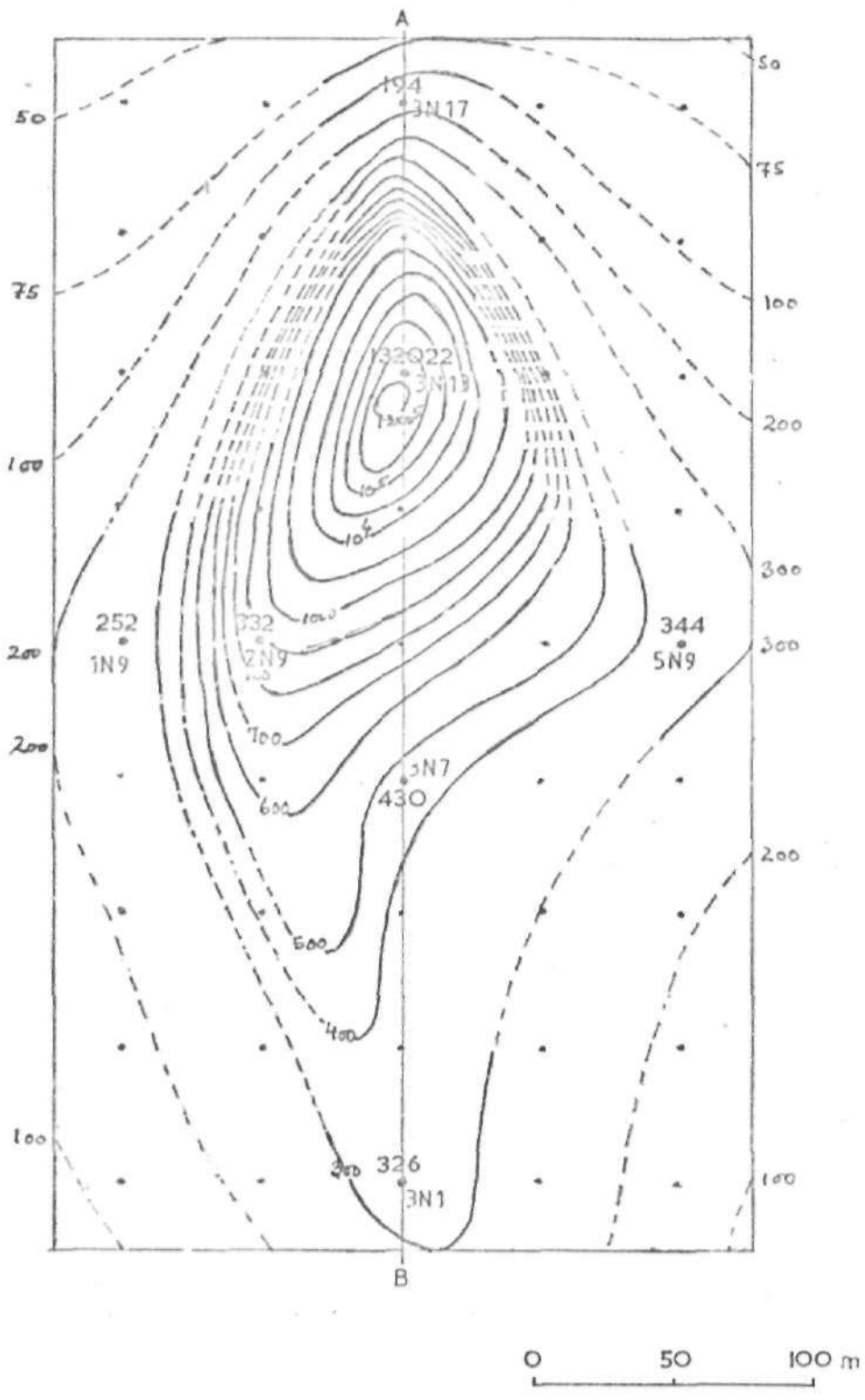


FIG. 6·9c

ISORESISTIVITY CONTOURED MAP AT AB/2=5 m.

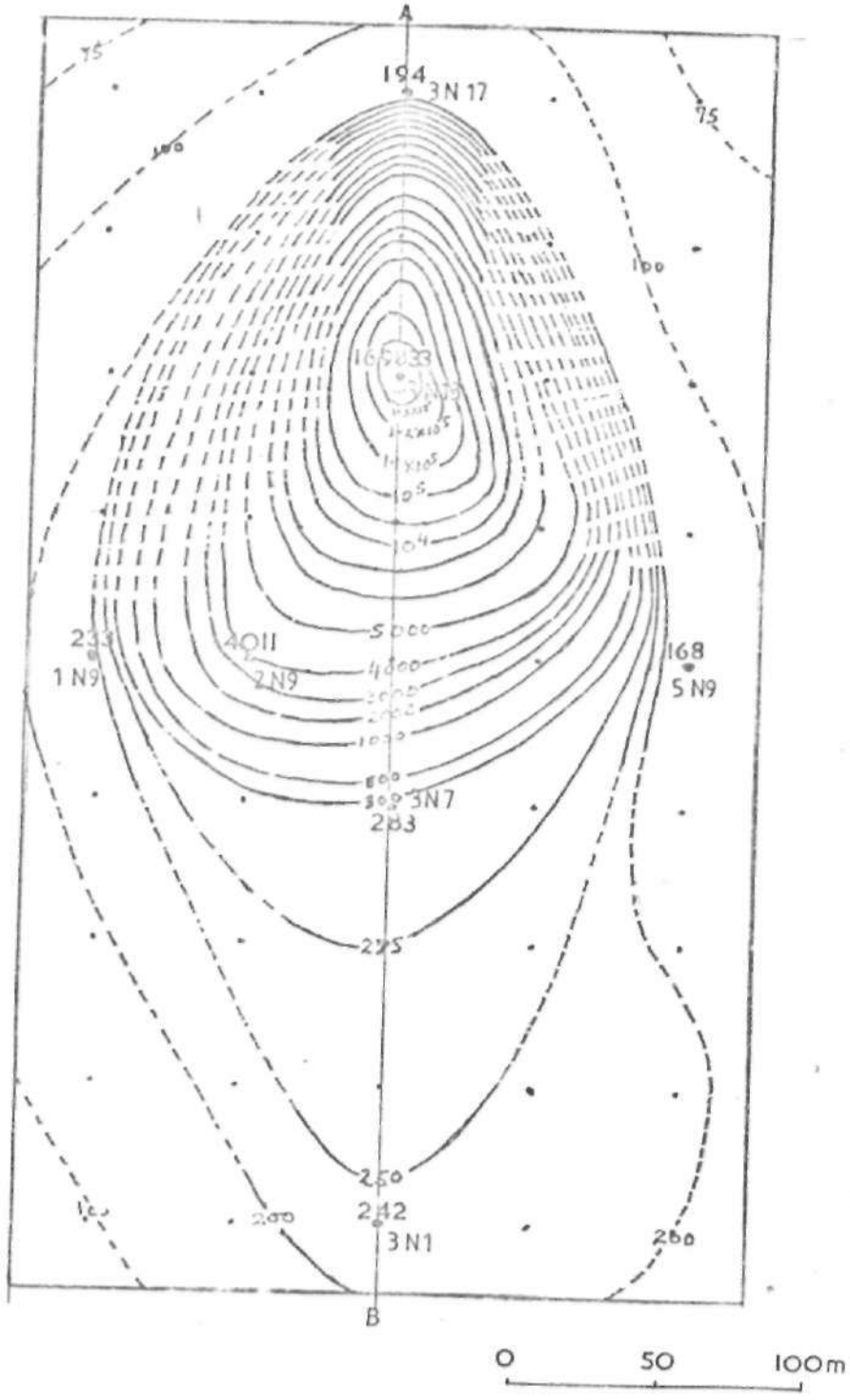


FIG. 6.9d

ISORESISTIVITY CONTOURED MAP AT AB/2 = 8 m.

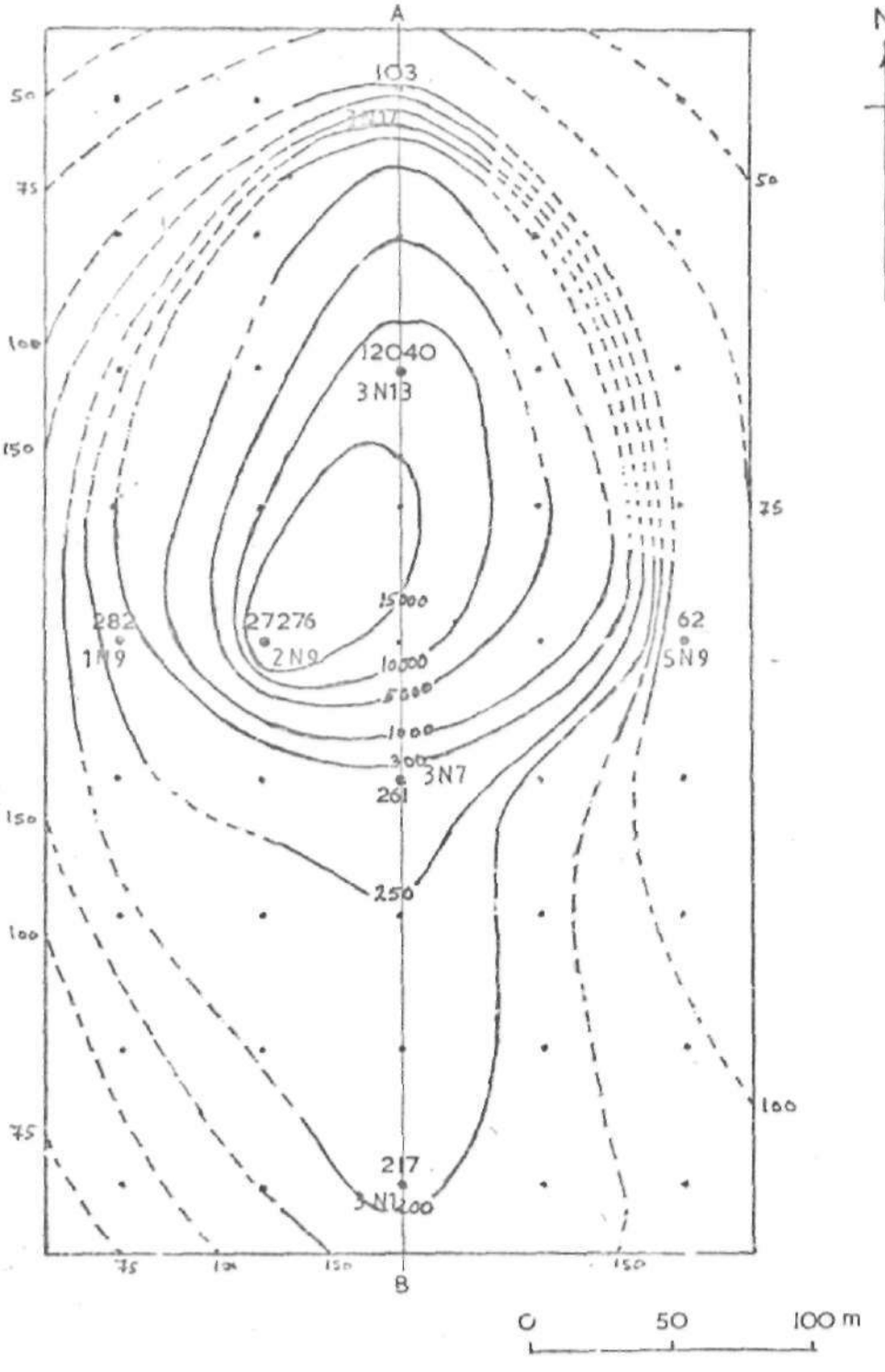


FIG. 6·9e

ISORESISTIVITY CONTOURED MAP AT AB/2 =10 m.

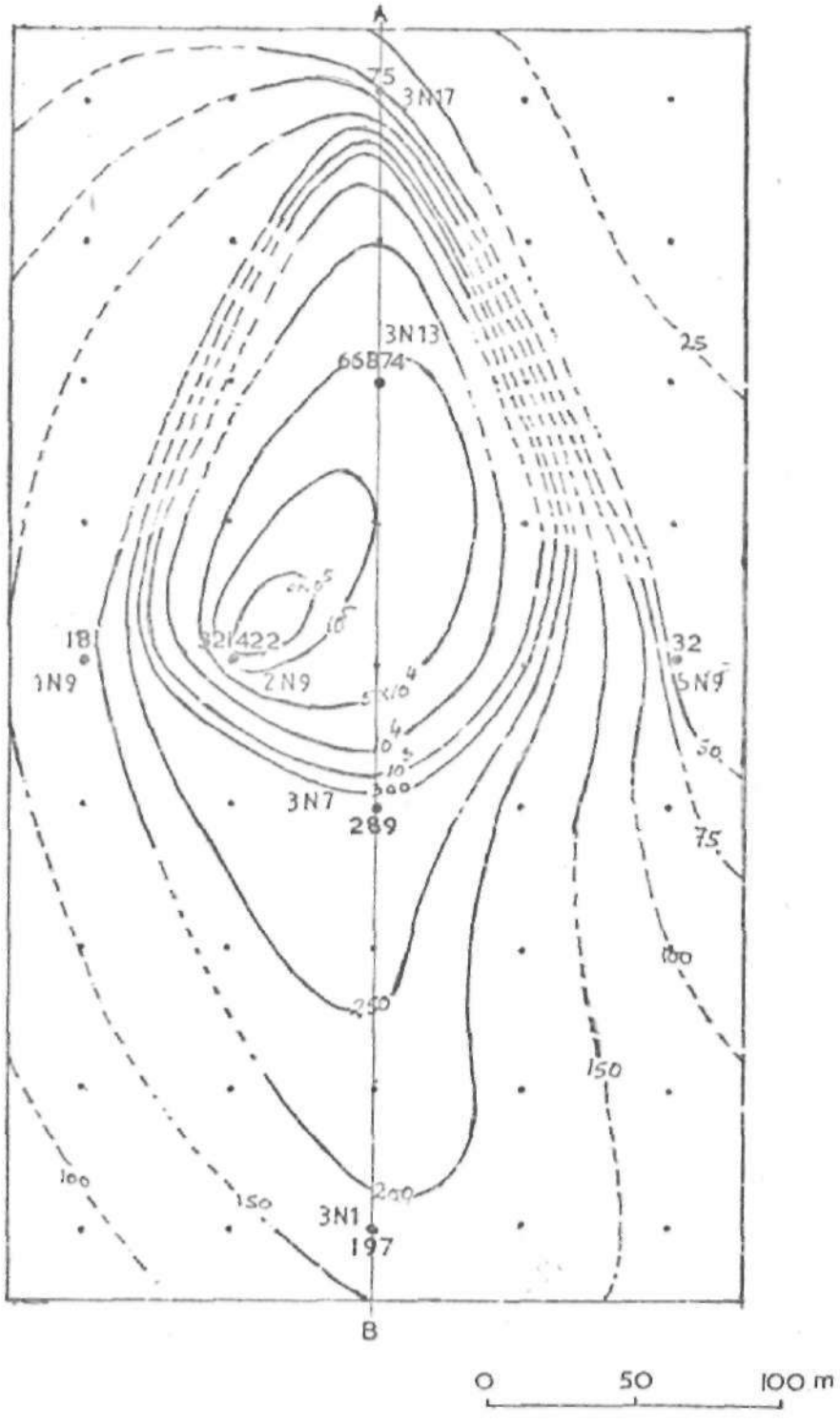


FIG. 6·9f

ISORESISTIVITY CONTOURED MAP AT AB/2 = 12 m.

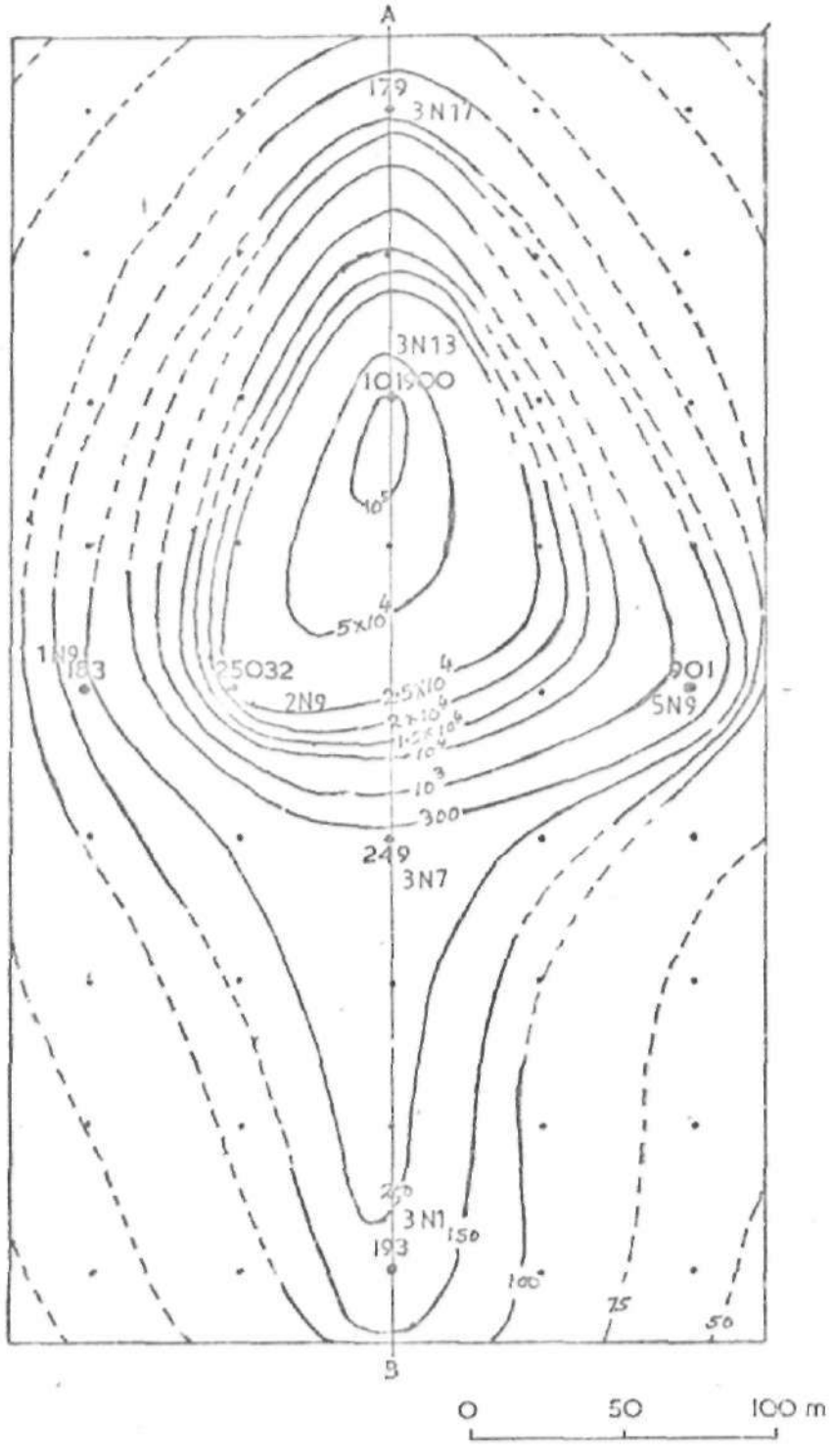


FIG. 6·9g

ISORESISTIVITY CONTOURED MAP AT AB/2 =16 m.

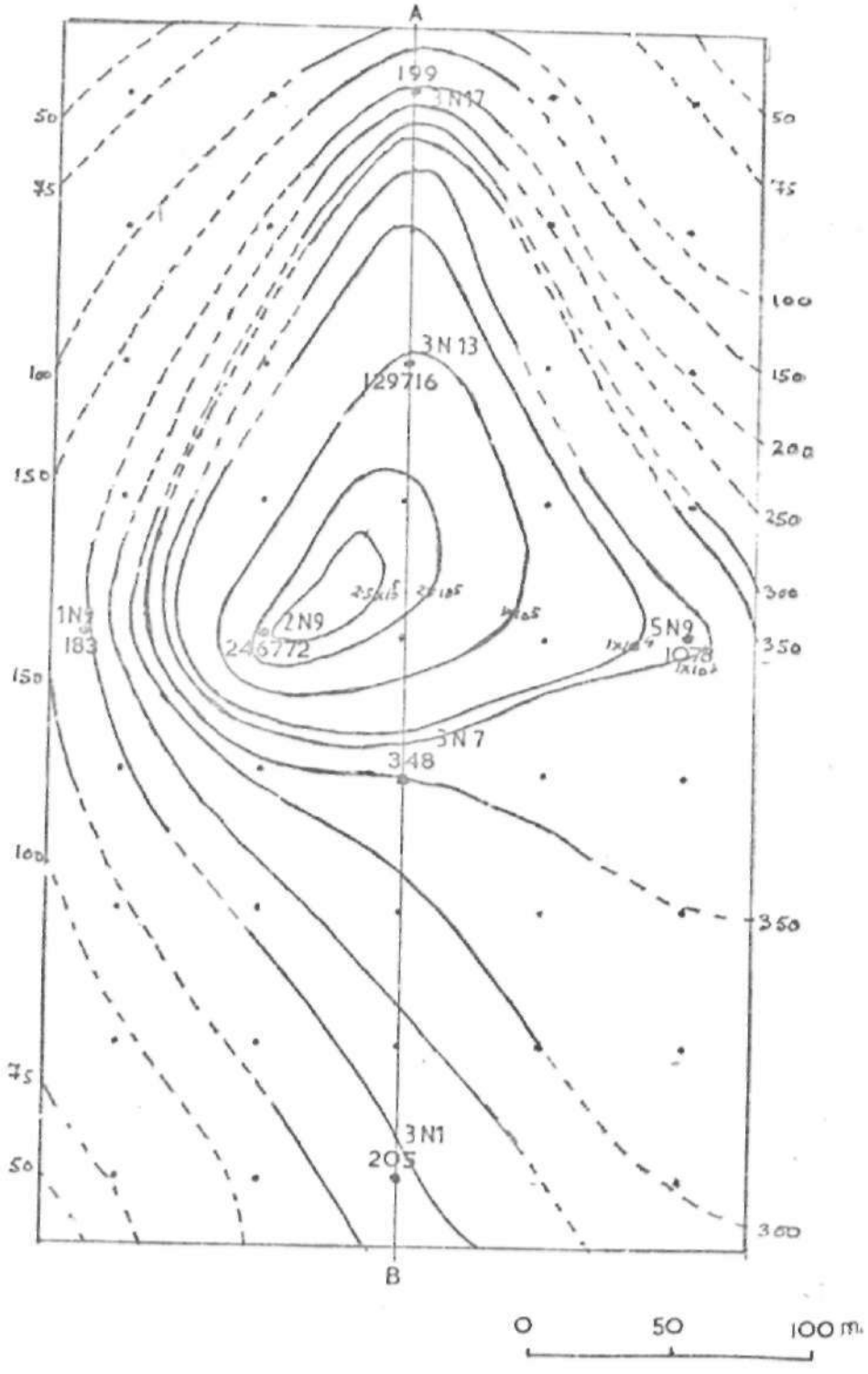


FIG. 6·9h

ISORESISTIVITY CONTOURED MAP AT AB/2=20 m.

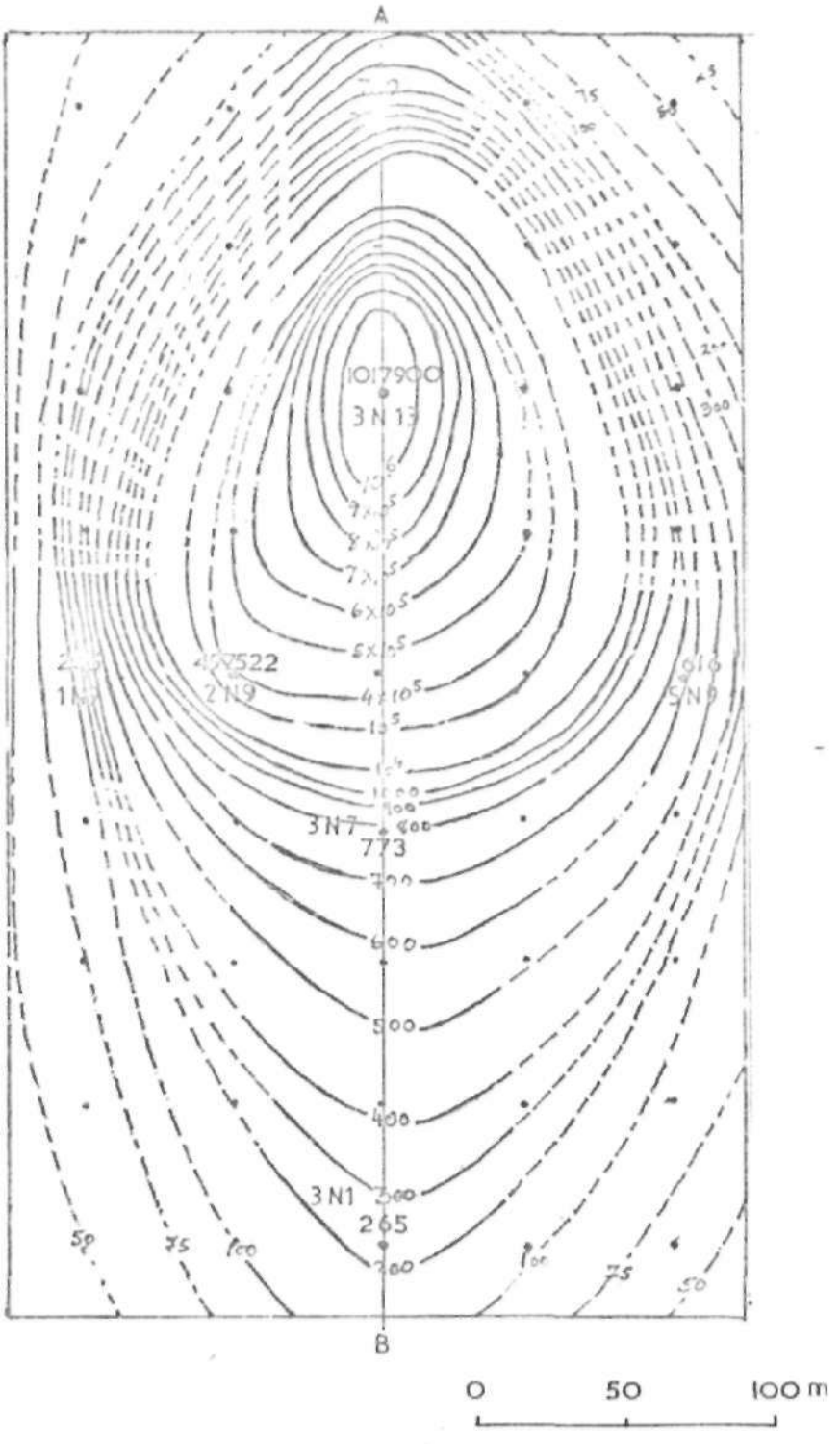


FIG. 6·9 i

ISORESISTIVITY CONTOURED MAP AT AB/2 =40 m.

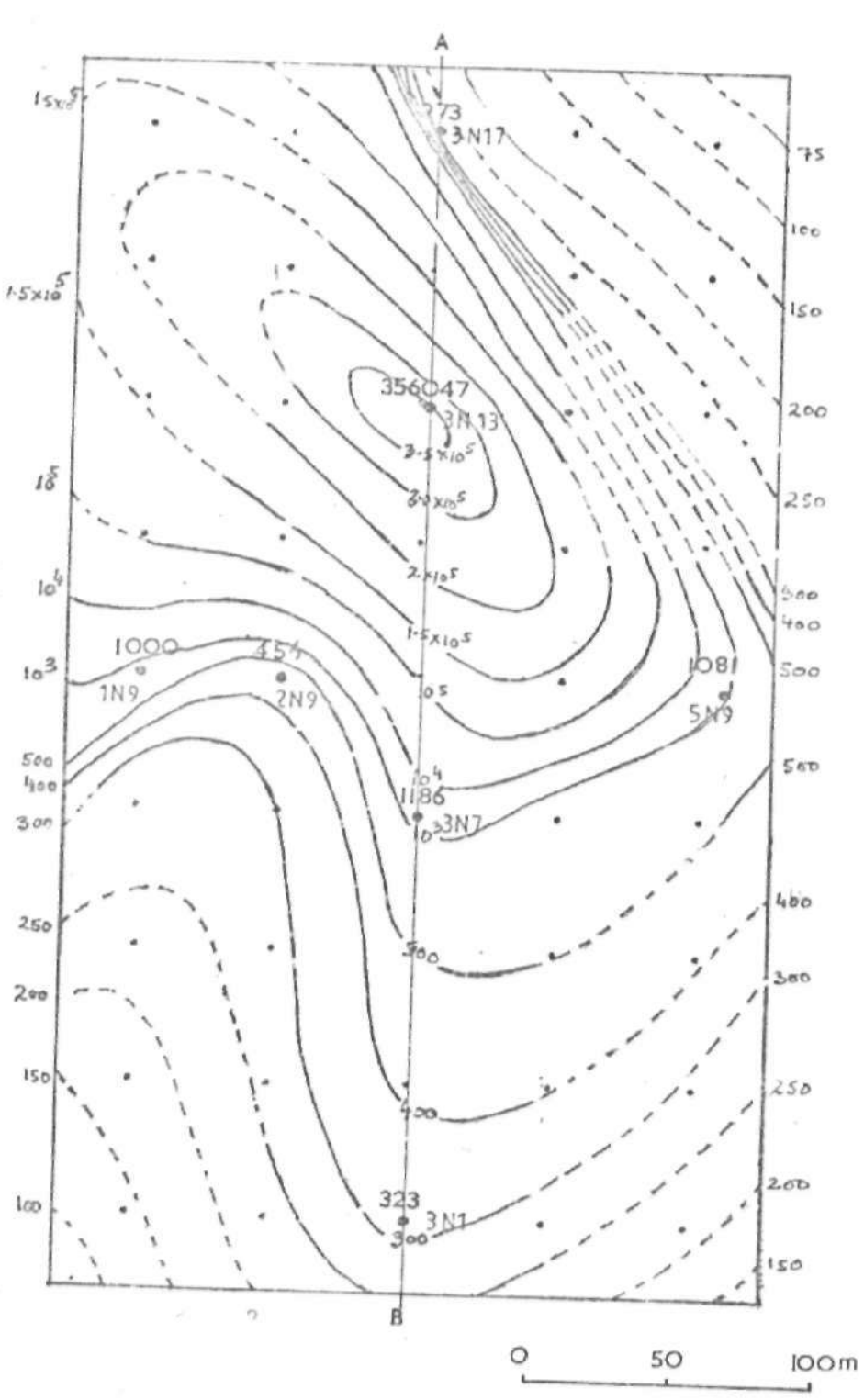


FIG. 6.9j

ISORESISTIVITY CONTOURED MAP AT AB/2 = 80 m.

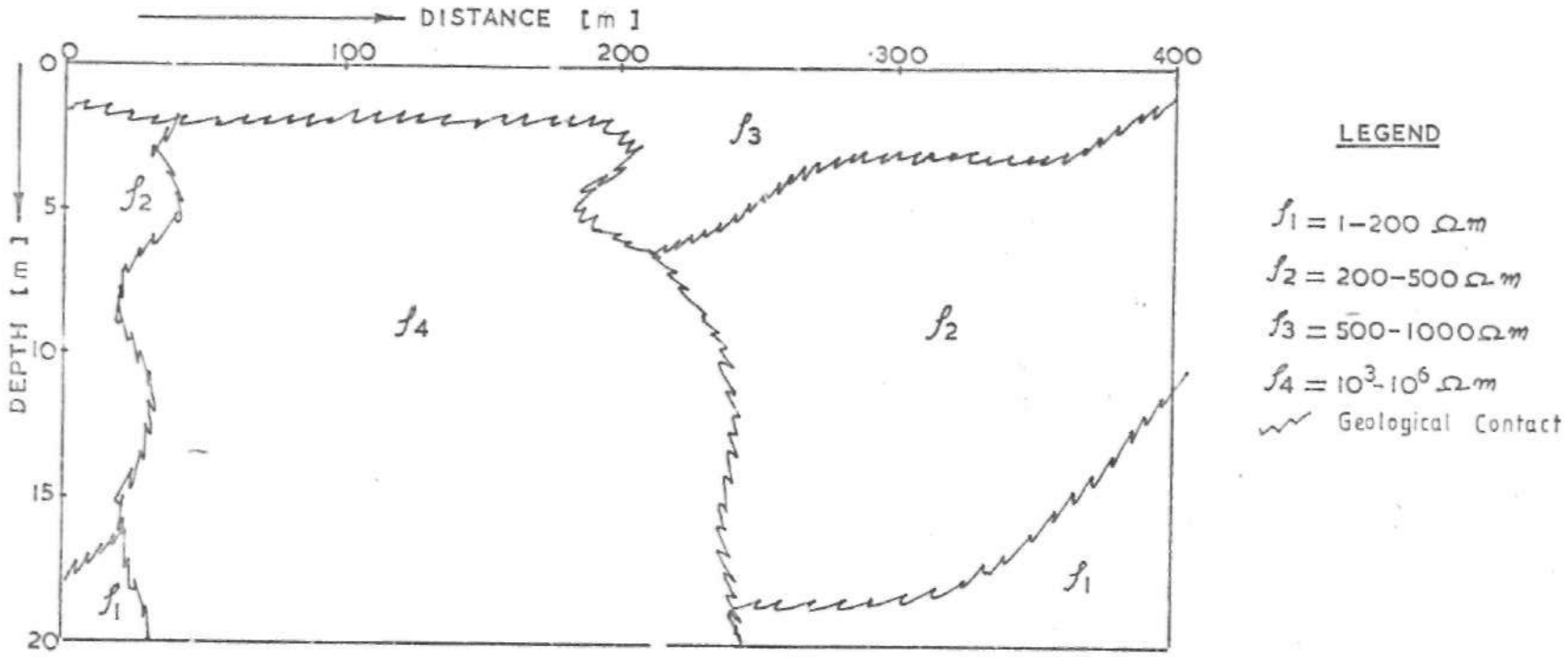


FIG. 6·10

CROSS SECTION OF THE SURVEYED AREA AS DEDUCED FROM THE VES RESULTS.

history of the area is deduced. As this region lies within the undifferentiated basement complex, the major rocks are granitic. It would be observed from Figs. 6.9b to 6.9j that there is a very high resistive body having an anomalous value of 10^3-10^6 Ω m in all these diagrams. This anomalous body is probably a burried outcrop or a ridge of granite, Fig. 6.11a. With passage of time, weathering of this ridge occured. The weathered decomposed material was deposited on the sides, and it formed a layer of low resistivity of value 1-200 Ωm, Fig. 6.11b. As the process of weathering of this anomalous body progressed, the deposition of the material continued in a way that the top most layer formed was of slightly higher resistivity value, 200-500 Ωm, Fig. 6.11c. This could be explained that the bottom layer was saturated with water. Then came the period of denudation after which there was deposition of fine wind-blown sand, thus covering the ridge completely and bringing the sub-surface to the present day topography, Fig. 6.11d.

Referring to Fig. 6.10 it would be seen that this anomalous body with resistivity ρ_4, of 10^3-10^6 Ωm lies beyond 2m below the ground surface and extends downwards. The top-most layer, ρ_3, having resistivity between 500-1,000 Ωm has a maximum depth of 6m and is most probably composed of dry sandy soil. It is underlain by another layer, ρ_2 of resistivity between 200-500 Ωm having varying depth and extending at certain points to a maximum

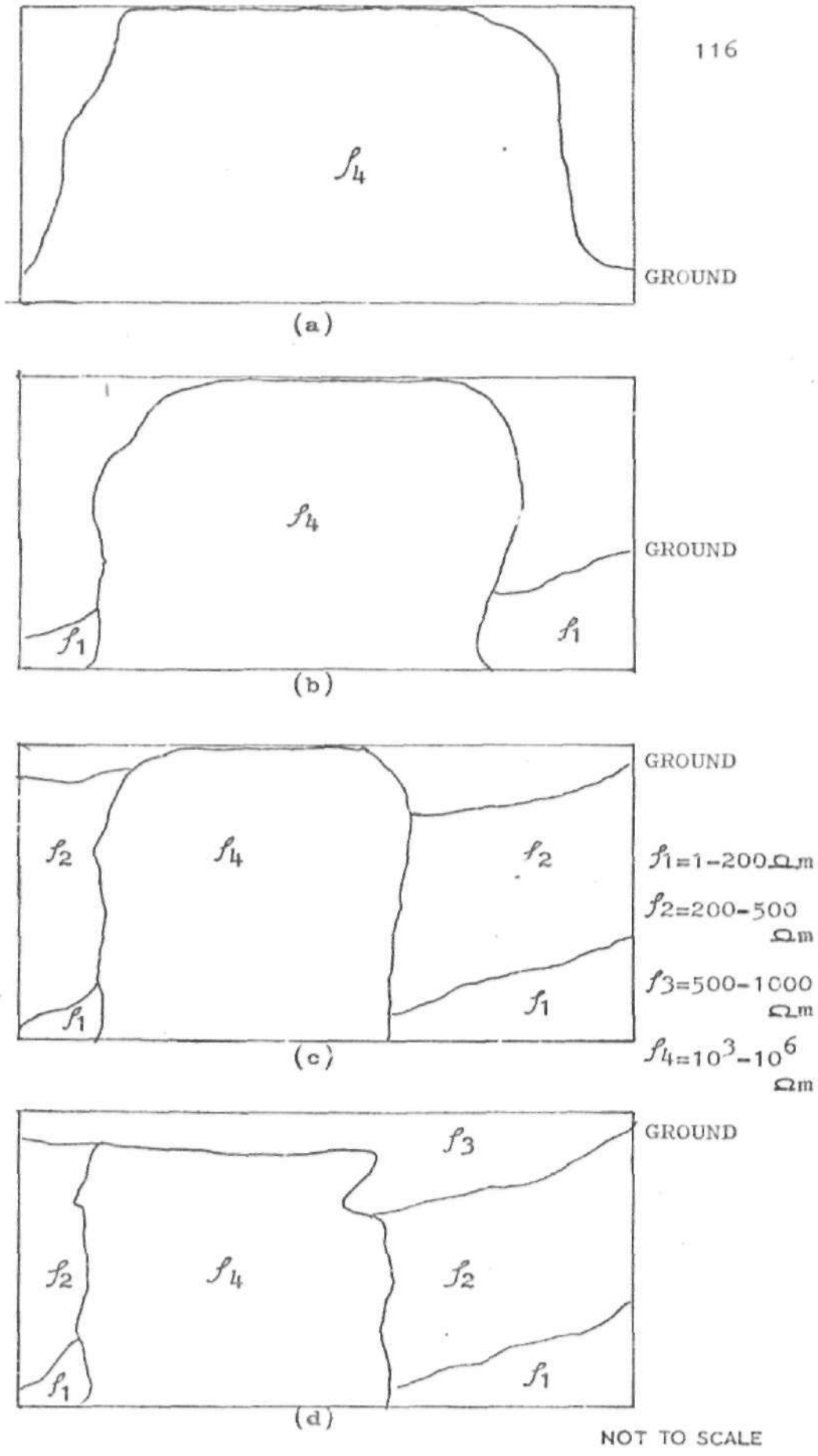


FIG. 6·11

SCHEMATIC DIAGRAM OF THE INFERRED SEQUENCE OF GEOLOGICAL HISTORY OF SURVEYED AREA.

of 19 m. This layer could be of kaolin. The layer, ρ_1 below this is of a slight less resistivity value. This also is probably composed of kaolin but highly saturated with water.

The ground water will tend to accumulate in the vicinity of the anomalous body which is impervious and shall act as a barrier. Such a site would be suitable for ground water prospecting as water will be obtained throughout the year.

6.3.4 Deduction of Sub-surface Structure of the Area Surrounding the Kaolin Pit from Anomalous Body Characteristics:

Referring to Figs. 6.9b-6.9j, it would be seen that resistivity contours at different depths for values 10^3 to 10^6 Ωm have appeared in almost all the figures. This range of resistivity values, from 10^3 to 10^6 Ωm has been attributed to an anomalous body, section 6.3.3.

The relief, maximum gradient, mean radius and area of this anomalous body for different depths was calculated, given in Table 6.3. Also graphs were drawn, Figs. 6.12 to 6.15. The relief showed the dominating effect of one layer over the other layer. From the maximum gradient, the contact points of different layers were obtained since maximum gradient is got just at the inflection points. The area and the radius of the anomalous body gave its volume.

TABLE 6.3

Calculated values of Relief, Maximum Gradient, Mean Radius and Area of Anomalous Body with respect to various Depths.

Depth (m)	Relief (Ω-m)	Maximum Gradient	Mean Radius (m)	Area x 10^3 (m^2)
3	23,500	5,020	64.1	12.53
5	120,700	5,000	56.3	10.06
8	125,000	4,201	83.4	24.49
10	16,570	2,405	73.7	25.00
12	58,075	705	69.8	20.03
16	130,000	760	87.6	28.32
20	225,000	5,203	76.0	27.24
40	740,565	15,008	93.8	31.00
80	421,780	4,108	149.6	76.57

TABLE 6.4

Calculated Volume of Anomalous Body with respect to Depths.

Depth (m)	Volume x 10^4 (m^3)
3 - 7	3.75
7 - 11	10.72
11 - 19	15.98
19 - 80	272.25

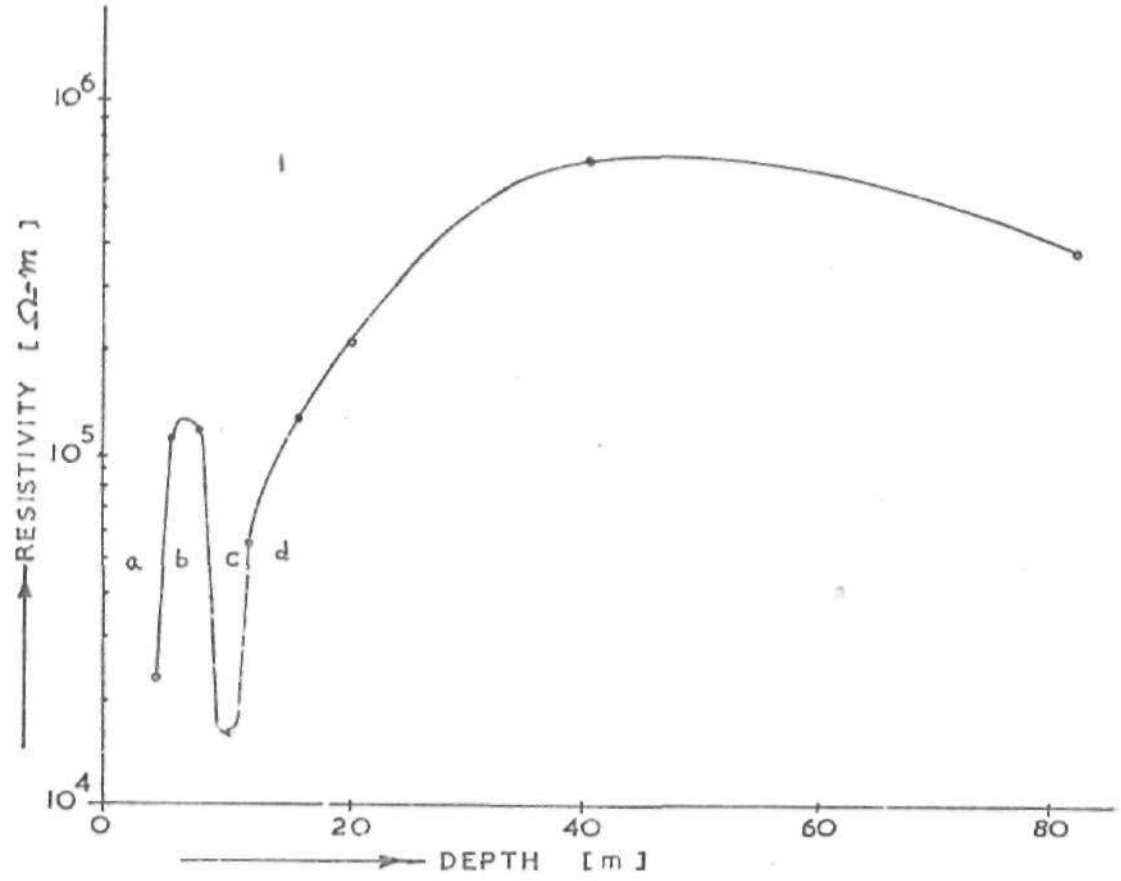


FIG. 6·12

GRAPH SHOWING VARIATION IN RESISTIVITY RELIEF WITH DEPTH IN THE SURVEY AREA.

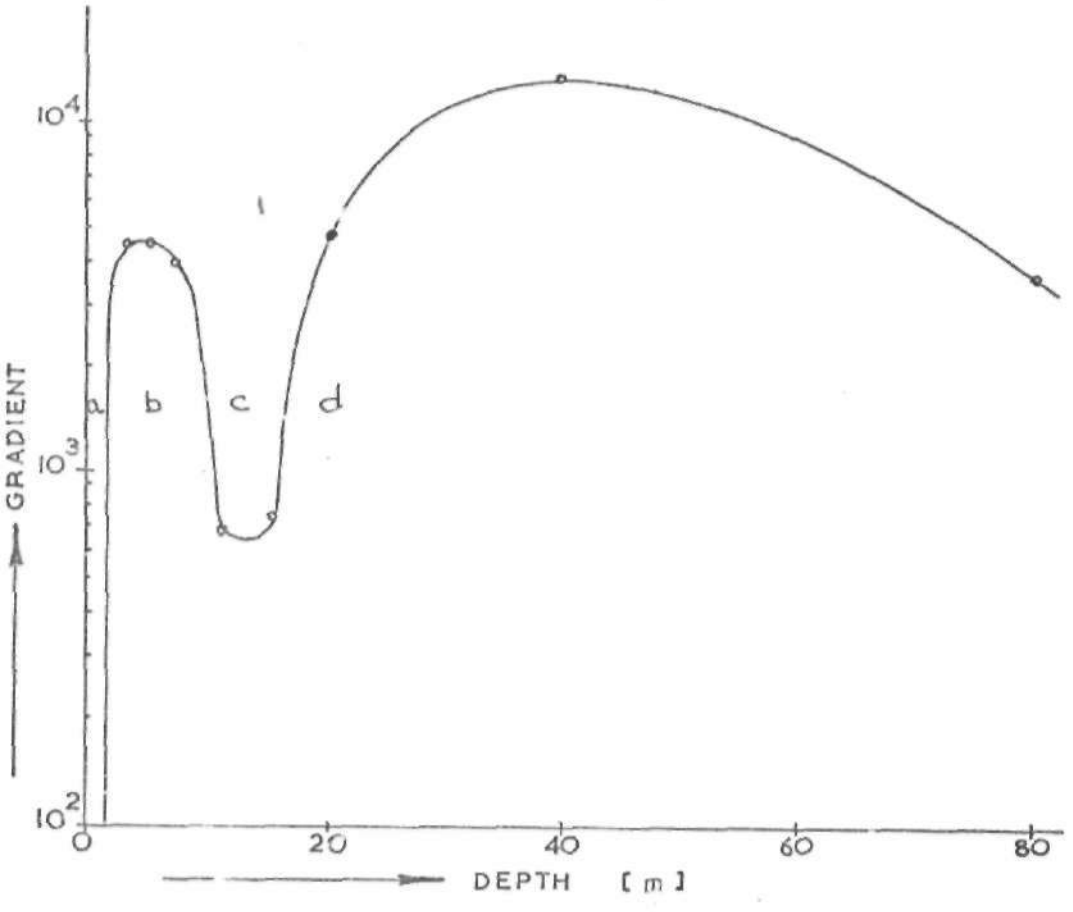


FIG. 6·13

GRAPH SHOWING THE VARIATION IN MAXIMUM GRADIENT WITH DEPTH IN THE SURVEY AREA.

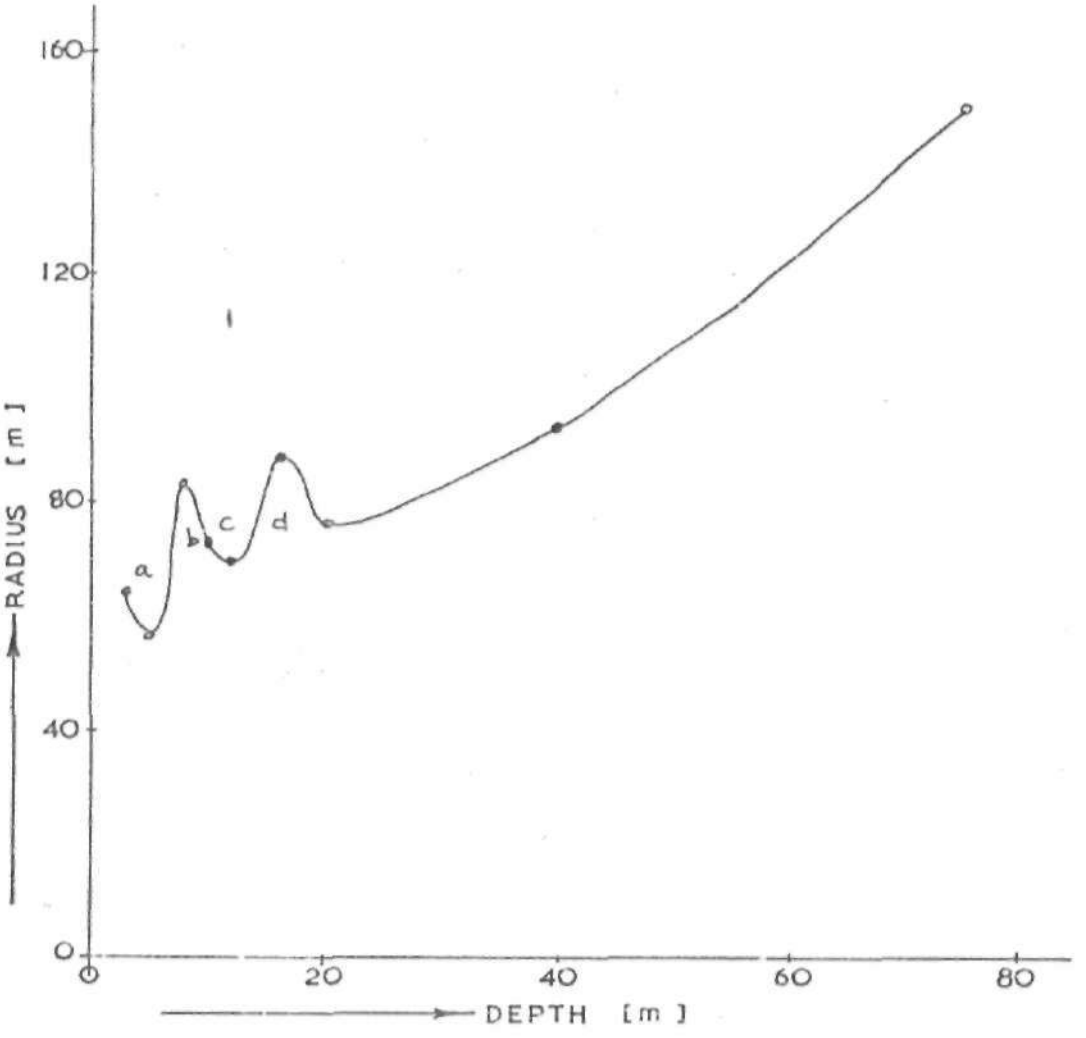


FIG. 6·14

GRAPH SHOWING THE VARIATION IN MEAN RADIUS WITH DEPTH IN THE SURVEY AREA.

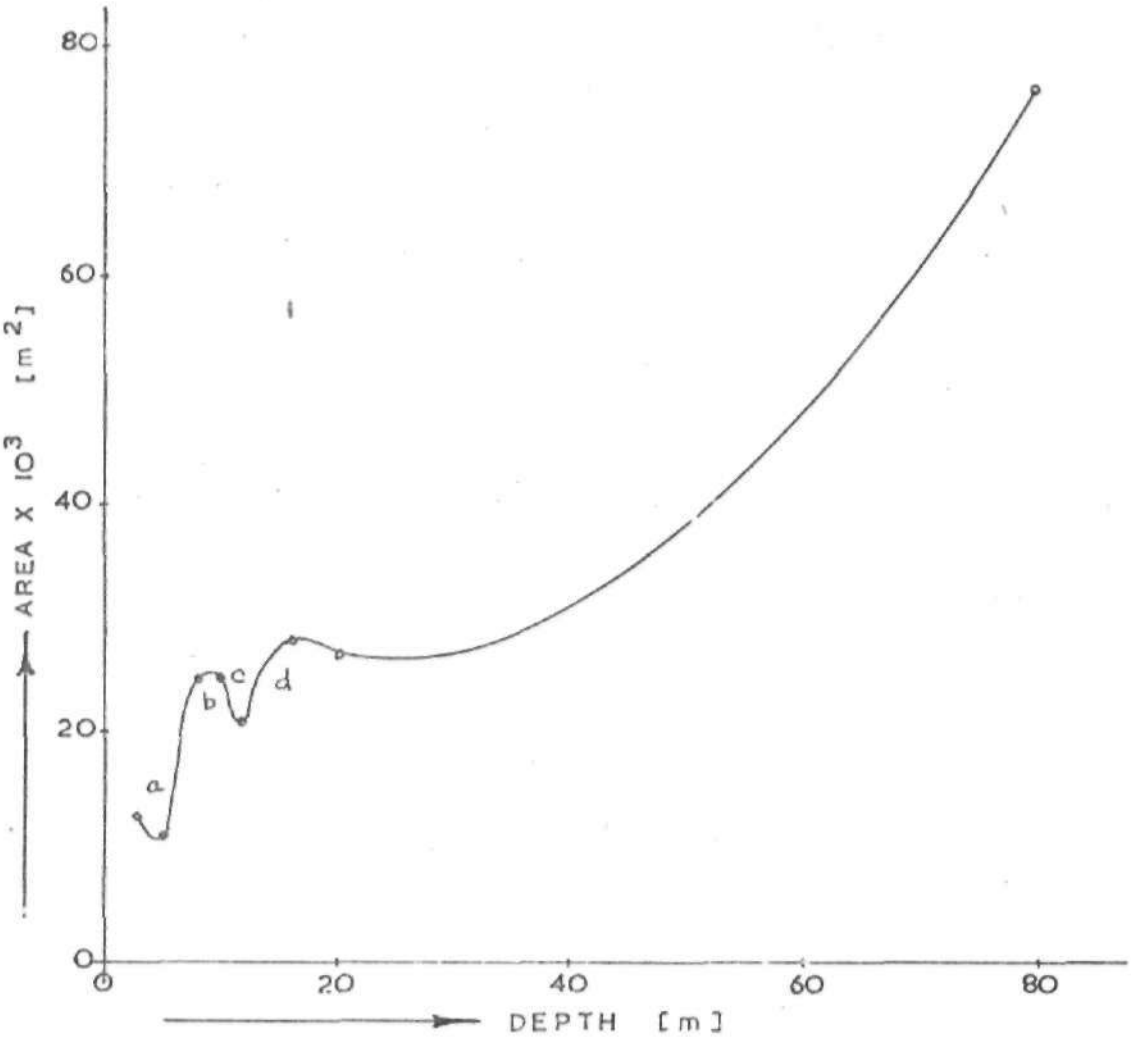


FIG. 6·15

GRAPH SHOWING THE VARIATION IN AREA WITH DEPTH IN THE SURVEY AREA.

The relief of the anomalous body was found by removing the background regional resistivity of the area at various depths. This graph gives a sort of resistivity log, Fig. 6.12. It can be seen from this figure that there are in all four layers and an anomalous body interacts with three different layers in the first 20m depth, which is indicated by the high and low resistive values. The fourth, 'd', layer, which is after 20 m depth could be part of the basement complex. This is in agreement with the lithology of the borehole, Fig. 2.5, and the geology of the sub-surface in section 6.3.3. The third layer 'c' is of a lower resistivity value than the second layer 'b' which is also in conformity with the findings in the previous section. The first layer 'a' has the lowest resistivity value from the relief graph. This may be due to the reason that it is a very thin layer and does not interact with the anomalous body.

The maximum gradients of this anomalous body at various depths are shown in Fig. 6.13. As would be seen from the graph, the contact points are between the four different layers. The first layer is at 2 m depth, the second layer ranges from 2 to 12 m, the third layer from 12 to 17 m and the fourth layer is encountered at depth greater than 17 m. This to a fair degree conforms with the depth of different layers deduced from the borehole data. The differences in depth of these layers could be due to the fact that the borehole is located 5.5 km away

from the survey area. The shallow thickness of 2 m of the first layer could be the result of deposition and or erosion at this location.

The area enclosed by the contour for resistivity value of 10^3 Ω.m, Figs. 6.9b to 6.9j, was determined by using a planimeter. The mean radius of the anomalous body was calculated from Figs. 6.9b to 6.9j by measuring the major and minor axis (as the anomalous body is of elliptical shape in these figures); thus finding its average radius. Figs. 6.14 and 6.15 show that the anomalous body is increasing at an exponential rate after 19 m depth. From the area diagram, the volume of this body was found out for different depths by fitting simple geometrical figures to the curves and a histogram was drawn, Fig. 6.16. The volumes are given in Table 6.4.

6.4 Resistivity Profiling:

The object of electrical profiling or mapping is to detect the lateral variation in apparent resistivity of the sub-stratum within a predetermined depth range. Under normal conditions, the effective depths of penetration of the current is considered roughly equal to the separation of the electrode. However due to the non-homogenous sub-surface, the assumption may not be fully true. During the survey process, the changes in strata lying under the path of the survey and above a depth roughly equal to the electrode separation could be

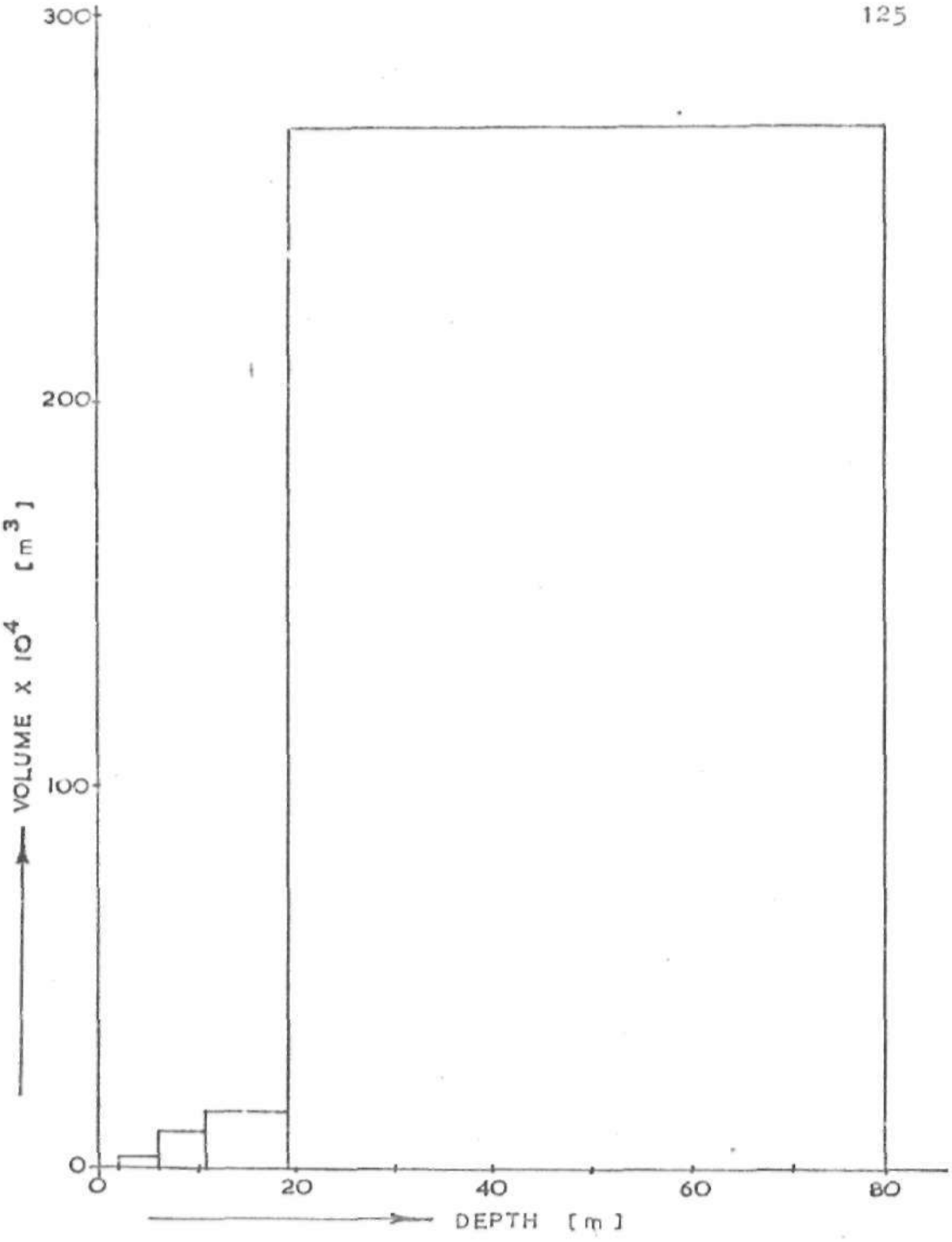


FIG. 6·16

ESTIMATED VOLUME OF HIGH RESISTIVITY ANOMALOUS BODY.

reflected in the reading.

During resistivity profiling, the entire electrode configuration was moved along the traverse at regular intervals. The Wenner profiling method, Fig. 3.3, using electrode spacings of 10 and 20 m chosen on the basis of the sounding curves was used. Profiling was done in both east-west and north-south directions. The apparent resistivities were calculated using equation 20 in chapter 3 and plotted against distance as shown in Figs. 6.17 and 6.18.

6.4.1 Interpretation of Resistivity Profiling:

A close investigation of the east-west profiling for 10 and 20 m electrode separations reveals that there is a sharp lateral contact between two different types of media, one of low resistivity range, 1 to 400 Ωm, and the other from 2,000 to 94,000 Ωm, Fig. 6.17. The low resistivity values could be attributed to kaolin while the high resistivity values could be attributed to granitic rocks within the basement complex. The effect of this highly resistive zone is more detectable using 20 m electrode spacing than at 10 m electrode spacing even though at few places such as 11N1, it is the reverse.

An anistropy effect was observed when profiling was done in the north-south direction, Fig. 6.18, even though the actual strike of the bedding plane was not

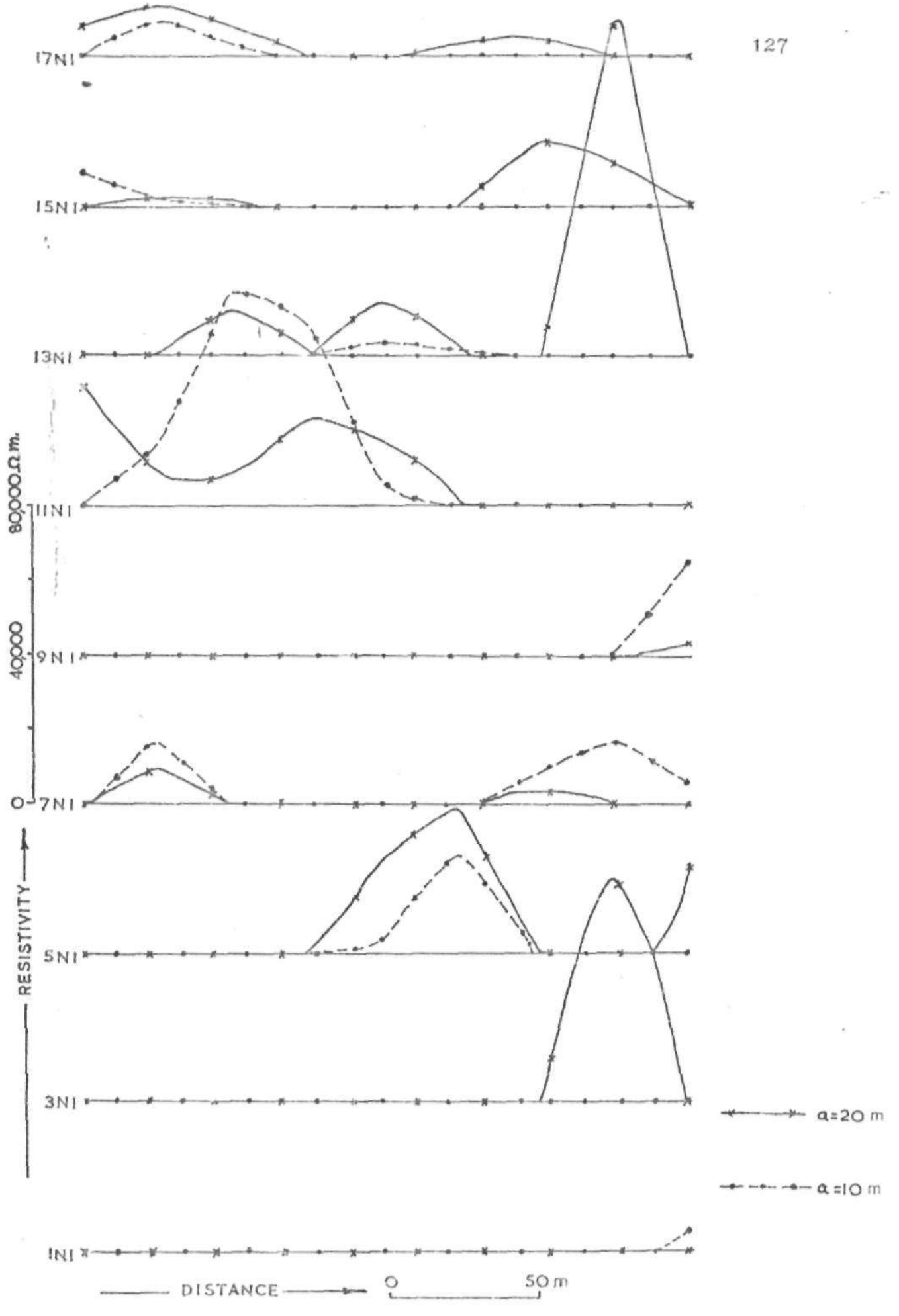


FIG. 6·17

WENNER RESISTIVITY PROFILING IN THE EAST-WEST DIRECTION.

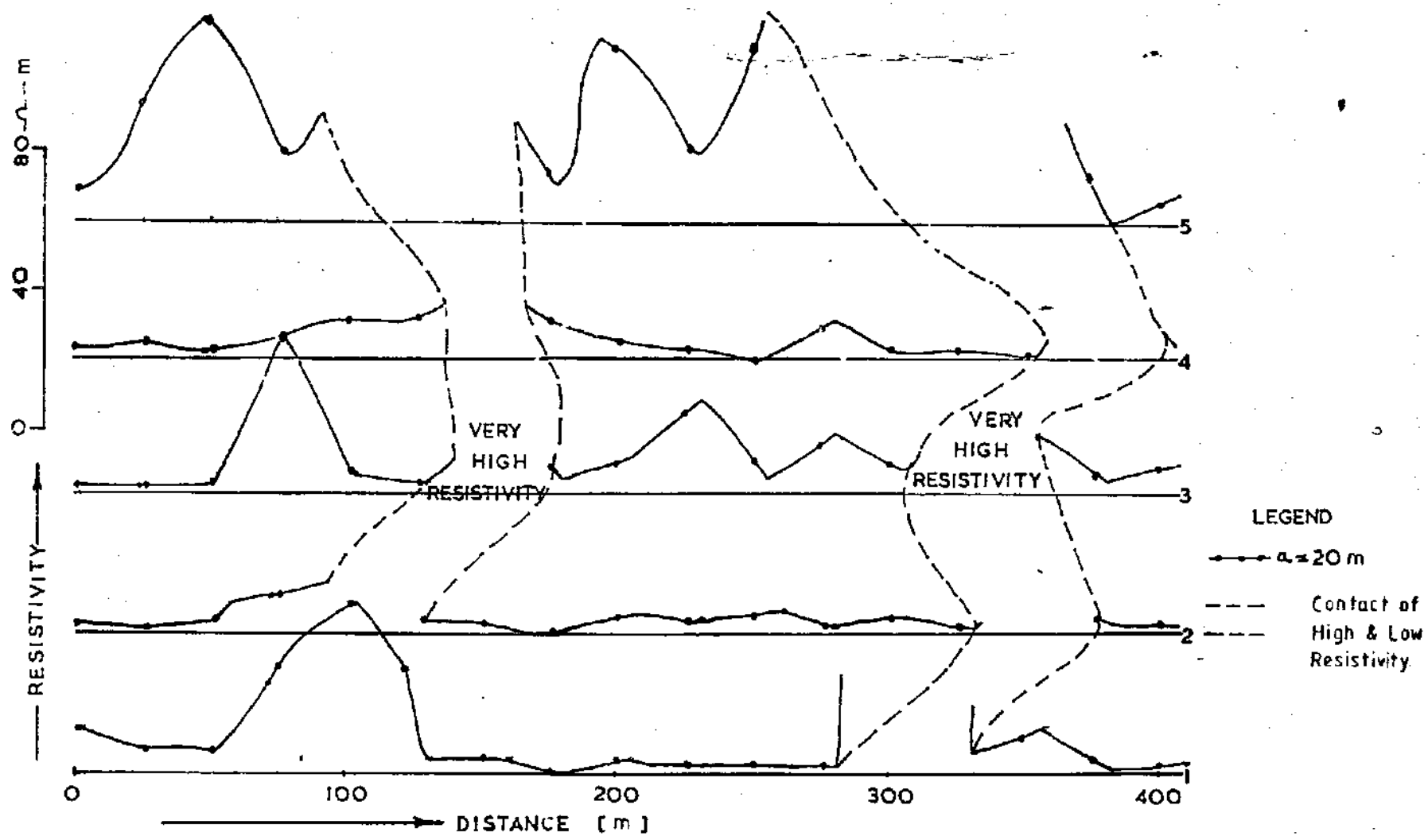


FIG. 6·18

WENNER RESISTIVITY PROFILING IN THE **NORTH–SOUTH DIRECTION.**

known. The low resistivity value in north-south direction ranged between 1 to 30 Ωm and the high value between 5,000 to 10,000 Ωm. According to Telford (1976), if the beds have a steep dip and the measurement is made with a spread perpendicular to the strike, the apparent resistivity will be smaller than the true resistivity, normal to the bedding. If the array is parallel to the strike of the dipping beds, the apparent resistivity will be too large. In resistivity surveys it is possible to estimate the true resistivity through cross profiling by taking the average of the resistivity values in the north-south and east-west directions, thus removing the anistropy effect. To determine this, their averages were taken, the regions of high resistivity were separated from the low ones by qualitative/semi-quantitative analysis. Referring to Fig. 6.19, it would be observed that the occurence of the mineral deposit is sporadic.

Since the thickness of the kaolin deposit (Fig. 6.19) varies from one location to the other as seen from the vertical soundings, the area indicating kaolin deposits was divided into small sectors. The area of these sectors was determined using a planimeter and multiplied by the dominating thickness of that particular sector calculated from the soundings nearest to that sector. The results show that the kaolin zone extends laterally over an area of 57,805 $\pm$ 200 m^2. Using the average bulk density of kaolin as $1.82 \times 10^3 \pm 0.2 \times 10^3$ kg/m^3

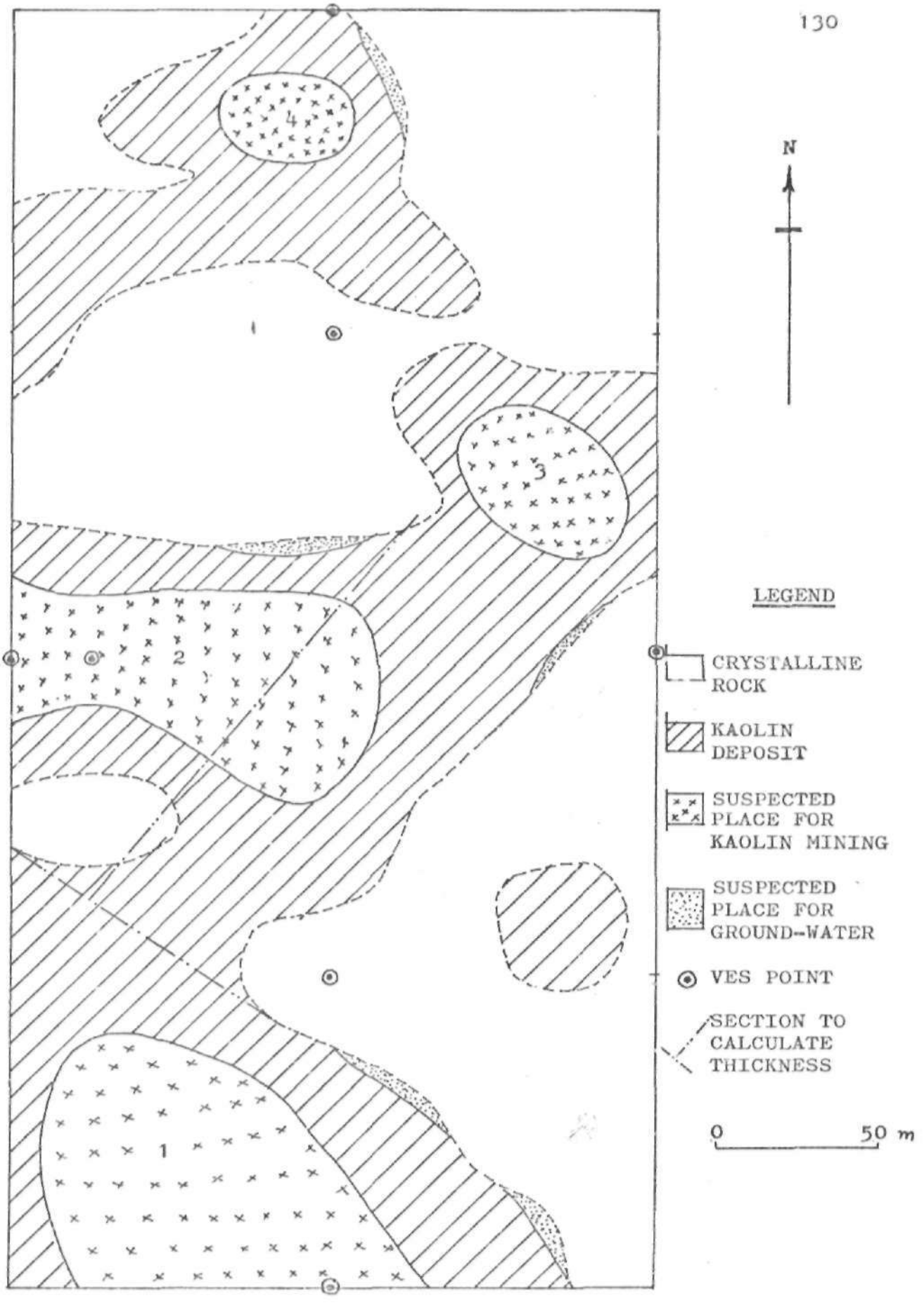


FIG. 6·19

MAP SHOWING POSSIBLE EXTENT OF KAOLIN DEPOSIT USING THE WENNER RESISTIVITY PROFILING METHOD.

determined from six different samples collected from the existing mining pit, its approximate mass is estimated to be 1.6 ± 0.2 million tons. The accuracy of the estimate would however be subject to variation in its thickness and its sporadic nature.

The best possible places suitable for constructing wells for ground water are shown at places marked in Fig. 6.19. These places have been recommended keeping in view the following:

i) very low resistivity values of less than 10 Ω m given by Wenner profiling of a = 10 m

ii) position and general shape of the border lines between the high and low resistivity regions (such as pocket or grab shape) as shown in Fig. 6.19, and

iii) being very close to the impervious highly resistive rock. The water gets accumulated there and the basin like structure makes it a good reservoir.

6.5 Interpretation of Self-Potential Survey:

The theory of S.P. has been discussed in chapter 3. The object of such a survey is to locate variations in rock properties or mineral contents at geologic contacts.

Terrameter SAS-300 was used for this survey. The field procedure involved using two electrodes which had a constant mutual separation of 25 m. These were advanced

together along the nine east-west traverses in steps of 25 m, so that the rear electrode occupied every time the position previously held by the front electrode.

The gradient at the point midway between the electrodes was plotted for the nine traverses, as shown in Fig. 6.20. It would be seen that the curves mostly show positive low S.P. deflections. These could be due to the background potential. The small negative values observed at traverses 3 and 17 could be attributed to groundwater. The resistivity values are also very low in this area, less than 10 Ω.m. This further confirms that ground-water should be available at shallow depth in this area. Along profile 9, there is hardly any change in S.P. readings which suggests that the zone is homogenous. This is in agreement with the resistivity profiling along the same traverse which too does not show any significant change in the readings.

Kaolin deposits usually give relatively positive S.P. values in comparison to shales which give zero value on the S.P. log. The exact range of S.P. values for kaolin is not yet known. To differentiate different media of the kaolin deposits and crystalline rock, the inflection points of the S.P. curves were taken into consideration, and respective areas were outlined, Fig. 6.21. The largest deposits of kaolin were given by the maximum positive S.P. value on the curves, Fig. 6.20.

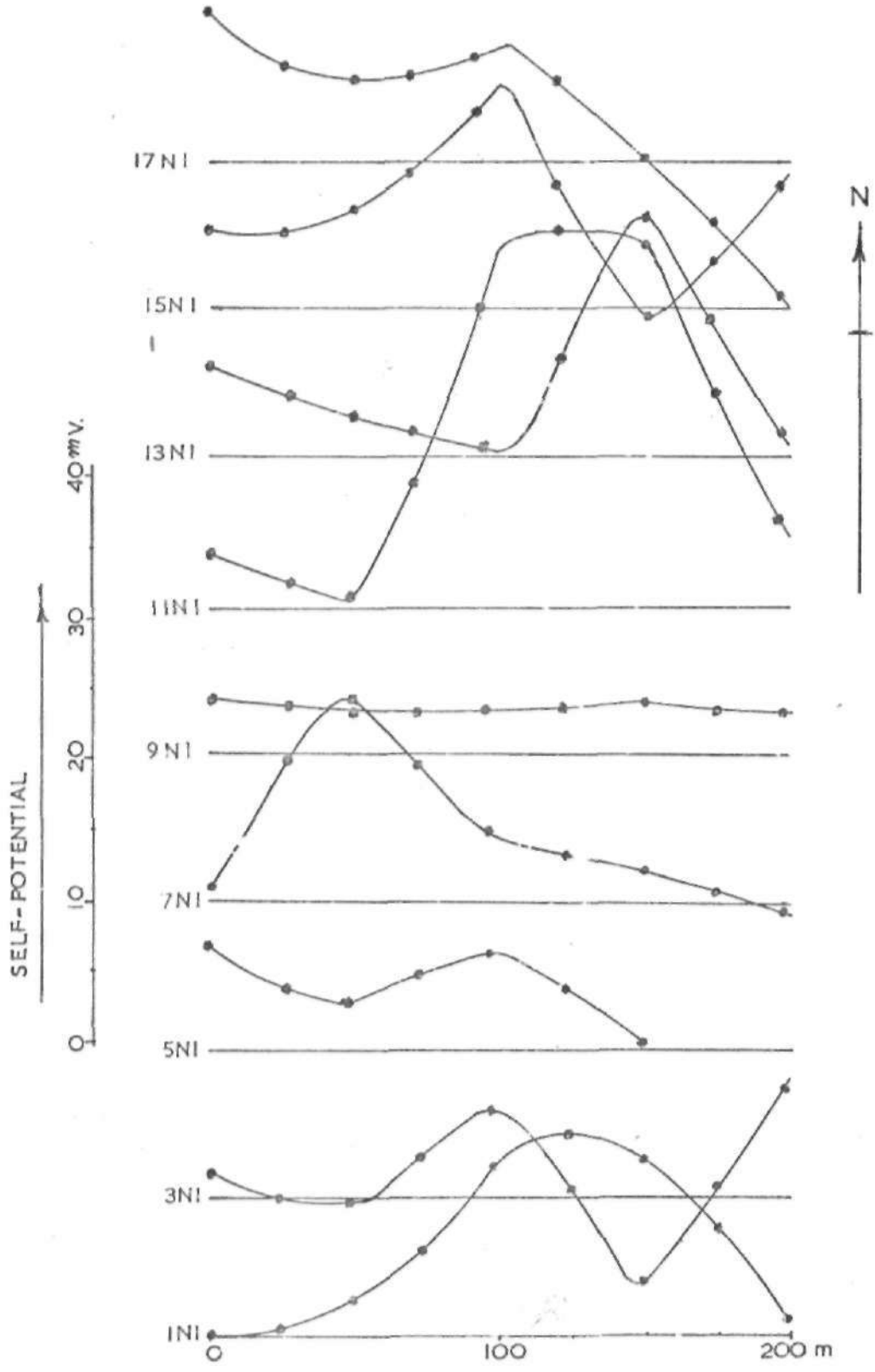


FIG. 6·20

SELF-POTENTIAL DATA IN THE EAST-WEST DIRECTION.

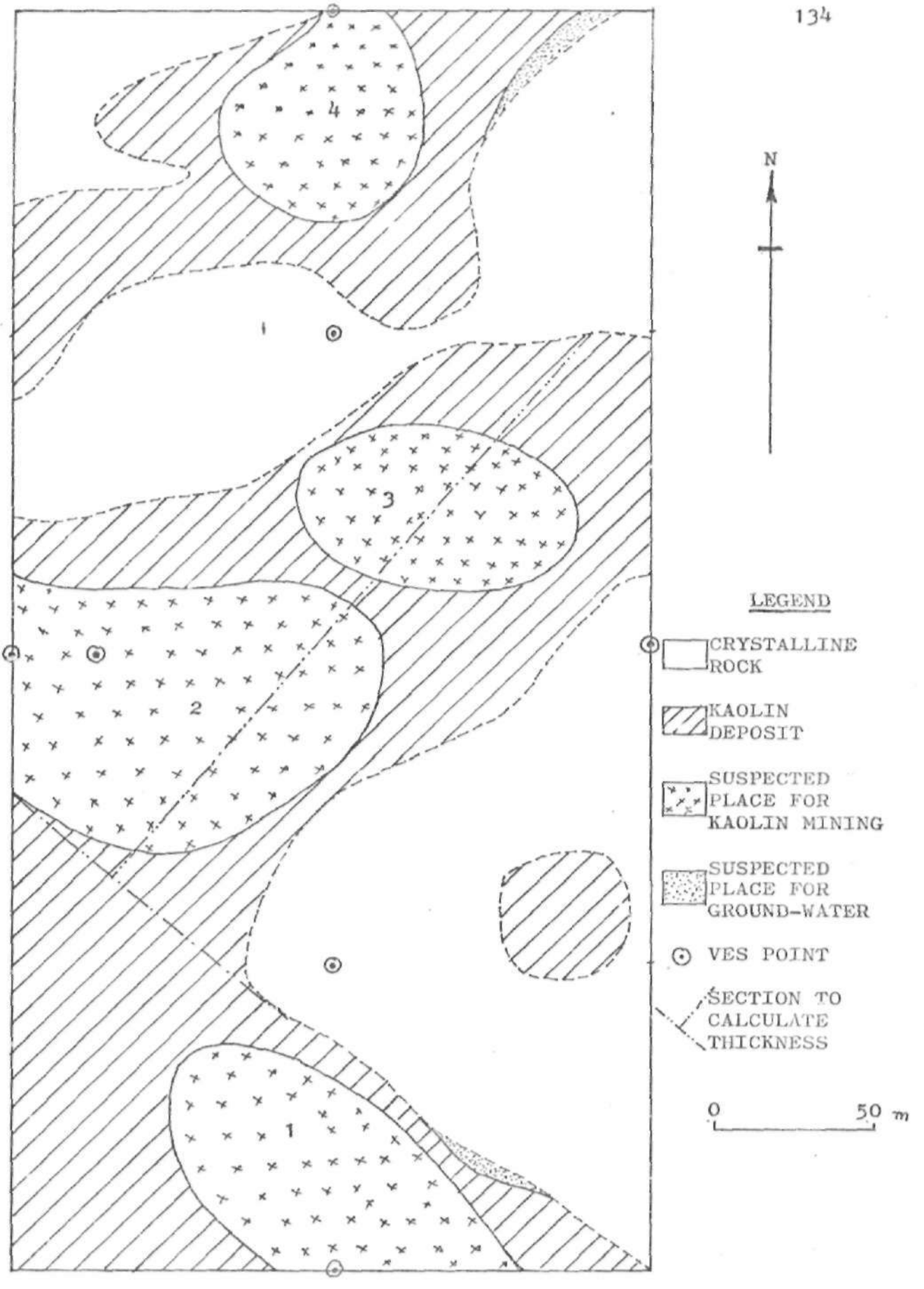


FIG. 6·21

LATERAL EXTENT OF KAOLIN DEPOSIT BY SELF-POTENTIAL SURVEY.

The total area and the mass of the kaolin deposit as deduced from the S.P. survey is 59,558 ± 200 m^2 and 1.7 ± 0.2 million tons respectively.

In the S.P. interpretation, the exact range of S.P. values for kaolin is not known, also the data points are very few. The results of resistivity profiling are considered more reliable than those of S.P. survey.

When comparing the outline of the area occupied by kaolin deposit as predicted from the qualitative/semi-quantitative analysis of both resistivity profiling and S.P. profiling, it would be noted that it is more or less similar, except slight variations, Figs. 6.19 and 6.21 respectively. These two figs. were superimposed on each other and the area where the two figs. intersect are recommended for mining of kaolin and prospecting for ground water (Fig. 6.22).

6.6 Interpretation of V.L.F. Survey:

This survey was carried out to delineate the contact points between different sub-surface media and to compare the results obtained from the resistivity survey for the same area. Both the in-phase and quad components were measured at intervals of 50 m along the nine traverses, using the Geonic VLF-EM unit, which is described in section 3.3.1. The V.L.F. transmitter station chosen was GBR f = 16 KHz.

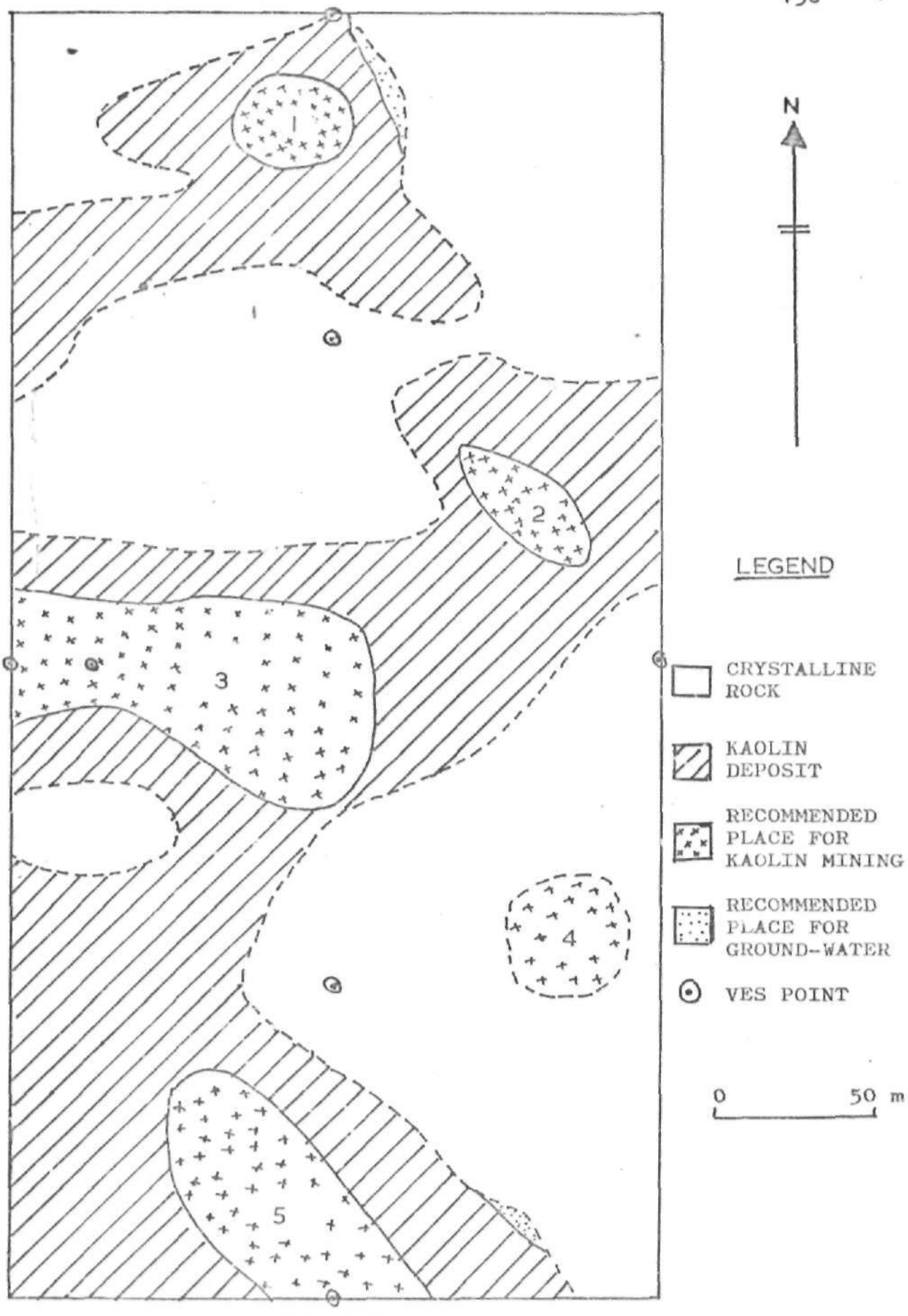


FIG. 6·22

MAP SHOWING EXTENT OF KAOLIN DEPOSIT AND POSSIBLE PLACES FOR GROUND-WATER PROSPECTING.

After applying Fraser's filtering method to the data, for the in-phase components, contouring was done as shown in Fig. 6.23. A cross-section running north to south at the middle of the grid was drawn, Fig. 6.24. It would be observed that this cross-section to a fair degree can be correlated to the one deduced from iso-resistivity maps, Fig. 6.10. On the basis of previous results obtained in section 6.3.3, it can be said that the negative in-phase values are due to the anomalous body, while the positive in-phase values are due to kaolin deposits. At places where the inphase component has zero value, those points indicate the demarcation line between the two different media, kaolin and the anomalous body. The position and the length of the anomalous body is generally similar to that deduced in section 6.3.3. Both V.L.F. and iso-resistivity maps have provided good correlation in delineating the kaolin deposits.

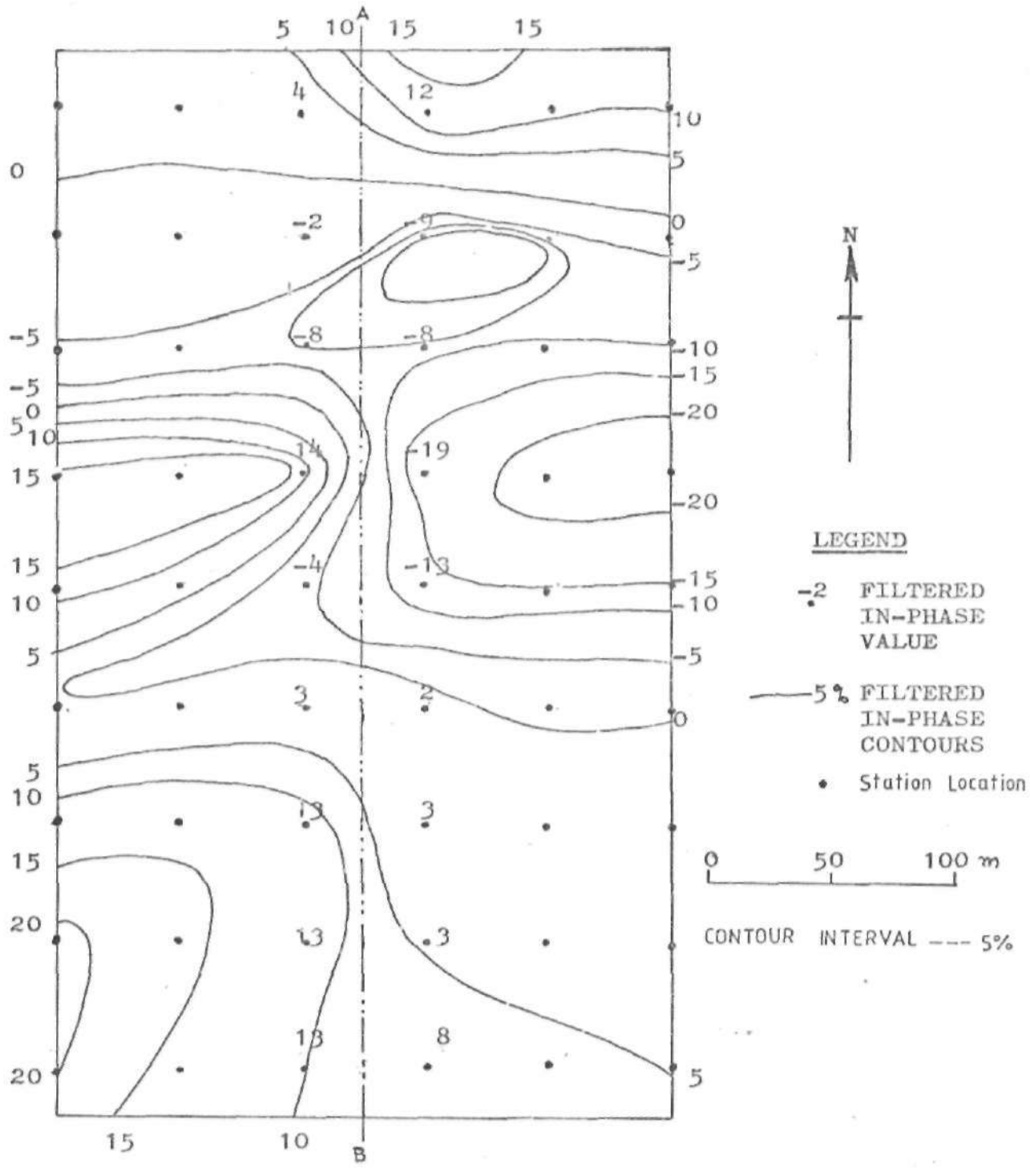


FIG. 6·23

CONTOUR PLOT OF THE V.L.F. IN-PHASE COMPONENT DATA AFTER APPLYING FRASER'S FILTERING.

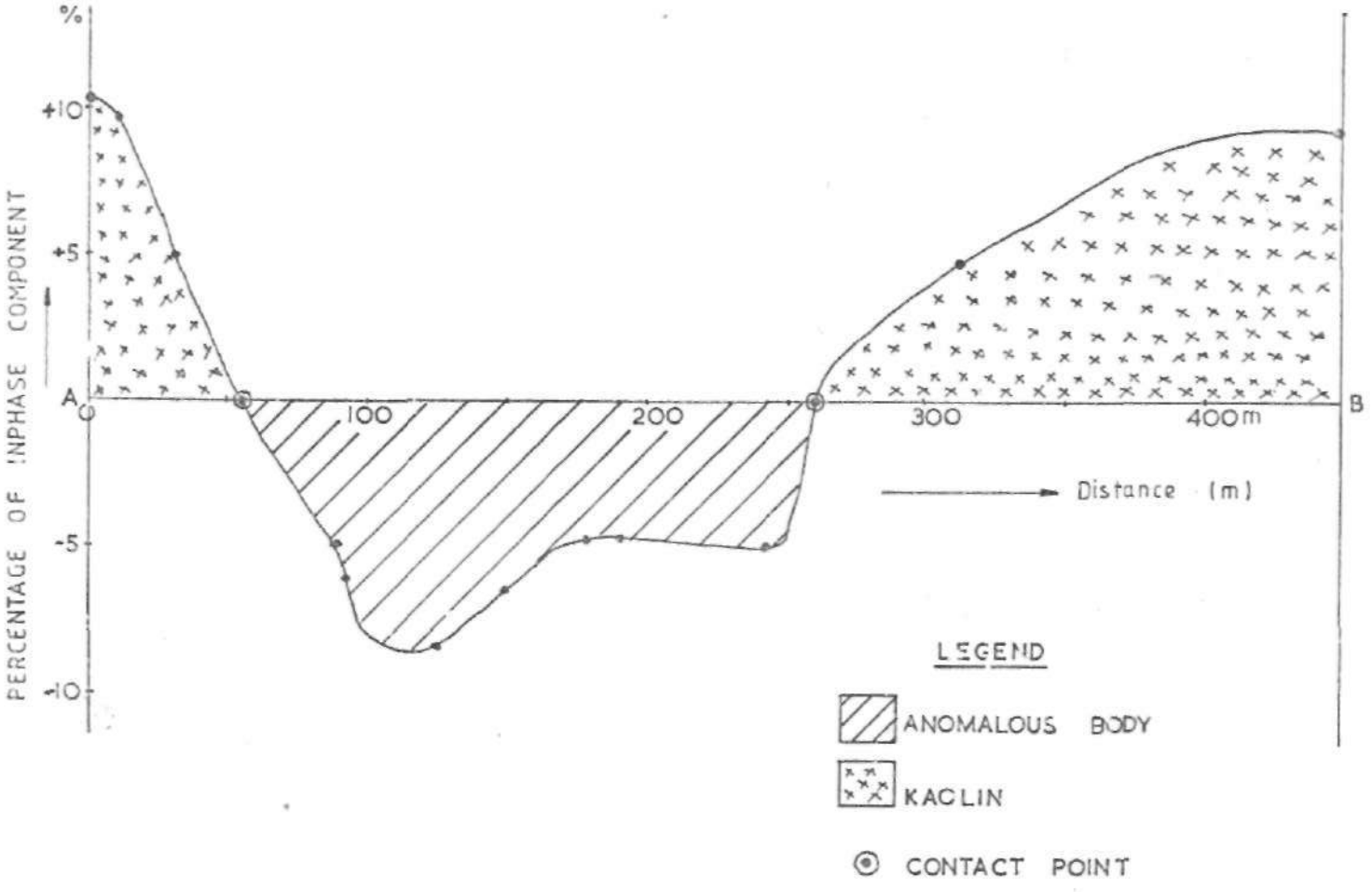


FIG. 6·24

CROSS-SECTION OF A-B AS DEDUCED FROM V.L.F. IN-PHASE COMPONENT DATA.

Chapter 7

CONCLUSIONS

7.1 Summary:

Regional geophysical survey carried out along the three profiles using mechanical analysis, resistivity, S.P., and V.L.F. have led to the following conclusions:

i) The results of mechanical analysis of the surface soils along three profiles have been correlated with their topographic heights. Silt and coarse sand gives the highest multiple correlation factor of about 0.6 with height.

ii) The resistivity profiling of Minjibir to Bagurawa has been correlated with observed geological exposures. It shows two peaks of very high resistivity values. The resistivity profiling of Minjibir to Wasai gives a very low resistivity of 30 Ωm at the Minjibir end indicating that ground-water is trapped there in. The resistivity profiling of dry river bed indicates the existence of buried channels.

iii) S.P. survey along Minjibir to Wasai and along the dry river bed shows that the shape of the S.P. curves is similar, thus indicating that sub-surface structure can be extended from the dry river to Minjibir-Wasai profile. It has been deduced that this is a shallow basin like structure, which is

filled with recent sediments. The basin is most likely an aquifer for groundwater and overlies the bedrock. The places giving negative S.P. values are recommended for groundwater prospecting.

iv) The regional V.L.F. and S.P. profiling methods provide a good correlation in respect of the sub-surface structure of that area.

Geophysical survey carried out in the vicinity of an existing kaolin pit using resistivity, S.P. and V.L.F. methods have led to the following conclusions:

i) The results of the vertical soundings indicate that the sub-strata is composed of three different layers. The first layer has resistivity value between 600 to 1,175 Ω-m and its thickness varies between 1.1 to 1.7 m. It is composed of sand and some laterite. The second layer is the least resistive and has a resistivity value between 100 to 235 Ωm. Its thickness varies from 11.3 ± 2.4 m to 21.7 ± 1.3 m and is composed of kaolin. The third layer has the highest resistivity value, above 2,400 Ωm and is the bed rock.

ii) An attempt has been made to deduce the sub-surface geology of the area by the use of iso-resistivity contoured maps. The two dimensional section drawn shows the existence of four layers. The top layer is of sand. The layer beneath it i.e. the second layer is composed of kaolin, having varying depth

upto 19 m. The third layer, most probably is also composed of kaolin, but highly saturated with water. It has a varying depth between 10 and 20 m below the ground surface. The last layer is the bed rock.

iii) The sub-surface structure of the highly resistive anomalous body has been deduced from various characteristics obtained from iso-resistivity contoured maps such as relief, gradient, mean radius and area. The sub-surface structure indicates four layer interacting with the anomalous body.

iv) The results of resistivity profiling survey indicates that the occurence of kaolin is sporadic. Its total mass is estimated to be 1.6 $\pm$ 0.2 million tons.

v) The S.P. method used to delineate kaolin deposits has given similar results as obtained by the resistivity profiling technique. The estimated mass of kaolin by this method comes to 1.7 $\pm$ 0.2 million tons.

vi) Suitable locations for groundwater prospecting as deduced from Fig. 6.22 have been recommended. This is due to the presence of impervious sub-strata, which would act as barriers and good accumulation of water would occur at these places.

vii) In the V.L.F. method, the in-phase component values were filtered using Fraser's method and contoured.

The negative in-phase values indicated the existence of anomalous body, while the positive in-phase values indicated kaolin deposits. The V.L.F. method provided a good correlation with the final cross-section arrived at from the iso-resistivity maps.

7.2 Suggestions:

i) The locations as indicated in Fig. 6.22 are suggested for mining of kaolin.

ii) The locations as shown in Fig. 6.22 and also the areas on both ends of the Minjibir to Wasai profile are suggested for ground-water prospecting.

iii) A larger area surrounding the existing kaolin pit should be surveyed, and other geophysical methods such as seismic and induced polarization should also be deployed for better delineation and quantification of kaolin deposits.

iv) Where there are indications of groundwater, the area should be surveyed using smaller electrode spacing for an accurate determination of the water table depth.

v) Mechanical analysis of soils should be carried out for more profiles in this area to confirm the results obtained during this survey.

REFERENCES

Ahn, P.M. (1970), "West African Soils", London, Oxford.

Ajayi, L.A. (1983), "Geotechnical Properties of a Deep Organic Clay Stratum Underlying Lagos Area of Nigeria", edited by S.A. Ola, Tropical Soils of Nigeria in Engineering Practice. A.A. Balkema Publ., Netherlands.

Atlas Copco ABEM, (1981) Geophysical Instruments Ltd., ABEM Terrameter SAS-300 Instrument Manual.

Barber, A. and Akano, G., "A note on Resistivity Measurements at Kano Province, Geol. Survey Nigeria", Rept. No. 1380.

Bateman, A.M. (1967), Economic Mineral Deposits, John Wileys Sons Inc., London.

Bayoumi, A.I. and Sayed, M.A. (1973), Geoelectrical Investigation on the Underground Water Resources of Ras El-Hekma, Mediterranean Littoral Zone, Egypt. Bulletin of the Faculty of Science, Cairo University.

Bowden et al, (1976), "Geochemical Studies on Younger Granites of Nigeria", edited by C.A. Kogbe, Geology of Nigeria, Elizabethan Publ. Co., Lagos.

De-Witte, L. (1948) "A New Method of Interpretation of Self-Potential Field Data", Geophysics, Vol. 13, pp. 233-244.

D'Hoore, J.L. (1964), Soil Map of Africa, Explanatory notes, CCTA, Lagos.

Dobrin, M.B. (1976), Introduction to Geophysical Prospecting, McGraw Hill Book Co., Inc., New York.

Ebifegha, M.E. (1977) "Geophysical Exploration for Buried Kaolin Mineral near Kankara, Katsina Province, Kaduna State, Nigeria", M.Sc. Thesis, Dept. of Physics, A.B.U., Zaria, Nigeria.

El-Kadi, H. (1973), "Introduction to the Interpretation of Resistivity Curves", The Arab Sc. Congr. Cairo. Vol. IV, pp 211-223.

_____, (1973), "Electrical Prospecting in Wadi El-Natrun Area", Seventh Arab Sc. Congr., Cairo. Vol. IV, pp 191-210.

Faseke, O.O. (1977), "Reconnaissance Survey of the Kaolin Deposit at Bagurawa, Southwest of Minjibir", Geol. Survey Nigeria.

Fraser, D.C., (1969), "Contouring of VLF-EM Data", Geophysics, Vol. 34, pp 958-967.

Geonics Ltd. (1979), VLF-EM 16 Operating Manual, 2 Thorncliffe, Park Drive, Toronto.

George, A. (1976), "Analytical Interpretation of High Frequency E.M. Prospecting Data (VLF System)", M. Sc. Thesis, International Institute for Aerial

Survey and Earth Sciences, Delft, Netherlands.

Ginzburg, A. (1974), "Resistivity Surveying", Journ. of Geophy. Surveys. Vol. I, No.3, pp 325-355.

Grant, F.S. and West, G.F. (1965), Interpretation Theory in Applied Geophysics. McGraw Hill Book Co., Inc., New York.

Grant, N.K. (1971), "A Compilation of Radiometric Ages from Nigeria", Journ. Min. and Geol. Vol.VI, pp 37-54.

Griffiths, D.H. and King, R.F. (1965), Applied Geophysics for Engineers and Geologists. Pergamon Press, London.

Grimshaw, R.W. (1971), The Chemistry and Physics of Clays and other Ceramic Materials. Ernest Benn Ltd., London.

Jackson, P.D. and Stanford, P.N. (1978), "Resistivity-Porosity- Particles Shape Relationships for Marine Sands", Geophysics. Vol. XXXXIII, pp 1250-1268.

Johnstone, S.J. and Johnstone, M.G. (1961), Minerals for the Chemical and Allied Industries. Chapman and Hall, London.

John, C.D. (1973), Statistics and Data Analysis in Geology, John Wiley and Sons Inc., London.

Keller, G.V. (1967), Methods in Mineral and Groundwater Exploration in Mining and Groundwater Geophysics, edited by L.W. Monley, Geol. Survey Can. Econ. Geol. Rep. No. XXVI.

_____, and Frischnecht, F.C. (1966), Electrical Methods in Geophysical Prospecting, Pergamon Press, Oxford.

Kiakkonon, P. (1979), "Numerical VLF Modelling", Geophs. Prosp. Vol. XXVII, pp 815-834.

Kirsch, H. (1968), Applied Mineralogy for Engineers, Technologists and Students. Chapman and Hall, London.

Koefoed, O. (1969), "An Analysis Of Equivalence in Resistivity Sounding", Geophysical Prosp. Vol. XVII, No. 8.

Kollert, R. (1969), "Groundwater Exploration by the Electrical Resistivity Method", Geophysical Memorandum 3/69. Atlas Copco ABEM AB.

Macleod, W., "Kaolin Deposits near Bichi, Kano Province and Near Kankara, Katsina Province", Geol. Survey Nigeria, Unpub. Rept. No. 1,442.

Maignion, R. (1966), "Review of Research on Laterites', UNESCO Nat. Res. Series. IV Paris, UNESCO.

McCurry, P. (1976), "The Geology of the Precambrian to Lower Palaezoia Rocks of Northern Nigeria", edited by C.J. Kogbe, Geology of Nigeria. Elizabethan Publ. Co., Nigeria, pp 15-35.

Millot, G. (1970), Geology of Clay. Springer- Verlag, New York.

Mooney, H.M. (1973), Handbook of Engineering Geophysics, Bison Instrument Inc., Minnesota.

Nkuesunam, O.E. (1976), "Investigation of the Extent of Kaolin Deposit near Tsanyawa, Kano State, Nigeria, using Geo-electrical and Seismic Refraction Methods", M.Sc. Thesis. Dept. of Physics, A.B.U., Zaria, Nigeria.

Ojanuga, A.G. (1979), "Clay Mineralogy of Soils in the Nigerian Tropical Savannah Regions", Soil Sc. Soc., America, pp 43.

_____ and Lee, G.B. (1973), "Characteristics, Distribution and Genesis of Nodules and Concentrations in Soils of the Southwestern Upland of Nigeria", Soil Sci., Vol. 116, pp 282-291.

Ola, S.A. (1983), "Geotechnical Properties and Behaviour of some Nigerian Lateritic Soils", edited by S.A. Ola, Tropical Soils of Nigeria in Engineering Practice. Balkema Publ., Netherlands.

Olsson, O. (1980), "VLF Anomalies for Perfectly Conducting Half-plane below an Over-burden", Geophs. Prosp. Vol. XXVIII, pp 415-434.

Oyawoye, M.O. (1964), "Geology of the Nigeria Basement Complex", Journ. of Min. and Geol. Vol. I, pp 87-102.

Oyeka, A.N. (1976), "Report on Kankara Kaolin Deposits, Kankara, Katsina Province, North Central State with notes on Marble Occurence", Geol. Survey Nigeria, Unpub. Rept. No. 1,529.

Parasnis, S.D. (1973), Mining Geophysics, Elsevier Scientific Publ. Co., Netherlands.

Paterson, N.R. and Ronka, V. (1969), "Five years of Surveying with the VLF-EM Method", Annual International Meeting Soc. of Explor. Geophys.

Rahaman, M.A. (1976), "Review of the Basement Geology of Southwestern Nigeria", edited by C.J. Kogbe, Geology of Nigeria. Elizabethan Publ. Co., Nigeria.

_____, et al (1977), "Detailed age study of the Migration of Ring Complexes in Northern Nigeria", Journ. Min. and Geol. Vol. XIV.

_____, and Malomo, S. (1983), "Sedimentary and Crystalline Rocks of Nigeria", edited by S.A. Ola, Tropical Soils of Nigeria in Engineering Practice, A.A. Balkema Publ., Netherlands.

Rijkswaterstaat, (1975), Standard Graphs for Resistivity Prosp. EAEG, The Hague, Netherlands.

Sato, M. and Mooney, H.M. (1960), "The Electrochemical Mechanism of Sulphide Self-potentials", Geophysics. Vol. XXV(1), pp 226-249.

Saydam, A.S. (1981), "Very Low Frequency Electromagnetic Interpretation using the Tilt Angle and Ellipticity Measurements", Geophysics. Vol. XXXXVI(2), pp 1,594-1,605.

Telford, W.M. et al (1976), Applied Geophysics. Cambridge Univ. Press, Cambridge.

Vingoe, P. (1972), "Electrical Resistivity Surveying", Geop. Memorandum 5/72. Atlas Copco ABEM AP.

Walpole, R.E. (1974), Introduction to Statistics. Macmillan Publ. Co., New York.

Worral, W.E. (1968), Clay - Their Nature, Origin and General Properties. Maclaren and Sons, London.